

Nanocellulose, a Versatile Green Platform: From Biosources to Materials and Their Applications

Bejoy Thomas,^{*,†} Midhun C. Raj,[†] Athira K. B,[†] Rubiyah M. H,[†] Jithin Joy,^{†,‡} Audrey Moores,^{||} Glenna L. Drisko,^{*,§} and Clément Sanchez^{*,⊥}

[†]Department of Chemistry, Newman College, Thodupuzha, 685 585 Thodupuzha, Kerala, India

[‡]International and Interuniversity Centre for Nanoscience and Nanotechnology (IIUCNN), Mahatma Gandhi University, 686 560 Kottayam, Kerala, India

[§]CNRS, ICMCB, Université de Bordeaux, UMR 5026, F-33600 Pessac, France

^{||}Centre in Green Chemistry and Catalysis, Department of Chemistry, McGill University, 801 Sherbrooke Street West, Montreal, Quebec H3A 0B8, Canada

[⊥]UPMC Université Paris 06, CNRS, UMR 7574 Laboratoire Chimie de la Matière Condensée de Paris, Collège de France, 11 place, Marcelin Berthelot, F-75005, Paris, France

ABSTRACT: With increasing environmental and ecological concerns due to the use of petroleum-based chemicals and products, the synthesis of fine chemicals and functional materials from natural resources is of great public value. Nanocellulose may prove to be one of the most promising green materials of modern times due to its intrinsic properties, renewability, and abundance. In this review, we present nanocellulose-based materials from sourcing, synthesis, and surface modification of nanocellulose, to materials formation and applications. Nanocellulose can be sourced from biomass, plants, or bacteria, relying on fairly simple, scalable, and efficient isolation techniques. Mechanical, chemical, and enzymatic treatments, or a combination of these, can be used to extract nanocellulose from natural sources. The properties of nanocellulose are dependent on the source, the isolation technique, and potential subsequent surface transformations. Nanocellulose surface modification techniques are typically used to introduce either charged or hydrophobic moieties, and include amidation, esterification, etherification, silylation, polymerization, urethanization, sulfonation, and phosphorylation. Nanocellulose has excellent strength, high Young's modulus, biocompatibility, and tunable self-assembly, thixotropic, and photonic properties, which are essential for the applications of this material. Nanocellulose participates in the fabrication of a large range of nanomaterials and nanocomposites, including those based on polymers, metals, metal oxides, and carbon. In particular, nanocellulose complements organic-based materials, where it imparts its mechanical properties to the composite. Nanocellulose is a promising material whenever material strength, flexibility, and/or specific nanostructuring are required. Applications include functional paper, optoelectronics, and antibacterial coatings, packaging, mechanically reinforced polymer composites, tissue scaffolds, drug delivery, biosensors, energy storage, catalysis, environmental remediation, and electrochemically controlled separation. Phosphorylated nanocellulose is a particularly interesting material, spanning a surprising set of applications in various dimensions including bone scaffolds, adsorbents, and flame retardants and as a support for the heterogenization of homogeneous catalysts.



CONTENTS

1. Introduction	11576	5.1. Imparting Ionic Charges to Nanocellulosic Surfaces	11587
2. Cellulose Structuration and Subunit Composition	11577	5.1.1. Phosphorylation of Cellulose	11588
2.1. Cellulose Nanocrystals (CNCs)	11579	5.1.2. Carboxymethylation	11589
2.2. Nanofibrillated Cellulose (NFC)	11580	5.1.3. Oxidation	11589
2.3. Bacterial Nanocellulose (BNC)	11580	5.1.4. Sulfonation	11589
3. Biomass Sources	11580	5.2. Generation of Nanocellulosic Materials with Hydrophobic Surfaces	11591
4. Nanocellulose Isolation	11583	5.2.1. Acetylation	11591
4.1. Mechanical Treatments	11583	5.2.2. Etherification	11591
4.2. Chemomechanical Treatment (Kraft Pulp- ing)	11586	5.2.3. Silylation	11591
4.3. Enzymatic–Mechanical Treatment	11586	5.2.4. Urethanization	11592
5. Chemical Modifications of Nanocellulose	11587		

Received: December 12, 2017

Published: November 7, 2018





Research article

Chitin nanowhisker – Inspired electrospun PVDF membrane for enhanced oil-water separation

Sreerag Gopi^a, Rupert Kargl^b, Karin Stana Kleinschek^b, Anitha Pius^{a,*}, Sabu Thomas^{c,**}^a Department of Chemistry, Gandhigram Rural Institute - Deemed University, Gandhigram, Dindigul District, 624302, Tamilnadu, India^b Faculty of Mechanical Engineering, University of Maribor, Smetanova 17, 2000, Maribor, Slovenia^c International and Inter University Centre for Nanoscience and Nanotechnology, Mahatma Gandhi University, Kottayam, 686560, Kerala, India

ARTICLE INFO

Keywords:

Polyvinylidene fluoride
Biopolymer
Chitin
Wastewater treatment
Oil
Advanced materials

ABSTRACT

The requirement of promoting a revolution in filtration technology has led to growing devotion in advanced functional materials such as electrospun membranes for filtering devices as a solution for providing water at lower energy costs. In this study, electrospun polyvinylidene fluoride membranes were fabricated by reinforcing 0.5 and 1 wt. % of chitin nanowhiskers in order to improve their thermal stability, mechanical properties, pure water flux and oil-water filtration performance for the possible application as filtration membranes. Morphological analysis revealed the porous and fibrous structure of membranes which confirmed by BET surface area analysis. Incorporation of chitin nanowhiskers improved the mechanical properties of the membranes such as elongation at break and tensile strength (specifically at 1 wt. % of chitin nanowhisker) while resulted in substantial enhancement of their thermal properties. Furthermore, polyvinylidene fluoride/chitin nanowhisker membranes showed enhanced oil-water separation ability, while reinforcement of chitin nanowhisker led to increase pure water flux rate, which measured as a crucial point in filtration membranes. The oil-water separation results compared with a commercial polyvinylidene fluoride membrane and the results signified the potential of electrospun polyvinylidene fluoride/chitin nanowhisker to be used for filtration application.

1. Introduction

Water is one of the most vital component in the world and it is being polluted to a critical limit. The increase in water pollution has significant impact on environment and the shortage of drinking water calls for the development of high performance water purification techniques. Due to their adverse effects on human health and environment, the removal of numerous pollutants like dyes, pesticides, heavy metals, herbicides, oils, and other agriculture wastes from waste water is becoming a critical problem to mankind (Huang et al., 2011). Water contamination by oil spills, especially in the areas that have industrial and urban development, is a major problem which is leading to damage aquatic and marine ecosystems (Lee et al., 2013). Conventional methods employed for oil-water separation like coagulation-flocculation, centrifugation, gravity separation, and skimming exhibit major drawback such as low separation efficiency, high processing costs and use of secondary pollutants (Lee and Baik, 2010). Therefore, new alternative adsorbent materials such as zeolites (Radetić et al., 2003), organoclays (Adebajo et al., 2003), activated carbon, gelators from

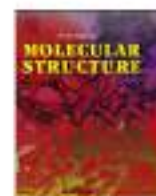
sugar or straw (Choi and Cloud, 1992), carbon nanotubes sponges (Lee et al., 2011), wool fibers (Annunciado et al., 2005), hair (Bayat et al., 2005), and others (Nadargi et al., 2009) are investigated as potential candidates for oil-water separation.

A variety of research articles, dealing with alternative approaches for oil-water filtration were published recently. Makaremi et al. fabricated polyacrylonitrile electrospun nanofibrous membranes reinforced with halloysite nanotubes for oil-water separation and heavy metal adsorption, concluded that, membrane activity increased by increasing the percentage of nanoparticles (Makaremi et al., 2015). Chaudhary et al. developed porous aerogel based on chitosan using bio-originated genipin as crosslinking agent and utilized for oil-water emulsion separator (Chaudhary et al., 2015). Cheng et al. fabricated cellulose nanocrystals based superhydrophilic membrane having contact angle of 31.6° and claimed that fabricated membranes were novel materials for oil-water separator reported for the first time (Cheng et al., 2017). A superhydrophilic and underwater superoleophilic polyvinylidene fluoride membrane based on chitosan-silica nanoparticle was reported by Liu. et al. (Liu et al., 2016). Surface modification using

* Corresponding author.

** Corresponding author.

E-mail addresses: dranithapius@gmail.com (A. Pius), sabuthomas@mgu.ac.in (S. Thomas).



Supramolecular framework of conjugated nitro-alkenes: Crystallographic and hirshfeld surface scan

Monu Joy, Nirmala Joseph, Varughese Mary, Vibin Jose, C. Sudarsanakumar*

School of Pure & Applied Physics, Mahatma Gandhi University, Kerala, 686503, India

ARTICLE INFO

Article history:

Received 10 May 2018

Received in revised form

8 July 2018

Accepted 9 July 2018

Available online 17 July 2018

Keywords:

Crystal structure analysis

Hirshfeld surfaces

Supramolecular interactions

ABSTRACT

Structural exploration of functionalised organic materials is the forefront of current research including crystal engineering. Six conjugated nitroalkene mediated heterocyclic analogs were crystallized and investigated its supramolecular characteristics systematically through Hirshfeld surface analysis with special reference to both *inter* and *intra* molecular hydrogen bonding patterns leading to its stability in the solid state. Herein the compounds **1–4** are α -aminoalkylated nitroalkenes, where **5** and **6** belong to α -hydroxy methylated nitroalkenes. Those interactions applicable to the present work include H...H, S...H, C...H, N...H, O...H and π -based interactions together with N... π , H...H contact majoring in **1–3** and the mainstream interaction of compounds **4–6** are O...H/H...O while nitro- π interactions are limited in number but present in variants **1, 5** and **6**. Besides the mentioned short contacts, various non-covalent interactions are also involved in the molecular architecture of the organic scaffolds (**1–6**) are also reported.

© 2018 Elsevier B.V. All rights reserved.

1. Introduction

Accurate three-dimensional structural treatments of highly challenging materials are forefront of current research. Recently much attention has been given to the design and developments of crystal structures. The quantitative estimation of their non-covalent interactions through Hirshfeld surfaces and thereby estimating the chemical performance of molecules is a long-lasting target of structural chemistry [1,2]. This is swiftly getting hold of popularity and seeks to figure out non-covalent interactions to restructuring the molecules in the atomic level so as to realize the goal of fabricating functionalised materials with tunable activities [3–5]. The most fashionable supramolecular approaches concerning non-covalent interactions including both *inter* and *intra* molecular hydrogen bonding lead to the stability in the solid-state with an extension of its activity [6]. In a crystal engineering perception, hydrogen bonds take part in the molecular assembly and restructuring of organic building blocks utilizing the conception of motifs and synthon through a diverse array of interactions, guide to propose the synthesis of new solid-state compounds with attractive properties [7]. Cooperativity of hydrogen bonds is very

important to the stability of organic materials since the donor-acceptor polarization of interconnected hydrogen bonds increases mutually and it leads to strengthening individual bonds. Besides strong hydrogen bonding interactions, weak short contacts viz. C–H...X (X = O, N, S) and π ... π stacking including C/N–H... π bonds control the self-assembly of organic compounds appreciably [8–10]. Non-covalent interactions are generally weaker and geometrically obscured, but their mutual effects, however, can be equally significant as covalent bonding. To the structural exploration of weak supramolecular interactions, the NO₂ group plays a significant role, is well thought-out by structural experts and crystal engineers where Wuest et al. establish the prospective of N...O interactions through crystal engineering [11]. Further, the advantages of nitro groups in the solid state synergy have also been studied by Daszkiewicz [12]. Consequently, the understanding of such interactions is essential and appealing for structural chemists and material scientist.

Besides their structural interest, nitrocompounds are versatile substrates which undergo a variety of useful synthetic alterations in organic chemistry. Nitro group has ability to transform into a legion of diverse functionalities as it can be reduced to oximes, ketones, hydroxyl amines, oxidized to carboxylic acids and conversion to primary alkyl radicals and 1,3 dipoles [13–16]. Conjugated nitro alkenes are readily reduced by a variety of borane and borohydride reagents and it provides an access to a number of nitrogen and

* Corresponding author.

E-mail address: c.sudarsan.mgu@gmail.com (C. Sudarsanakumar).

RESEARCH ARTICLE

Open Access



Tailoring of nanostructured material as an electrochemical sensor and sorbent for toxic Cd(II) ions from various real samples

Archana Aravind and Beena Mathew* 

Abstract

The aim of the present study is the fabrication of electrochemical sensor and sorbent for toxic Cd(II) ion using ion-imprinting technique on vinyl-functionalized multiwalled carbon nanotube. Multiwalled carbon nanotube-based ion-imprinted polymer (MWCNT-IIP) were synthesized using meth acrylic acid as the functional monomer, *N,N'* methylene-bis-acrylamide as the cross linking agent, and potassium peroxy disulphate as an initiator. The template and porogen used were cadmium chloride and water. To know the importance of MWCNT, ion-imprinted polymer without MWCNT was also prepared. For the purpose of comparison, non-imprinted polymers were also synthesized. The synthesized products were analyzed by FT-IR, XRD, TEM, EDAX, and TGA. An electrochemical sensor was made up by modifying platinum electrode with MWCNT-IIP. Experimental factors that control the routine of the sensor were investigated and optimized. Under optimal conditions, a calibration curve was obtained with a detection limit of 0.03 μM by using differential pulse voltammetric technique. Selectivity studies show irrelevant significance with Zn (II), Cu (II), and Ni (II) ions. The feasibility of modified platinum electrode shows a prospective application in real water sample collected from a lake, pigments, cosmetics, and fertilizers. The synthesized nanostructured material is also used for the extraction of Cd(II) ion from real water samples. The maximum adsorption of Cd(II) by various imprinted and non-imprinted sorbents was calculated, and it was found that maximum adsorption takes place at pH 6. The kinetic studies show that the adsorption of Cd(II) increases with time and reaches equilibrium at 70 min and the kinetic data follow pseudo-second-order kinetics. The adsorption data fitted to the Langmuir adsorption model which confirms the monolayer formation of an IIP layer on MWCNT surface. The selectivity co-efficient of the imprinted sorbent shows high selectivity and specificity towards Cd(II) ion than other metal ions.

Keywords: Cadmium (II), Molecular imprinting, MWCNT, MWCNT-IIP, Cyclic voltammetry

Highlights

- A new method for Cd(II) ion sensing with the advantage of ion-imprinted and electrochemical sensor.
- The sensor displays lower detection limit compared with the existed methods.
- MWCNT-IIP sensor displays good selectivity towards Cd(II) ion over other metal ions.
- Sensor with high sensitivity can be used for sensing and extraction of Cd(II) ion in real samples.

Introduction

Metal pollution in the environment is generally due to the industrial development (Das et al. 2016). Heavy metal ions such as cadmium, lead, chromium, and arsenic are highly toxic to the human health (Das et al. 1997). Cadmium grades ninth among the toxic substance by US disease and poison registry. Cadmium is a dispensable heavy metal which inhibits the enzyme, and it has been considered as the most hazardous pollutant due to its solubility and toxicity in the surroundings. Cd(II) is classified as a type I carcinogen. Exposure to cadmium leads to a variety of undesirable effects such as cancer, growth in the liver and kidney, and softening of bones (Waalkes 2003; Parameswaran and Mathew 2014). There are lots of methods which reported the detection of cadmium ions such as

* Correspondence: beenamscs@gmail.com
School of Chemical Sciences, Mahatma Gandhi University, Kottayam, Kerala 686560, India

Acknowledgements

The analytical facilities from Cashew Export Promotion Council of India, Kollam, Kerala, is gratefully acknowledged.

Funding

There is no funding for this study.

Availability of data and materials

The authors have no data to share since all data are revealed in the submitted manuscript.

Authors' contributions

MWCNT-based ion-imprinted polymer used as an electrochemical sensor and sorbent for toxic Cd(II) ions from real samples was discussed in this paper. Both authors read and approved the final manuscript.

Ethics approval and consent to participate

Not applicable.

Consent for publication

Not applicable.

Competing interests

The authors declare that they have no competing interests.

Publisher's Note

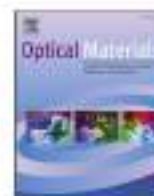
Springer Nature remains neutral with regard to jurisdictional claims in published maps and institutional affiliations.

Received: 16 June 2018 Accepted: 13 September 2018

<https://doi.org/10.1007/s12048-018-0218-8>

References

- Afkhami A, Soltani-Shahrivar M, Ghaedi H, Madrakian T. Construction of modified carbon paste electrode for highly sensitive simultaneous electrochemical determination of trace amounts of copper (II) and cadmium (II). *Electroanalysis*. 2015;28:296–303.
- D'Ilio S, Petrucci F, D'Amato M, Di Gregorio M, Senofonte O, Violante N. Method validation for determination of arsenic, cadmium, chromium, and lead in milk by means of dynamic reaction cell inductively coupled plasma mass spectrometry. *Anal Chim Acta*. 2005;624:59–67.
- Das N, Bhattacharya S, Maiti MK. Enhanced cadmium accumulation and tolerance in transgenic tobacco overexpressing rice metal tolerance protein gene OsMTP1 is promising for phytoremediation. *Plant Physiol Biochem*. 2016;105:297–309.
- Das P, Samantary S, Rout GR. Studies on cadmium toxicity in plants: a review. *Environ Pollut*. 1997;98:29–36.
- Diouf A, Motia S, El Alami El Hassani N, El Bari N, Bouchikhi B. Development and characterization of an electrochemical biosensor for creatinine detection in human urine based on functional molecularly imprinted polymer. *J Electroanal Chem*. 2017;788:44–53.
- L. Fotouhi, A. B. Hashkavayi, and M. M. Heravi, "Electrochemical behaviour and voltammetric determination of sulphadiazine using a multi-walled carbon nanotube composite film-glassy carbon electrode," *J Exp Nanosci*, 8, 947–956 (2012). X. Fu, Q. Yang, Q. Zhou, Q. Lin, and C. Wang, "Template-monomer interaction in molecular imprinting: is the strongest the best?," *Open J Org Polym Mater*, 2, 58–68 (2015).
- Gong K, Dong Y, Xiong S, Chen Y, Mao L. Novel electrochemical method for sensitive determination of homocysteine with carbon nanotube-based electrodes. *Biosens Bioelectron*. 2004;20:253–9.
- Gumpu MB, Sethuraman S, Krishnan UM, Rayappan JBB. A review on detection of heavy metal ions in water – an electrochemical approach. *Sensors Actuators B Chem*. 2015;213:515–33.
- Y. Han, J. Zheng, and S. Dong, "A novel nonenzymatic hydrogen peroxide sensor based on Ag–MnO₂–MWCNTs nanocomposites," *Electrochim Acta*, 90, 35–43 (2013). G. Fan, "Highly sensitive electrochemical determination of cadmium (II) in environmental water based on the electrodeposited bismuth nanoparticles," *Int J Electrochem Sci*, 4362–4370 (2016).
- Kan X, Zhao Y, Geng Z, Wang Z, Zhu J-J. Composites of multiwalled carbon nanotubes and molecularly imprinted polymers for dopamine recognition. *J Phys Chem C*. 2008;112:4849–54.
- Lee S, Oh J, Kim D, Piao Y. A sensitive electrochemical sensor using an iron oxide/graphene composite for the simultaneous detection of heavy metal ions. *Talanta*. 2016a;160:528–36.
- Lee SM, Zirliangura JA, Tiwari D. Electrochemical sensor for trace determination of cadmium(II) from aqueous solutions: use of hybrid materials precursors to natural clays. *Int J Environ Anal Chem*. 2016b;96:490–504.
- Legeai S, Vittori O. A Cu/Nafion/Bi electrode for on-site monitoring of trace heavy metals in natural waters using anodic stripping voltammetry: an alternative to mercury-based electrodes. *Anal Chim Acta*. 2006;560:184–90.
- Martínez-Huitle CA, Fernandes NS, Cerro-Lopez M, Quiroz MA, Quiroz MA. Determination of trace metals by differential pulse voltammetry at chitosan modified electrodes. *Port Electrochim Acta*. 2010;28:39–49.
- Mazzotta E, Malatesta C. Electrochemical detection of the toxic organohalide 2, 4-DB using a Co-porphyrin based electrosynthesized molecularly imprinted polymer. *Sensors Actuators B Chem*. 2010;148:186–94.
- Mhammedi MAE, Achak M, Hbid M, Bakasse M, Hbid T, Chtaini A. Electrochemical determination of cadmium(II) at platinum electrode modified with kaolin by square wave voltammetry. *J Hazard Mater*. 2009;170:590–4.
- Parameswaran G, Mathew B. Bioremediation of waste water containing hazardous cadmium ion with ion imprinted interpenetrating polymer networks. *Adv Environ Chem*. 2014;2014:1–10.
- Parham H, Pourreza N, Rahbar N. Solid phase extraction of lead and cadmium using solid sulfur as a new metal extractor prior to the determination by flame atomic absorption spectrometry. *J Hazard Mater*. 2009;163:588–92.
- Rezaei B, Rahmani O. Direct nanolayer preparation of molecularly imprinted polymers immobilized on multiwalled carbon nanotubes as a surface-recognition sites and their characterization. *J Appl Polym Sci*. 2011;125:798–803.
- Roy E, Patra S, Madhuri R, Sharma PK. Simultaneous determination of heavy metals in biological samples by a multiple-template imprinting technique: an electrochemical study. *RSC Adv*. 2014;4:56690–700.
- Shen J, Hu Y, Qin C, Ye M. Layer-by-layer self-assembly of multiwalled carbon nanotube polyelectrolytes prepared by in situ radical polymerization. *Langmuir*. 2008;24:3993–7.
- M. P. Sooraj and B. Mathew, "Structure-specific sorbent based on nanostructures for selective recognition of cimetidine from its structural analogues," *J Appl Polym Sci*, 131, (2014).
- A. Trani, R. Petrucci, G. Marrosu, D. Zane, and A. Curulli, "Selective electrochemical determination of caffeine at a gold-chitosan nanocomposite sensor: may little change on nanocomposites synthesis affect selectivity?," *J Electroanal Chem*, 788, 99–106 (2017).
- Veerakumar P, Veeramani V, Chen S-M, Madhu R, Liu S-B. Palladium nanoparticle incorporated porous activated carbon: electrochemical detection of toxic metal ions. *ACS Appl Mater Interfaces*. 2016;8:1319–26.
- Waalkes M. Cadmium carcinogenesis. *Mutation Research/Fundamental and Molecular Mechanisms of Mutagenesis*. 2003;533:107–20.
- Wei Y, Gao C, Meng F-L, Li H-H, Wang L, Liu J-H, Huang X-J. SnO₂/reduced graphene oxide nanocomposite for the simultaneous electrochemical detection of cadmium(II), lead(II), copper(II), and mercury(II): an interesting favorable mutual interference. *J Phys Chem C*. 2012;116:1034–41.
- Wong A, Foguel MV, Khan S, de Oliveira FM, Tarley CRT, Sotomayor MDPT. Development of an electrochemical sensor modified with MWCNT-COOH and MIP for detection of diuron. *Electrochim Acta*. 2015;182:122–30.
- Zougagh M. Determination of cadmium in water by ICP-AES with on-line adsorption preconcentration using DPTH-gel and TS-gel microcolumns. *Talanta*. 2002;56:753–61.



Eu³⁺ activated terbium oxalate nanocrystals: A novel luminescent material with delayed concentration quenching and tunable multicolour emission



Dinu Alexander, Kukku Thomas, S. Sisira, Linju Ann Jacob, Subash Gopi, Ajeesh Kumar S, P.R. Biju, N.V. Unnikrishnan, Cyriac Joseph*

School of Pure and Applied Physics, Mahatma Gandhi University, Kerala, 686360, India

ARTICLE INFO

Keywords:
Nanocrystals
Photoluminescence
Energy transfer
Multicolour phosphors

ABSTRACT

Tunable multicolour emitting Eu³⁺ activated Terbium oxalate nanophosphors synthesised by simple microwave assisted co-precipitation method is being forth. The powder X-ray diffraction analysis confirmed the crystal system of synthesised nanophosphors as monoclinic system with space group P2₁/c. The photoluminescence properties and energy transfer from Tb³⁺ to Eu³⁺ ions were analyzed systematically. The luminescence emission spectra and decay curves were analyzed based on the relative fraction of Tb³⁺/Eu³⁺ ions in oxalate matrix. Evidences for efficient energy transfer and the subsequent multicolour emission from green to red in the oxalate matrix were established by photoluminescence excitation, emission and decay kinetics. The present investigation revealed a dipole-dipole interaction mechanism for energy transfer between Tb³⁺ and Eu³⁺ with an energy transfer efficiency of 90%. The quenching free nature of oxalate matrix provided by the structure specificity ensures higher luminescence performance and makes it a suitable candidate for optical applications.

1. Introduction

Colour tunable rare earth based inorganic phosphors have sparked research to develop single phased phosphors for various applications because their multicolour luminescence emission in different regimes of visible spectra arising from the inherent 4f - 4f electronic transitions of rare earth ions [1–3]. The development of phosphors with more than one type of RE³⁺ in to the host matrix have opened up the possibilities of detailed spectroscopic investigation of the energetics between the two luminescent centres providing the multicolour emission under a single excitation wavelength. There are several parameters affecting the energy transfer mediated multicolour emission in phosphors such as concentration of sensitizer and receptor ions, type of interaction governing the energy transfer, intensities of intraconfigurational 4f - 4f transition in RE³⁺ ion and the energy transfer dynamics etc [3–5]. The detailed investigation on the energy transfer mechanism between rare earth ions is significant as it give information relating the possibility of multicolour emission and concentration of sensitizer and activator.

Tb³⁺ and Eu³⁺ ions are used in various luminescent materials because of their green and red emissions at 543 nm and 616 nm arising from the transitions ⁵D₄ - ⁷F_{0,5,8,3} and ³D₀ - ⁷F_{0,1,2,3,4} respectively. The Tb³⁺ to Eu³⁺ energy transfer processes are well discussed in various hosts ScPO₄:Tb³⁺/Eu³⁺, NaLa(PO₃)₄:Tb³⁺/Eu³⁺, La_{2-x}

y(MoO₄)₂:Tb³⁺/Eu³⁺, Y₂(Si₃O₉)₂:Tb³⁺/Eu³⁺ etc while the detailed reports on the energy transfer mechanism in Eu³⁺ activated Tb-concentrated host materials are limited [2,4,6,7]. Depending on the structural characteristics of the host, different luminescence behaviour can be seen. These differences may govern the luminescence emission colour of the material, depending on the energy transfer between sensitizer to sensitizer and sensitizer to activator. In Terbium concentrated host materials, the energy transfer between Terbium - Europium depends mainly on two factors; Tb³⁺-Tb³⁺ energy migration and Tb³⁺ - Eu³⁺ energy transfer. The energy migration again depends on parameters like site of symmetry of the RE³⁺ ion, distance between ions and the disorder in the lattice [8,9].

In our recent publications, we have proved the potentiality of Terbium oxalate as an efficient green emitting phosphor without substantial luminescence quenching [10–12]. The detailed single crystal structure analysis of Terbium oxalate crystals was reported describing the symmetry around the terbium ion and its nature of coordination with the oxalate ligand, revealing the structural peculiarities assisting efficient photoluminescence emission without concentration quenching [10]. The asymmetric unit of Terbium oxalate contains one crystallographically independent Terbium metal center (Tb³⁺ ion), one and half oxalate ligands, three coordinated water molecules and two lattice water molecules. The 9-fold coordination polyhedra of Tb³⁺ ion adopt

* Corresponding author.

E-mail address: cyriacjg@gmail.com (C. Joseph).



Research paper

Biomass yield and biochemical profile of fourteen species of fast-growing green algae from eutrophic bloomed freshwaters of Kerala, South India

Prasanthkumar Santhakumaran, Santhosh Kumar Kookal, Joseph George Ray^{*}

Laboratory of Plant Science and Ecology, School of Biosciences, Mahatma Gandhi University, Kottayam, 686560, Kerala, India

ARTICLE INFO

Keywords:

Algal-biomass
Algal-protein
Algal-lipid
Bloomed-waters
Microalgae
Omega fatty acids

ABSTRACT

Eutrophic, bloomed waters are known for fast-growing microalgae of high biomass yield. The biochemical composition of algae may vary from species to species. Identification of fast-growing local algal species, their experimental culture for assessing biomass yield and biochemical screening of the same for desirable metabolites is crucial to the prospects of algal technology. The freshwater algal diversity of Kerala - one of the biodiversity hotspots of the world, remains poorly explored. In this context, we assessed the yield and biochemical profile of hitherto uninvestigated 14 fast-growing microalgae of eutrophic bloomed freshwaters of Kerala. The biomass yield, carbohydrate, protein, pigment and lipid content of these species were significantly different. The alga *Pseudococcomyxa simplex* showed the highest biomass yield of $196.5 \pm 3.04\%$ increase $L^{-1} day^{-1}$. The alga *Kirchneriella lunaris* with 58.95% protein was found superior to the other algae in this regard. The species *Scenedesmus obliquus* was significantly higher in total lipids (32.05% of dry biomass) than the other algae. The alga *Monoraphidium griffithii* with 42.92% of omega groups of fatty acids in its lipid appeared a highly valuable species. The algae, *Rhodococcus ruber* ($12.77 \pm 2.31 mg g^{-1}$ of chlorophyll *a*), *Myrmecia bisecta* ($5.87 \pm 0.01 mg g^{-1}$ of chlorophyll *b*) and *Monoraphidium griffithii* ($7.50 \pm 0.02 mg g^{-1}$ carotenoid) appeared superior to the others in pigment content. Fourier-Transform-Infrared Spectroscopy of the biodiesel prepared from the lipids of all the algae confirmed the biodiesel feasibility of the same. The bioresource potentials of the 14 algal species revealed are new to science.

1. Introduction

Many species of algae are well-known bioresources, especially for nutraceutically valuable compounds, oil and minerals [1]. Since thousands of years, several algae have been used as a direct source of human food or for the preparation of various kinds of nutrient-rich functional foods in different parts of the world [2]. In general, the nutritional value of many species of microalgae is quite high, as they contain a high proportion of proteins, carbohydrates, lipids and vitamins [3]. Today, many algae are commercially cultivated for food [4], nutraceutical [5] and biofuel purposes [6]. Algae have now emerged as a stable economic crop [7].

Isolation of species and production of specific biomolecules from algal biomass for food and feed [8] is not new. Many species of polyunsaturated fatty acid yielding green algae are currently used for the feedstock preparations in the aquaculture industry [9]. Algae, rich in essential fatty acids are beneficial in the treatment of some illness and metabolic disorders in vertebrates [10–12]. Nutraceutical and toxicological evaluations of specific algal biomass have demonstrated

microalgae as a valuable feed supplement, which can easily replace the conventional protein supplements in animal feeds [13]. Algal proteins and other energy supplements from algal biomass form a prebiotic for enhancing production and maintaining the health of livestock [14]. In general, algae can provide a high yield of nutrient-rich biomass, which is readily convertible to animal feed at a minimum cost of production [15,16]. In addition to these aspects, certain green algal species are rich sources of pigments, antioxidants, vitamins, immune-stimulants as well as specific plant hormones such as the Chloro-Growth-Factor compounds [17] for various human purposes and medicinal applications. Many species of algae with high photosynthetic efficiency can produce oil in the form of tri-acyl-glycerol as storage lipids [18], which are valuable in the biofuel industry as a renewable source of energy and fuel. The annual productivity and the lipid content of certain species of algae are found to be far higher than that of seed crops [19].

Currently, the biomass and biofuel extraction from algae is well known as an industrially reliable process. Although reports on the biochemical potentials of few limited numbers of species exist in the literature [20], that of a large number of algae remain entirely

^{*} Corresponding author.E-mail addresses: prasanthsmg@gmail.com (P. Santhakumaran), sknairbt@yahoo.in (S.K. Kookal), jgray@mgu.ac.in (J.G. Ray).

Electrochemical sensor based on nanostructured ion imprinted polymer for the sensing and extraction of Cr(III) ions from industrial wastewater

Archana Aravind and Beena Mathew* 

ABSTRACT

In the present study we prepared a novel ion imprinted polymer as a sensitive electrochemical sensor for the determination of Cr(III) ion. The Cr(III) ion imprinted polymer was fabricated on a platinum electrode. Due to the presence of a nanolayer on the ion imprinted polymer with specific binding sites, the sensor reacted quickly to Cr(III) ion and can be used for selective extraction of Cr(III) ion. The Cr(III) ion imprinted polymer was prepared by using methacrylic acid as the functional monomer, *N,N'*-methylene-bis-acrylamide as the crosslinking agent, potassium peroxydisulfate as initiator and Cr(III) ion as the template molecule. Non-imprinted polymers were also prepared for comparative studies. The synthesized polymer was characterized using Fourier transform IR spectroscopy, TEM, Energy-dispersive X-ray spectroscopy and XRD. The limit of detection of the platinum–multiwalled carbon nanotube ion imprinted polymer sensor was found to be $0.051 \mu\text{mol L}^{-1}$ using differential pulse voltammetry. Moreover, the proposed method was effectively used for the sensing and extraction of Cr(III) ion in real samples collected from the metal plating industry.

© 2018 Society of Chemical Industry

Keywords: ion imprinted polymer (IIP); MWCNT; cyclic voltammetry; differential pulse voltammetry

INTRODUCTION

Heavy metals can gather and be preserved in the environment which makes them a hazardous health issue for human beings. Among various toxic heavy metals, chromium is one such heavy metal which enters the body and can cause various diseases such as cancer, chronic ulcers, autoimmune disease and even death.¹ The permissible limit of chromium in drinking water is $50\text{--}200 \mu\text{g dL}^{-1}$.² The main sources of chromium discharges into the environment causing ecological problems are electroplating, textile production, paint pigments, metal plating, wood industries and so on.³ Thus it is necessary to design an appropriate way to sense chromium ions in environmental samples before they enter into our body.

In earlier periods many methods were reported for the trace determination of chromium ions, e.g. HPLC,⁴ inductively coupled plasma mass spectrometer,⁵ solid phase extraction,⁶ electrothermal atomic absorption spectrometry⁷ etc. Even though these methods have achieved much attention for the determination of chromium ions, they have some drawbacks such as expense, sample pre-treatment, time and high sample consumption etc. Thus there is a significant need to overcome these disadvantages and make a selective and inexpensive tool for the determination of chromium ions in the environment.

Recently ion imprinted polymers (IIPs), a branch of molecular imprinting technology, have attracted great attention in many fields such as sensors, drug delivery and so on. However, IIPs have a few disadvantages such as a small binding capacity, slow mass transfer, low recognition sites etc.⁸ The disadvantages of

these polymers are overcome by adapting nanofabrication on IIPs. Multiwalled carbon nanotubes (MWCNTs) were used in this study since they have a high surface area and good electrical, chemical and mechanical stability. MWCNTs⁹ have also been used for electrochemical sensing as the supporting materials for IIPs due to their ability to ease electron transfer which has been accredited to the ends of the carbon nanotubes behaving similarly to edge plane graphite.^{10,11}

The main objective of the present work was to prepare an electrochemical sensor with Cr(III) ion imprinted MWCNT-IIP with high adsorption rate, selectivity and sensitivity. Cr(III) ion imprinted MWCNT-IIP was created using vinyl group functionalized MWCNTs; methacrylic acid (MAA), *N,N'*-methylene-bis-acrylamide (NNMBA) and chromium chloride were used as the monomer, crosslinking agent and template. The electrochemical behaviour and selectivity studies were carried out using cyclic voltammetry. The limit of detection of the modified electrode was determined using differential pulse voltammetry. The developed sensor was effectively used for the sensing of Cr(III) ion from environmental samples. After the sensing of Cr(III) ion from the collected samples, MWCNT-IIP was used for the extraction of Cr(III) ion from the sample itself.

* Correspondence to: B Mathew, School of Chemical Sciences, Mahatma Gandhi University, Kottayam, Kerala 686560, India. E-mail: beenams@scs@gmail.com

School of Chemical Sciences, Mahatma Gandhi University, Kottayam, India

Home > [Archive](#)

Volume: 8, Issue: 12, December, 2018

DOI: 10.7324/JAPS.2018.81214



Research Article

Mesoporous silica loaded caffeine inhibits inflammatory markers in lipopolysaccharide-activated rat macrophage cells

 Mahesh Babu¹, Chinnu Jerard², Bibin Punnoose Michael², Sini Suresh², Rajesh Ramachandran²

Author Affiliations

¹School of Medical Education, M G University, Kottayam, India.

²Molecular Biology and Applied Science, Biogenix Research Center, Thiruvananthapuram, India.

[Abstracts](#) | [Full-text \(HTML\)](#) | [References](#) | [Article Metrics](#) | [Similar Articles](#)

INTRODUCTION

Inflammation, a localized rejoinder towards cellular wound, is manifested by redness, heat, pain, capillary dilatation, and leukocyte infiltration, and is also obliged as a mechanics initiating the obliteration of pestiferous agents and impaired tissue (Nagarkar and Jagtap, 2017; Ryan and Majno, 1977). Inflammation ranges from acute to chronic inflammation which may evolve to cancer, allergies, asthma, and diabetes (Lawrence and Gilroy, 2006; Straub and Schradin, 2016).

Inflammation advances mainly through the arachidonic acid pathway which is conciliated via the enzyme-mediated action of cyclooxygenase-I (COX-I) or prostaglandin-endoperoxide synthase (Ricciotti and FitzGerald, 2011; Samuelsson, 1991). Nuclear factor kappa-light-chain-enhancer of activated B cells (NF-κB) is the paramount transcriptional factor in the synchronization of pro-inflammatory genes, such as interleukin-6 (IL-6), nitric oxide, inducible nitric oxide synthase (iNOS), and COX-2 (Dlaska and Weiss, 1999; Hwang et al., 2016). Its activation is widely stigmatized in inflammatory diseases and considerable scrutiny on the advancement of anti-inflammatory drugs targeting NF-κB was reported (Yin et al., 1998). Although several chemical classes of NF-κB inhibitors have been recognized, it is only for a few of those that a safety analysis based on a comprehensive interpretation of their pharmacologic mechanism of action has been recorded (Gupta et al., 2010; Mora et al., 2012). The evolution of tumor necrosis factor-alpha (TNF-α) inhibitors has, moreover, been one of the most vigorous fields of therapeutics more than a decade for the management of inflammatory diseases (Baugh and Bucala, 2001; Jackson, 2007).

Inflammatory response preceding tissue injury is quite cardinal in playing a key role both in normal and pathological healing which includes the activation of the innate immune system, enrollment of inflammatory cells to the site of injury etc. (Koh and DiPietro, 2011; Kokkas, 2010). The wound-healing progression involves four vastly incorporated along with super-imposing phases, such as hemostasis, inflammation, proliferation, and tissue remodeling or resolution (Broughton et al., 2006; Pugin, 2012). Delayed acute plus chronic injuries immigrate a pathologic inflammation due to partial or uncoordinated healing process (Koh and DiPietro, 2011). Characteristic of both chronic wounds and acute wounds that fail to heal is enormous leukocytosis and abridged matrix deposition (Ashcroft et al., 2003). The factors that impact repair can be assorted into local and systemic (Guo and DiPietro, 2010).

Caffeine, a phytochemical found in coffee plants is recognized to have biological characteristics, such as anti-oxidant, anti-aging, and anti-obesity effects (DaSilva et al., 2017). The well-acknowledged starting place of caffeine is the *Coffea Arabica* plant seed (Patay et al., 2017). This white crystalline Xanthine alkaloid analeptic drug is observed in the seeds, coffee plant, and the leaves of the tea bush (Ashihara et al., 2017; Hwang et al., 2016). It was revealed to have less IL-6, TNF-α (Horrigan et al., 2006; Popko et al., 2010), cell death, and inflammation, such as COX-2 in caffeine-infused rats than in those who had the placebo (Li et al., 2011). In the last two decennaries, mesoporous silica nanoparticles (MSN) have acquired increased attention for medical applications because of their humongous biocompatibility, biodegradability, storage stability, controllable diameter, maximum drug loading efficiency, and large amendable surface potential (Brezániová et al., 2018). To this regard, caffeine-loaded silica nanoparticles (CSNP) authenticate higher penetration rate when juxtaposed with caffeine.

Download Fulltext:

PDF (1.5 MB)

Abstract

[Print this Article](#)

How to cite this article

Download XML

Next article

Previous article

[Table of contents](#)

Share This Article on:



- > Email this to a friend
- > Request Permissions
- > Import into EndNote
- > Import into Bibtext

Related Search:

Author(s):

- Babu M
[PubMed] [Scholar]
- Jerard C
[PubMed] [Scholar]
- Michael B P
[PubMed] [Scholar]
- Suresh S
[PubMed] [Scholar]
- Ramachandran R
[PubMed] [Scholar]

Article(s):

- Related Article in PubMed
- Related Article in Google Scholar

Create Citaion Alert via Google Scholar





Ionic liquid functionalised reduced graphene oxide fluoroelastomer nanocomposites with enhanced mechanical, dielectric and viscoelastic properties

Grace Moni^{a,b}, Anshidha Mayeen^c, Amalu Mohan^a, Jinu Jacob George^d, Sabu Thomas^{e,h}, Soney C. George^{a,b,*}

^a Centre for Nanoscience and Technology, Department of Basic Sciences, Amal Jyothi College of Engineering, Kanjirappally, Kerala, India

^b School of Chemical Sciences, MG University, Kottayam, Kerala, India

^c School of Pure and Applied Physics, MG University, Kottayam, Kerala, India

^d Department of Polymer Science and Rubber Technology, Cochin University of Science and Technology, Cochin 682022, Kerala, India

^e International and Inter University Centre for Nanoscience and Nanotechnology, Mahatma Gandhi University, Kottayam, Kerala, India



ARTICLE INFO

Keywords:

Fluoroelastomers

Graphene

Ionic liquids

Viscoelastic characterisation

Dielectric properties

ABSTRACT

Utilization of Ionic Liquids (IL) as suitable candidate for nanofiller modification is of considerable interest in the current scenario owing to its peculiar properties. In the present study reduced graphene oxide (rGO) is modified with varying amount of IL to improve the dispersibility and interaction with fluoroelastomer (FKM) matrix. The surface modification of rGO using IL, its dispersion and incorporation into the FKM matrix was confirmed by FTIR, Raman, XRD, and AFM surface roughness analysis. The prepared nanocomposites achieved better static and dynamic mechanical properties by the addition of 2 phr of IL to rGO. Moreover the nanocomposites showed an increase in glass transition temperature from DSC (-18.82 for FIL 0 to -14 for FIL 2) analysis that supports the enhanced interaction between FKM and modified filler. Dynamic mechanical analysis of the nanocomposites proved the reinforcing ability and the effectiveness of ILrGO to enhance the properties as a whole. The dielectric study of the nanocomposites showed improved AC conductivity, dielectric constant value (60 with 2 phr of IL content) and a decrease in dielectric heating coefficient value with increase in ILrGO content. These property combinations make the nanocomposites a multifunctional material.

1. Introduction

Fluoroelastomers are well known for their chemical resistivity especially to acids, bases and organic solvents along with improved thermal stability and mechanical properties due to the presence of the stable C–F bond in the polymeric structure [1,2]. The strong van der Waals interaction between F and H atoms (intermolecular and intramolecular) supplied by the C–C and C–F bonds is responsible for the improved properties of FKM. But on the other hand the low surface energy and low dielectric constant value limits the application of fluoroelastomer to be used as sensors, actuators, super capacitors, etc. The incorporation of carbon based fillers finds its application in this loop hole. Carbon based fillers especially graphene and its counterparts with increased surface area, improved thermal, mechanical and dielectric properties [3] when incorporated into the polymer matrix will dramatically influence the properties of nanocomposites [4–8].

Graphene is ideally a flat, single layered material with 2D honeycomb lattice. The superior property of graphene is due to the presence of aromatic structure with extended conjugation and the presence of carbon atoms with enhanced chemical stability [9–11]. Reinforcement effect of graphene in the fluoroelastomer matrix can be improved by proper dispersion and with the presence of some interfacial interaction between the filler and the polymer matrix. When graphene in the pristine form is added to the polymer matrix the reinforcement effect cannot be achieved completely because of the agglomerating tendency of graphene in the polymer matrix by the π - π stacking and the van der Waals interaction between the graphene layers. Hence the modification of the graphene filler by covalent or non-covalent functionalization is essential to improve the dispersion and compatibility with the polymer matrix [7,12].

Ionic liquids which are known as 'greener solvents' have some peculiar properties such as polarity, thermal stability, non-volatility and

* Corresponding author at: Centre for Nanoscience and Technology, Department of Basic Sciences, Amal Jyothi College of Engineering, Kanjirappally, Kerala, India. E-mail address: sonygeo@gmail.com (S.C. George).



Novel core-shell dextran hybrid nanosystem for anti-viral drug delivery

K.S. Joshy^a, Anne George^c, S. Snigdha^a, Blessy Joseph^a, Nandakumar Kalarikkal^{a,b},
Laly A. Pothan^d, Sabu Thomas^{a,c,e,*}

^a International and Inter University Centre for Nanoscience and Nanotechnology, Mahatma Gandhi University, Kottayam 686 560, Kerala, India

^b School of Pure and Applied Physics, Mahatma Gandhi University, Kottayam 686 560, Kerala, India

^c Department of Anatomy, Government Medical College, Alappuzha, India

^d Department of Chemistry, Bishop Moore College, Mavelikkara, India

^e School of Chemical Sciences, Mahatma Gandhi University, Kottayam 686 560, Kerala, India



ARTICLE INFO

Keywords:
Nanoparticles
Blood compatibility
Dextran
Drug delivery
Lipid-polymer nanoparticle

ABSTRACT

Zidovudine (AZT) is an antiviral drug extensively used for combating the global pandemic- HIV/AIDS. However, its uses are overshadowed by its short half-life, poor aqueous solubility and inability to cross physiological barriers. This study highlights a nanosystem consisting of dextran and stearic acid for AZT delivery. This hybrid nanoparticle was prepared by double emulsion solvent evaporation method. The morphological analysis of the prepared nanoparticles was carried out by transmission electron microscopy (TEM) and structural analysis through FTIR spectroscopy. Haemolysis, blood cell aggregation and cytotoxicity evaluations were also performed. These biological evaluations indicated that the nanoparticles were compatible and fluorescence microscopy studies demonstrated increased cellular internalization of drug loaded hybrid nanoparticles when compared with free drug molecules. The experimental outcomes indicate that the prepared nanoparticles are highly biocompatible haemocompatible and effective in getting internalized into cells of neural origin. These results highlight the feasibility and efficacy of the hybrid nanoparticles for effective delivery of zidovudine.

1. Introduction

Zidovudine (3'-Azido-3'-deoxythymidine or AZT), was the first approved drug for the treatment of acquired immune deficiency syndrome (AIDS). AZT has also been found to be effective against hepatitis and cancer. Comparatively short *in vivo* half-life (about 1 h) in circulation and dose dependant side effects are the major drawbacks of this drug [1]. Several nanoparticle-based therapeutic formulations have been used for achieving controlled release and improved targeting of drugs [2]. The advent of nano emulsion has drastically improved the pharmacokinetic properties and therapeutic index of numerous drug delivery systems [3]. Lipid-polymer hybrid nanoparticles which incorporate the advantages of both lipid and polymer nanoparticles have proved to be very promising for the delivery of drug with short half-lives.

Recent years have seen the development of various lipid coated nanoparticles [4–7]. The biocompatibility and biodegradability of the drug delivery systems are sources of major concerns. Dextran (Dex), a branched polysaccharide of natural origin consists of 1,6- α -glucopyranosyl linkages. Due to their exceptional biocompatibility they are currently used in many biomedical applications like plasma volume

extenders, lubricants and an interesting candidate in drug delivery. Their inimitable physicochemical properties make them suitable for the synthesis of bioconjugates, nanogels etc. The glucose units of dextran can easily bond with molecules like amines or fatty acids to create self-assembled nanoparticles, moreover it has been shown to reduce plasma protein adsorption [8,9]. The long-chain fatty acid stearic acid (SA), has been already proven as an excellent matrix for the antiviral drug AZT [10]. Poly (ethylene glycol) (PEG) has been in high demand in drug delivery vehicles due to its stability, biocompatibility and biodegradability [11]. In addition, PEG coating on the surface of nanoparticles has been linked to reduced phagocytic uptake of nanoparticles by the immune system. They also extend the circulation time of nanoparticles thereby preventing their accumulation in tissue [12].

To date, there have been only a few studies examining the use of hybrid nanosystems in the loading and delivery of zidovudine. Further, none of this previous work investigated the use of dextran based hybrid nanoparticles for drug delivery. In this study, we used a double emulsion solvent evaporation technique to form a stable core-shell nanoparticle, thus allowing us to combine the advantages of lipid with those of polymer. We designed three different formulations with varying amount of drug to optimize the particle size, drug loading and

* Corresponding author at: Pro-Vice-Chancellor, Mahatma Gandhi University, Kottayam, Kerala 686560, India.

E-mail address: sabuthomas@mgu.ac.in (S. Thomas).



Original research article

Structural, optical and dielectric properties of gadolinium incorporated laser ablated ZnO thin films

R. Vinodkumar^{a,b,*}, Jeena Varghese^a, Jiji Varghese^a, Saji S.K^a, N.V. Unnikrishnan^c^a Department of Physics, University College, Thiruvananthapuram, Kerala, India^b Department of Optoelectronics, University of Kerala, Thiruvananthapuram, Kerala, 695581, India^c School of Pure and Applied Physics, Mahatma Gandhi University, Kottayam, 686560, Kerala, India

ARTICLE INFO

Keywords:

Thermal annealing
 Optoelectronic materials
 Photoluminescence
 Loss factor

ABSTRACT

Gadolinium doped ZnO nanostructured thin films were prepared on quartz substrates by pulsed laser ablation. The effects of thermal annealing at temperatures 400 to 600 °C on the structural, optical and dielectric properties were investigated. The as deposited film is amorphous in nature and all the annealed films show polycrystalline nature with hexagonal wurtzite crystal structure. The AFM images of the doped films show a porous structure for the films. An enhanced transmittance and surface smoothness with increase in annealing temperature were observed. The band gap energy was increasing with decrease in particle size. The porosity and refractive indices of the films were calculated from the transmittance and reflectance spectra. The complex dielectric constant and the loss factor of the ZnO thin films were calculated. From the Photoluminescence spectra all the films show PL emission in the UV and visible region. The O_i type defects are responsible for the enhanced green emission.

1. Introduction

Developments in the fabrication of devices like nanoscale lasers, electrochemically gated quantum doted transistor and the highly efficient exciton UV lasing action under optical pumping from the nanoclusters and thin films indicate that ZnO is a very promising material for applications in modern nanoelectronics and nano photonics. Zinc oxide (ZnO) is an *n*-type semiconductor with a wide band gap of 3.37 eV, high chemical and thermal stability, large mechanical strength and large piezoelectric coefficients [1–6]. The most important advantage of ZnO is its large exciton binding energy of about 60 meV even at room temperature, which makes it a suitable material for to realize room temperature excitonic devices. Zinc oxide thin films are one of the most promising transparent conducting oxides for window layer in heterojunction solar cells, heat mirrors, piezoelectric devices, multilayer photo-thermal conversion systems and solid state gas sensors etc. [6]. A lot of studies have focused on changing various techniques, parameters and the dopant concentrations to improve the performance of ZnO [7–16]. However, only a few studies on the effects of doping and thermal annealing on the micro structural and optical properties of gadolinium (Gd) doped ZnO nanostructured films have been reported. It is generally considered that the ionic radii of dopants for transparent and conductive ZnO films should be small and close to that of Zn²⁺. But the doping effect of a material having a big ionic radius like Gd has not much investigated. Gd has been shown to be a UV light emitter if implanted in to a SiO₂ matrix. Gd has certain and useful physical properties in optical applications [17].

In this work, we report the preparation of laser ablated gadolinium doped ZnO nanostructured films on quartz substrate. We also studied the effect of annealing on its structural and optical properties. The dielectric properties of the material were calculated from

* Corresponding author at: Department of Physics, University College, Thiruvananthapuram, Kerala, India.

E-mail address: vinodkopto@gmail.com (V. R.).



Nonlinear optical single crystal of L-Cystine hydrochloride: Insights into the crystalline perfection, thermal, mechanical and optical properties for device fabrication

Mahak Vij^{a,b}, Sonia^{a,b}, Hemant Kumar Verma^{a,b}, M.S. Jayalakshmy^c, Budhendra Singh^d, Sunil Verma^e, K.K. Maurya^{a,b,*}

^a Academy of Scientific and Innovative Research, CSIR-National Physical Laboratory, New Delhi 110 012, India

^b CSIR-National Physical Laboratory, Dr. K.S. Krishnan Road, New Delhi 110 012, India

^c International and Interuniversity Centre for Nanoscience and Nanotechnology, Mahatma Gandhi University Kottayam, Kerala 686 560, India

^d TEMA-NIRD, Mechanical Engineering Department and Aviro Institute of Nanotechnology (AIN), University of Aveiro, 3810-193 Aveiro, Portugal

^e Laser Materials Development and Devices Division, Raja Ramanna Centre for Advanced Technology, Indore 452013, India



ARTICLE INFO

Keywords:

Powder X-Ray diffraction
Specific heat
Thermal conductivity
Thermal diffusivity
Nanoindentation

ABSTRACT

Now days, nonlinear optical materials are subjected to extensive research owing to their versatility towards various photonic applications. In the present article, twin free L-Cystine hydrochloride single crystals were grown using conventional slow evaporation solution technique. The powder X-ray diffraction pattern confirmed that the titled compound belongs to monoclinic crystal system having space group C_2 . Using FWHM of each diffracting peak, the strain present within the lattice was calculated. Through High Resolution XRD, the crystal quality was scrutinized and found that the grown single crystal is free from any type of defects and grain boundaries. For examination of optical homogeneity of the crystal, birefringence studies were conducted which revealed that there is only one fringe in the interferogram suggesting a good optical homogeneity. Further, various thermal transport parameters were calculated using Photopyroelectric technique. Apart from that, its mechanical strength was assessed at nanoscale through Nano indentation technique. Piezoelectric and ferroelectric studies were also carried out on the titled compound.

1. Introduction

Nonlinear optics (NLO) and Material science are the vibrant fields of research producing various technological applications like optical switching, optical computing, optical data storage, and optical bi-stability [1,2]. It is important to understand the synergies between these two fields in order to design viable devices. Since material science enables the study of physical and structural properties of a material, it enhances the scope of practical application in nonlinear optics. There are numerous organic as well as inorganic compounds known for being good candidates in laser applications [3–5]. Inorganic crystals show high stability but exhibit low NLO responses while on the other hand, suitability of organic compounds over inorganic is defined by their large Nonlinear efficiency, ultra-fast response time and most importantly their flexibility towards structure modifications [6,7]. However, the shortcomings of both organic and inorganic crystals are eradicated by semi-organic class of materials. The criteria of high order

nonlinearity and sufficient mechanical and thermal stability is fulfilled by organic and inorganic counterpart respectively. Inorganic salt of amino acids are the suitable example of this class as most of the amino acids crystallize in non-centrosymmetric crystal structure owing to their zwitterionic structure and π -electron delocalization [1]. L-Cystine hydrochloride (LCH) is one such semi-organic nonlinear optical crystal which shows second harmonic generation 1.2 times that of KDP [8]. Although the absence of center of symmetry is the key criteria for a material to show nonlinear optical behavior, its usefulness cannot be ascertained until its physical properties are studied. To ensure material's compatibility for device fabrication, it is equally important to study other properties like mechanical and thermal stability which additionally proves its benefits towards Photonic crystal devices [7]. In this view, work presented in this paper aims at determining the properties like Optical homogeneity, polarizability, piezoelectric, crystalline perfection, mechanical strength, thermal and ferroelectric behavior of LCH.

* Corresponding author. Indian Reference Material, CSIR-National Physical Laboratory, Dr. K.S. Krishnan Road, New Delhi 110012, India.
E-mail address: kkmaurya@nplindia.org (K.K. Maurya).



Recent developments in nanocellulose-based biodegradable polymers, thermoplastic polymers, and porous nanocomposites

H. Kargarzadeh^{a,*}, J. Huang^{b,c}, N. Lin^b, I. Ahmad^{d,e}, M. Mariano^{e,f}, A. Dufresne^e, S. Thomas^{g,h}, Andrzej Gałęski^a

^a Center of Molecular and Macromolecular Studies, Polish Academy of Sciences, Sienkiewicza 112, 90-363 Łódź, Poland

^b School of Chemistry, Chemical Engineering and Life Sciences, Wuhan University of Technology, Wuhan 430070, China

^c School of Chemistry and Chemical Engineering, Southwest University, Chongqing 400715, China

^d Polymer Research Center (PORCE), Faculty of Science and Technology, School of Chemical Sciences and Food Technology, Universiti Kebangsaan Malaysia (UKM), 43600 Bangi, Selangor, Malaysia

^e Univ. Grenoble Alpes, CNRS, Grenoble INP, LGP2, F-38000 Grenoble, France

^f Brazilian Nanotechnology National Laboratory (LNANO), CNPq, 13083-970 Campinas, Brazil

^g School of Chemical Science, Mahatma Gandhi University, Kottayam, Kerala 686 560, India

^h International and Inter University Centre for Nano Science & Nanotechnology, Mahatma Gandhi University, Kottayam, Kerala 686 560, India

ARTICLE INFO

Article history:

Received 14 November 2017

Received in revised form 23 July 2018

Accepted 27 July 2018

Available online 2 August 2018

Keywords:

Cellulose nanocrystals

Cellulose nanofibrils

Nanocomposites

Biodegradable polymers

Thermoplastic

Porous

ABSTRACT

Nanocellulose has generated a great deal of interest as a source of nanometer-sized reinforcement, because of its good mechanical properties. In the last few years, nanocellulose has also attracted much attention due to environmental concerns. This review presents an overview of recent developments in this area, including the production, characterization, properties, and range of applications of nanocellulose-based biodegradable polymers, thermoplastic polymers, and porous nanocomposites. After explaining the unique properties of nanocellulose and its various preparation techniques, an orderly introduction of various nanocellulose-reinforced biodegradable polymers such as starch, proteins, alginate, chitosan, and gelatin is provided. Subsequently, the effects of nanocellulose on the properties of thermoplastic polymers such as polyamides, polysulfone, polypropyrol, and polyacrylonitrile are reported. The paper concludes with a presentation of new finding and cutting-edge studies on nanocellulose foam and aerogel composites. Three different types of aerogels, i.e., pristine nanocellulose-based aerogels, modified nanocellulose-based aerogels, and nanocellulose-based templates for aerogels, are discussed, as well as their preparation techniques and properties. In the case of foam composites, the research focus has been on two major preparation techniques, i.e., solvent-mixing/foaming and melt-mixing foaming, their respective challenges, and the properties of the final composites. In some cases, a comparison study between cellulose nanocrystals and cellulose nanofiber-reinforced biodegradable polymers, thermoplastics, and porous nanocomposites was carried out. Considering the vast amount of research on nanocellulose-based composites, special emphasis on such composites is provided at the end of the review.

© 2018 Elsevier B.V. All rights reserved.

Abbreviations: ABS, acrylonitrile butadiene styrene; AFM, atomic force microscopy; AP, amylopectin; AS, anisic starch; BC, bacterial cellulose; BSA, bovine serum albumin; C₁₈H₁₇NCO, n-octadecyl isocyanate; CEMD/C, contrast-enhanced microscopy digital image correlation; CNC, cellulose nanocrystal; CNCSFD, spray-freeze-dried CNC; CNF, cellulose nanofibrils; CS, cationic starch; CTE, coefficient of thermal expansion; DMTA, dynamic mechanical thermal analysis; DSC, differential scanning calorimetry; EDC, 1-ethyl-3-(3-dimethylaminopropyl) carbodiimide; EVOH, ethylene vinyl alcohol; L/D, aspect ratio; LbL, layer-by-layer; LCNs, lignin-coated CNFs; LDPE, low-density polyethylene; MA, maleic anhydride; MA/PP, maleic anhydride-grafted PP; MCC, microcrystalline cellulose; NMP, N-methylpyrrolidone; NR, natural rubber; OCNs, oxidized cellulose nanocrystals; OCNFs, oxidized cellulose nanofibrils; OMMT, organophilic montmorillonite; PA, polyamides; PAN, polyacrylonitrile; PBS, poly(butylene succinate); PC, polycarbonate; PCL, polycaprolactone; PDLA, poly(D-lactide); PE, polyethylene; PEG, poly(ethylene glycol); PEO, poly(ethylene oxide); PES, poly(ethersulfone); PFA, poly(furfuryl alcohol); PHA, poly(hydroxy alkanate); PHB, poly(hydroxy butyrate); PLA, poly(lactid acid); PLLA, poly(L-lactide); PMMA, poly(methyl methacrylate); PP, polypropylene; PPy, polypyrrole; PR, phenolic resin; PS, polystyrene; PSfs, polysulfones; PU, polyurethane; PVA, poly(vinyl alcohol); PVAc, poly(vinyl acetate); PVC, poly(vinyl chloride); PWF, pure water flux; SB, star burst; SEM, scanning electron microscopy; SF, silk fibroin; SIPN, semi-interpenetrating polymer network; SNPs, silica nanoparticles; SP, soy protein; T_d, decomposition temperature; TEM, transmission electron microscopy; TEMPO, (2,2,6,6-Tetramethylpiperidin-1-yl)oxy; T_g, transition temperature; TGA, thermogravimetric analysis; T_m, maximum melting temperature; T_m, melting point temperature; TOBC, TEMPO ultrathin BC; WPU, waterborne polyurethane; WVTR, water vapor transmission rate.

* Corresponding authors.

E-mail addresses: hani.h.kargarzadeh@gmail.com (H. Kargarzadeh), gaaling@ukm.edu.my (I. Ahmad).

Space Based Spatio-Temporal Assessment of Land Surface Temperature in Karunagappally Municipality, a Fast Growing City in the Western Coast of India

Sumith Satheendran S.^{1,2,*}, Smitha Chandran S.¹, Abin Varghese²

¹Department of Chemistry, Amrita Viswa Vidyapeetham, Amritapuri Campus, Kerala, India - smithachandran@am.amrita.edu

²Dr. R. Satheesh Centre for Remote Sensing and GIS, Mahatma Gandhi University, Kerala, India -remotesumithsat@gmail.com

Commission V, SS: Infrastructure and Development Planning

Keywords: Landsat, Thermal Band, Brightness Temperature, Karunagappally, Land Surface Temperature, Spatio-Temporal

Abstract

Urbanization is the process by which towns and cities are formed and become larger as more and more people begin living and working in central areas. According to 2001 census, the urban population of the country was 286.11 million, living in 5161 towns, which constitutes 27.81% of the total country's population. However, the same as per 2011 census has risen to 377.16 million viz. 32.16% of the total country's population and the number of towns has gone up to 7935. The rate of urban growth in the country is very high as compared to developed countries, and the large cities are becoming larger mostly due to continuous migration of population to these cities. India's current urban population exceeds the whole population of the United States, the world's third largest country. By 2050, over half of India's population is expected to be urban dwellers. This creates enormous pressure on existing urban infrastructure.

Urbanization trend in the State of Kerala shows marked peculiarities. The main reason for urban population growth is the increase in the number of urban areas and urbanization of the peripheral areas of the existing major urban centers. However, unlike the other parts of the country the Urbanization in Kerala is not limited to the designated cities and towns. The difference between rural and urban agglomerations is very negligible as far as Kerala is concerned. The Kerala society by and large can be termed as urbanized. Kerala has been witnessing rapid urbanization since 1980.

The present study, is an attempt to analyses the extent of land use/ land cover changes in the Municipality over the years from 2012 to 2017 and land surface variation over the years from 2000 to 2017. The land use/ land cover pattern of 2012 to 2017 was extracted from High resolution images of the study area were downloaded from Google Earth API and the Land Surface Temperature changes were analyzed from the thermal bands of the Landsat Imageries.

1. INTRODUCTION

1.1 The present study area

Karunagappally is a city in Kollam district of the Indian State of Kerala. The place has beautiful backwaters, which connects it to Kollam and Alappuzha. Padanayarkulangara, which forms part of the town, was once the military station of the Kayamkulam Rajas. An idol of Buddha, recovered from a local tank here, has raised speculations that Karunagappally was once a center of Buddhist teachings. The city is well connected by rail and road with other cities in the region. It has a thriving economy and boasts of well-developed commercial establishments and public infrastructure. Karunagappally is well known for its coir, fishing and tourism industries. It is an important township located on the backwaters of Kerala. The climate is tropical wet, with heavy rain in the monsoon season (May – August and October – November).

The geographical coordinates for Karunagappally extent from 9°3'11" to N latitudes and 76°32'4" to E longitudes (Figure 1). Karunagappally taluk covers an area of 66.34 km². The taluk is bound on the north by Kayamkulam, east by Kunnathur taluk, south by Kollam and on the west by the Arabian Sea.

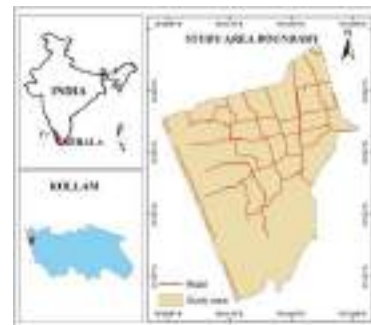


Figure 1 Study area

1.2 Studies on land use land cover changes

Land cover (LC) is defined as the features that are present on the earth's surface. Land use refers to the human induced changes for agricultural, industrial, residential or recreational purposes (Ramachandra and Bharath, 2012). Land cover changes refer to conversion and modification of vegetation, changes in biodiversity, soil quality, runoff, erosion, sedimentation and land productivity (Xiubin, 1996). Land use has been changing ever since humans first began to manage their environment. However, the changes that have taken place over the last 50 years have been especially important and intense as society is becoming increasingly urbanized, while natural ecosystems become deteriorated (Martinez et al., 2009). LULC changes are

* Corresponding author

In Situ Synthesis of Silver Nanospheres, Nanocubes, and Nanowires over Boron-Doped Graphene Sheets for Surface-Enhanced Raman Scattering Application and Enzyme-Free Detection of Hydrogen Peroxide

Anju K. Nair,^{†,‡} Kala Moolepparambil Sukumaran Nair,[‡] Sabu Thomas,^{†,§} Didier Rouxel,^{||} Subbiah Alwarappan,^{*,†,⊥} and Nandakumar Kalarikkal^{*,†,#}

[†]International and Inter University Centre for Nanoscience and Nanotechnology, Mahatma Gandhi University, Kottayam-686 560, Kerala, India

[‡]Department of Physics, St Teresas's College Ernakulam-682011, Kerala, India

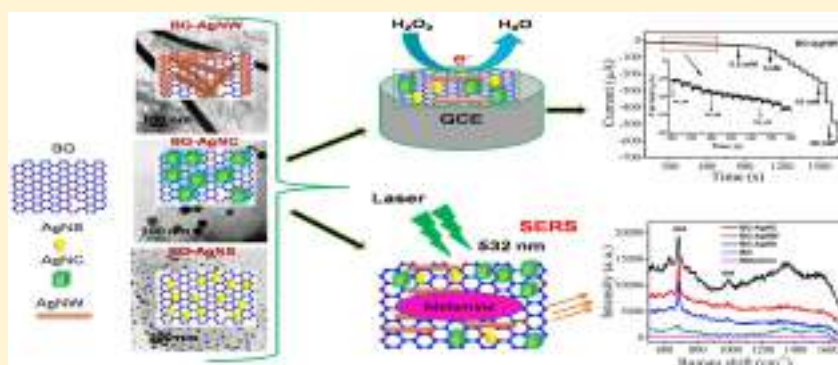
[§]School of Chemical Sciences, Mahatma Gandhi University, Kottayam-686 560, Kerala, India

^{||}UMR CNRS 7198, Faculté des Sciences et Techniques, Institut Jean Lamour, Campus Victor Grignard, BP 70239, 54506, Vandoeuvre-les-Nancy Cedex, France

[⊥]CSIR – Central Electrochemical Research Institute (CSIR-CECRI) Karaikudi-630 003, Tamil Nadu, India

[#]School of Pure and Applied Physics, Mahatma Gandhi University, Kottayam-686 560, Kerala India

Supporting Information



ABSTRACT: An effective *in situ* synthesis strategy is demonstrated for the preparation of silver nanostructures (nanospheres (NSs), nanocubes (NCs), and nanowires (NWs)) on the surface of boron-doped graphene (BG). Further, these functional nanomaterials are employed for the surface-enhanced Raman scattering (SERS) and non-enzymatic electrochemical detection of H_2O_2 . The results confirm the superior performance of BG-Ag nanostructures as SERS platform. Among various geometries of silver nanoparticles studied in this work, we find that the AgNCs over BG (BG-AgNC) present outstanding SERS performance for detecting 4-mercaptobenzoic acid, with a limit of detection of 1.0×10^{-13} M. Furthermore, BG-AgNC exhibits excellent capability to detect melamine as low as 1.0×10^{-9} M. Electrochemical results confirm that the BG-AgNW-based platform exhibits a superior biosensing performance toward H_2O_2 detection. The enhanced performance is due to the presence of graphene, which improves the conductivity and provides more active sites. The synthesis of doped graphene with metallic nanoparticles described in this work is expected to be a key strategy for the development of an efficient SERS and electrochemical sensor that offers simplicity, cost-effectiveness, long-term stability, and better reproducibility.

1. INTRODUCTION

Plasmonic nanostructures have received significant interest from scientists and industry for diverse applications due to their unique optical and chemical properties, such as energy conversion, surface-enhanced Raman scattering (SERS), catalysis, and biological and electrochemical sensing.^{1–4} All the above-mentioned properties and applications rely strongly on the surface morphology, size, edge composition, and crystal

structure of the metallic nanoparticles (NPs). Among various metallic NPs, silver nanoparticles (AgNPs) with well-defined shapes have practical applications in various fields due to their high plasmonic efficiency, biocompatibility, excellent con-

Received: June 14, 2018

Revised: September 30, 2018

Published: October 16, 2018



Development of Thick Superhydrophilic $\text{TiO}_2\text{-ZrO}_2$ Transparent Coatings Realized through the Inclusion of Poly(methyl methacrylate) and Pluronic-F127

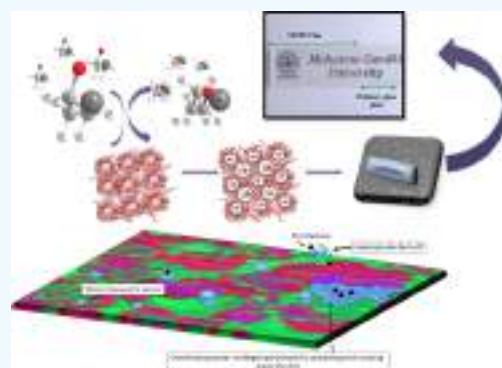
Sanu M. Simon,[†] Anoop Chandran,[‡] Gejo George,[†] M. S. Sajna,[†] Prakashan Valparambil,[†] Eric Kumi-Barmiah,[§] Gin Jose,[§] P. R. Biju,[†] Cyriac Joseph,[†] and N. V. Unnikrishnan^{*,†}

[†]School of Pure & Applied Physics, Mahatma Gandhi University, Kottayam 686 560, Kerala, India

[‡]Department of Physics, St. Cyril's College, Adoor 691 529, Kerala, India

[§]School of Chemical and Process Engineering, University of Leeds, Leeds LS2 9JT, U.K.

ABSTRACT: A thick coating of hierarchically porous double-templated $\text{TiO}_2\text{-ZrO}_2\text{-PMMA-PF127}$ with excellent self-cleaning properties and high transmittance has been developed for the first time on glass substrates using a simple dip-coating technique. Comparative studies of this sample with a thick and transparent coating of single-templated $\text{TiO}_2\text{-ZrO}_2\text{-PMMA}$ have been performed to probe the origin of its exceptional properties. The formation of the composites, successful incorporation of the polymer into the matrix, and the porous nature of the films have been studied. The presence of Ti^{2+} in the double-templated samples has been confirmed, which suggest the chemisorption of water on the surface of the film. The variation in the self-cleaning properties of the samples on UV-illumination has also been studied. The double-templated film is found to possess the capability of good hydrophilic retention even 2 days after UV-irradiation.



INTRODUCTION

It has been reported that hydrophilic coatings of inorganic metal oxides with large surface area and high porosity clean the surface quickly.¹ Addition of polymers to inorganic binary metal oxide composites, on the other hand, is known to facilitate the spreading nature of liquid, and the surface roughness can trap the water molecules.² Theoretical works of Wenzel and Cassie–Baxter suggest that maximal increase in wetting property of the surface can be achieved by the enhancement of its roughness.^{3–5} Also, there are many recent reports on hydrophilicity achieved through nanoporous structure formation on the film surface.^{2,6} Therefore, multi-functional polymer-incorporated inorganic composites in the form of meso/micro/macroporous films, membranes, and powders are of great significance as they have potential applications as self-cleaning glasses for solar cells, gas-sensing devices, photovoltaic devices, and window glass for green intelligent buildings.^{7–11}

TiO_2 as a self-cleaning coating has high transmittance and has the advantage to make use of both solar energy and rainfall to clean the surface, which reduces the cost of maintenance.¹² For further improving the transmittance, hydrophilicity, and mechanical and thermal stabilities, the general approach is to synthesize binary composites involving TiO_2 and a low refractive index material such as ZrO_2 , SiO_2 , and so forth.¹³ The excess amount of hydroxyl groups present in $\text{TiO}_2\text{-ZrO}_2/\text{TiO}_2\text{-SiO}_2$ hybrid composites trap photoinduced holes, which

increase the photocatalytic activity by delaying the recombination of electron–hole pairs.¹⁴ This implies that such a coating would be able to breakdown the dirt absorbed onto its surface in the presence of sunlight.¹⁵

The hydroxyl group-trapping ability of $\text{TiO}_2\text{-ZrO}_2/\text{SiO}_2$ along with high porosity of polymer-incorporated composites can be combined together in $\text{TiO}_2\text{-ZrO}_2/\text{SiO}_2\text{-polymer}$ coatings. Although there are a few reports on the hydrophilic nature of such coatings, some major disadvantages of such films remain unaddressed.^{16,17} The development of such coatings is of extreme significance, and efforts are underway to realize them. In most of the literature, which reports the formation of superhydrophilic transparent coatings, the thickness of the coating is on the nanoscale.^{12,14,17} Nevertheless, the large-scale production of such thin self-cleaning glasses is really expensive because of the sophisticated techniques involved. In this work, single-templated and double-templated porous, thick, yet transparent films of $\text{TiO}_2\text{-ZrO}_2\text{-pluronic F127}$ (PF127), and/or poly(methyl methacrylate) (PMMA) have been prepared via the sol-gel dip-coating method. The prepared samples are found to exhibit excellent self-cleaning properties, which can be substantially retained for hours. Such coatings have significant scientific and

Received: August 8, 2018

Accepted: October 19, 2018

Published: November 6, 2018



Effect of inorganic ions on the ultrasound initiated degradation and product formation of triphenylmethane dyes



Manoj P. Rayaroth^a, Usha K. Aravind^b, Charuvila T. Aravindakumar^{a,c,*}

^a School of Environmental Sciences, Mahatma Gandhi University, Kottayam, Kerala, India

^b Advanced Centre of Environmental Studies and Sustainable Development, Mahatma Gandhi University, Kottayam, Kerala, India

^c Inter University Instrumentation Centre, Mahatma Gandhi University, Kottayam, Kerala, India

ARTICLE INFO

Keywords:

Advanced oxidation processes

Sonolysis

Triphenylmethane dyes

Inorganic ions

End product analyses

LC-Q-TOF-MS

Carbonate radical

ABSTRACT

Triphenylmethane (TPM) dyes are an important category of dyes with a variety of industrial applications and consequently, these are found in the aquatic environment at relatively higher concentrations. Here, we report the degradation of two important TPM dyes (para rosaniline (PRA) and ethyl violet (EV)) in an aqueous medium by ultrasound which is one among the Advanced Oxidation Processes (AOPs). The main objective of this work is to study the effect of various inorganic ions on the degradation and the product formation of TPM dyes from the sonochemical reactions. Using a typical concentration of 10 ppm dyes and an ultrasonic frequency of 350 kHz and power of 60 W, a complete degradation of EV and PRA was observed with a pseudo first order rate constant of 0.2339 min^{-1} and 0.1956 min^{-1} , respectively. The product analyses using high-resolution mass spectrometry (LC-Q-TOF-MS) revealed the formation of hydroxylated, de-alkylated, and other collapsed conjugated structure destructed products. The evolution of these products in the presence of various inorganic ions (Cl^- , SO_4^{2-} , NO_3^- , and CO_3^{2-}) showed that only carbonate ions had a significant impact on the product evolution. The carbonate ions facilitated the formation of conjugated structure destructed product for both the dyes. This is attributed to the reactivity of carbonate radical, which facilitated the formation of carbon-centered radicals. This carbon-centered radical further undergoes reaction to cause the destruction of conjugated structures. This is confirmed by the identification of the corresponding product peaks in the mass spectra. The scavenging effect of carbonate ions was also reflected in the product study where there is a reduction in the formation of most of the hydroxylated products. One of the major inorganic species in any wastewater is carbonate ions and therefore the present result is very relevant to the understanding of oxidation based treatment protocol.

1. Introduction

The contribution of dye waste to water pollution has been on the rise due to their wide production (over 7×10^5 tons per year) and applications in textile, leather, jute, and food industries [1]. The important properties of the effluents from these industries are its intense color, high COD, and BOD values and its acidity. The effluent stream contains many heavy metals and other organic chemicals such as pesticides, various surfactants, and biocides [2] and therefore these effluents are reported to cause the notorious effect to the aquatic environment even though LD_{50} values of dyes are more than $2 \times 10^3 \text{ mg/kg}$ [3–6]. Since many inorganic ions like carbonates, chloride, nitrate, and sulfate are employed at some stages of dyeing processes, the dye house effluent is composed of these ions as well [7]. Triphenylmethane (TPM) dyes are an important class of intensely colored synthetic

organic dyes with various biological and histopathological applications along with other industrial applications [8,9]. The important structural feature of this type of dyes is that it shares three benzene rings with the formula $(\text{C}_6\text{H}_5)_3\text{CH}$ in common and are the precursor of many synthetic dyes such as triarylmethane dyes. The members of this family are basic green 4 (BG), bromocresol green, methyl violet, crystal violet, Victoria blue, brilliant green, ethyl violet, brilliant blue, pararosaniline, cresol red, bromophenol blue, methyl green and basic fuchsin [10–12].

There are many conventional techniques such as adsorption, flocculation, and coagulation, for the elimination of such chemicals from aqueous medium [13]. These methods are reported to be effective for the removal of color but fail in their complete mineralization. Moreover, the advanced oxidation processes (AOPs) have several advantages over the conventional techniques [13]. The degradation of some of the TPM dyes was reported using various AOPs like UV photolysis [14],

* Corresponding author at: School of Environmental Sciences, Mahatma Gandhi University, Kottayam 686560, Kerala, India.

E-mail address: cto@mgu.ac.in (C.T. Aravindakumar).

<https://doi.org/10.1016/j.ultsonch.2018.07.009>

Received 29 March 2018; Received in revised form 19 June 2018; Accepted 4 July 2018

Available online 05 July 2018

1350-4177/© 2018 Elsevier B.V. All rights reserved.

PAPER

Analysis of graphene films grown on copper foil at 845 °C by intermediate pressure chemical vapor deposition

Savitha Nalini¹, Subin Thomas², M K Jayaraj³ and K Rajeev Kumar¹

Published 12 September 2018 • © 2018 IOP Publishing Ltd

[Materials Research Express](#), Volume 5, Number 11

nsavitha01@gmail.com

¹ Department of Instrumentation, Cochin University of Science and Technology, Cochin, India

² School of Pure and Applied Physics, Mahatma Gandhi University, Kottayam, India

³ Department of Physics, Cochin University of Science and Technology, Cochin, India

Savitha Nalini  <https://orcid.org/0000-0002-6150-3942>

Received 7 July 2018

Accepted 4 September 2018

Accepted Manuscript online 4 September 2018

Published 12 September 2018



Original Research

Electrospun polyvinyl alcohol membranes incorporated with green synthesized silver nanoparticles for wound dressing applications

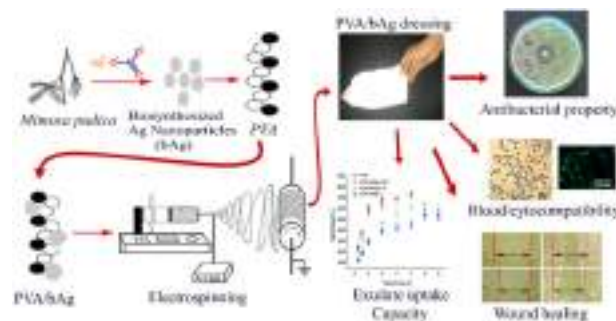
Robin Augustine^{1,2} · Anwarul Hasan^{1,2} · V. K Yadu Nath³ · Jince Thomas³ · Anitha Augustine⁴ · Nandakumar Kalarikkal^{3,5} · Ala-Eddin Al Moustafa^{2,6} · Sabu Thomas^{3,7}

Received: 9 March 2018 / Accepted: 12 October 2018
© Springer Science+Business Media, LLC, part of Springer Nature 2018

Abstract

Electrospun membranes have the potential to act as an effective barrier for wounds from the external environment to prevent pathogens. In addition, materials with good antibacterial properties can effectively fight off the invading pathogens. In this paper, we report the development of a novel electrospun polyvinyl alcohol (PVA) membrane containing biosynthesized silver nanoparticle (bAg) for wound dressing applications. Plant extract from a medicinal plant *Mimosa pudica* was utilized for the synthesis of bAg. Synthesized bAg were characterized by Ultraviolet-Visible (UV) Spectroscopy and Fourier Transform Infrared Spectroscopy (FTIR). The morphology of bAg was obtained from Transmission Electron Microscopy (TEM) and found that they were spherical in morphology with average particle size 7.63 ± 1.2 nm. bAg nanoparticles incorporated PVA membranes were characterized using several physicochemical techniques such as Scanning Electron Microscopy (SEM), Energy Dispersive X-Ray Spectroscopy (EDS) and X-Ray Diffraction (XRD) analysis. Experimental results confirmed the successful incorporation of bAg in PVA fibers. PVA nanofiber membranes incorporated with bAg showed good mechanical strength, excellent exudate uptake capacity, antibacterial activity, blood compatibility and cytocompatibility.

Graphical Abstract



✉ Robin Augustine
robin@robinlab.in
robin.augustine@qu.edu.qa

✉ Anwarul Hasan
ahasan@qu.edu.qa

¹ Department of Mechanical and Industrial Engineering, College of Engineering, Qatar University, Doha 2713, Qatar

² Biomedical Research Centre, Qatar University, Doha 2713, Qatar

³ International and Inter University Centre for Nanoscience and

Nanotechnology, Mahatma Gandhi University, Kottayam, Kerala 686 560, India

⁴ Department of Chemistry, Bishop Kurialacherry College for Women, Amalagiri, Kottayam, Kerala 686561, India

⁵ School of Pure and Applied Physics, Mahatma Gandhi University, Kottayam, Kerala 686 560, India

⁶ College of Medicine, Qatar University, Doha 2713, Qatar

⁷ School of Chemical Sciences, Mahatma Gandhi University, Kottayam, Kerala 686 560, India

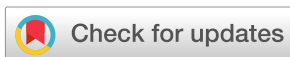
Issue 10, 2018

[Previous](#)[Next](#)

From the journal:

Environmental Science: Water Research & Technology

Green synthesized unmodified silver nanoparticles as a multi-sensor for Cr(III) ions

[Archana Aravind](#)^a, [Maria Sebastian](#)^a and [Beena Mathew](#) ^{*a}

Author affiliations

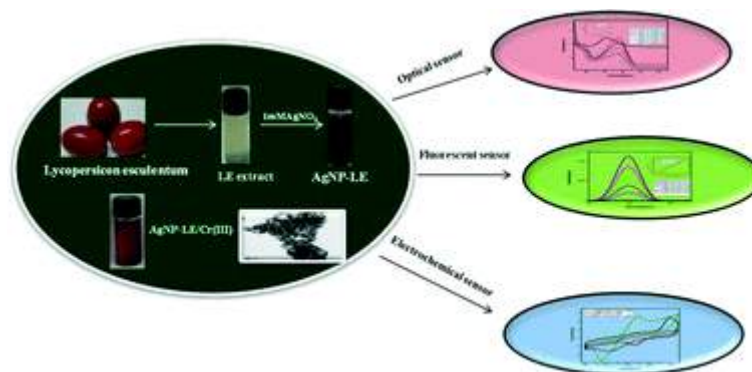
* Corresponding authors

^a School of Chemical Sciences, Mahatma Gandhi University, Kottayam, Kerala 686560, India

E-mail: beenamscs@gmail.com

Abstract

In this work we present optical, fluorescence and electrochemical sensing of Cr(III) ions using silver nanoparticles (AgNPs) synthesized by a green method using *Lycopersicon esculentum* (LE) extract without any surface functionalization. The synthesized AgNP-LE was analyzed by various techniques such as UV-visible absorption spectroscopy, infrared spectroscopy, X-ray diffraction and transmission electron microscopy. The principle behind the sensing involves the dispersion of nanoparticles followed by the aggregation of Cr(III) ions leading to a redshift of the surface plasmon resonance (SPR) peak in the UV-vis absorption spectra. The fluorescence sensing of Cr(III) ions using AgNP-LE was also studied by the changes in the fluorescence intensity. The electrochemical studies were carried out using a AgNP-LE modified platinum electrode. The linear calibration range was focused over the range of 10 to 90 μM and the limit of detection was found to be 0.804 μM using differential pulse voltammetry. This simple and sensitive method has a high selectivity towards Cr(III) ions over other metal ions. The modified sensor was also studied over real samples to determine the presence of Cr(III) ions. The synthesized AgNP-LE also exhibited antibacterial properties against waterborne pathogens like *Escherichia coli* and *Staphylococcus aureus* extracted from the water sample collected from the Ashtamudi lake, Kollam, Kerala.

[About](#)[Cited by](#)[Related](#)

Buy this article

£42.50*

* Exclusive of taxes

This article contains 12 page(s)

Other ways to access this content

Log in

Using your institution credentials

Sign in

With your membership or subscriber account

Publication details

The article was received on 06 Jun 2018, accepted on 06 Jul 2018 and first published on 10 Jul 2018



Protective effect of *Rotula aquatica* Lour against gentamicin induced oxidative stress and nephrotoxicity in Wistar rats

A. Vysakh, S. Abhilash, Kuriakose Jayesh, Sebastian Jose Midhun, Mathew Jyothis, M.S. Latha*

School of Biosciences, Mahatma Gandhi University, Priyadarshini Hills, Kottayam, Kerala, India



ARTICLE INFO

Keywords:
Gentamicin
Nephrotoxicity
Oxidative stress
Rotula aquatica

ABSTRACT

Gentamicin is an aminoglycoside antibiotic widely used for the treatment of life-threatening infections caused by Gram-negative bacteria. The use of gentamicin was limited due to its ototoxic and nephrotoxic adverse effects. The current study was designed to evaluate the protective effect of ethyl acetate fraction from *Rotula aquatica* (EFRA) against gentamicin induced nephrotoxicity. The antioxidant enzymes status, lipid peroxidation, nitrate and ROS level, serum markers like creatinine, Urea, BUN were estimated in the present study. The histopathological analysis of renal tissues was done by H&E and PAS staining. The mRNA level expression of KIM-1, NF- κ B, TNF- α , and IL-6 were measured by semi-quantitative reverse transcription-polymerase chain reaction. The changes in antioxidant parameters were restored by the treatment of EFRA at different dose (50 mg/kg bwt, 100 mg/kg bwt). The serum parameters, ROS, MDA and nitrate level were decreased by administration of EFRA. The EFRA ameliorates histological changes associated with gentamicin induced nephrotoxicity. The mRNA level expression of KIM-1, NF- κ B, TNF- α , and IL-6 were downregulated in EFRA treated groups. The results from present study reveals the role of EFRA as good anti-inflammatory and nephro protective drug.

1. Introduction

The aminoglycoside antibiotic gentamicin (GM) is broadly used in medical treatment for the management of acute Gram-negative bacterial diseases [1]. The main drawback in the consumption of aminoglycoside antibiotics is their potent nephrotoxicity [2]. It has been stated that around 30% of patients administered with GM results in renal impairment [3]. Although the exact mechanism involved in GM-induced nephro toxicity is not elucidated completely. Oxidative stress is considered as one of the key factor which plays a central role in pathophysiology of GM-induced nephrotoxicity. Oxidative stress is responsible for the development of toxic free radicals, increased cellular lipid peroxidation, insufficiency in cellular antioxidants and finally cellular necrosis in renal tubules [4,5]. The accumulation of GM in renal proximal convoluted tubules was responsible for its nephrotoxicity and leads to network damage in brush border cells, reduction in glomerular filtration rate, acute tubular necrosis etc [6]. In addition to tubular injury, histopathological evidences like cellular apoptosis, glomerular mesangial cells, proliferation and necrosis were also contributing to disease severity [7].

Nephrotoxicity induced by gentamicin is a complex condition characterized by an increase in serum urea and creatinine concentration with tubular necrosis [8]. During kidney injury, one of the major

injury marker molecule like kidney injury molecule-1 (KIM-1) is expressed in the tubules to support the removal of necrotic and apoptotic debris. The gene level expression of KIM-1 is very low in normal kidneys, but after ischemic injury, upregulation of the protein is increased in proximal tubules [9].

The nuclear factor kappa B (NF- κ B) is a key transcription factor, activated by a wide range of chemical and biological stimuli including ROS [10]. The oxidative stress generated during the GM induced nephrotoxicity stimulates the transcription factor NF- κ B. Upon stimulation, NF- κ B dissociates from the complex (NF- κ B-I κ B), translocates into the nucleus and subsequently enhances the transcriptional activation of target genes [10,11] including IL-6, iNOS, TNF- α , COX-2, which enhance the kidney damage [11]. Thus, a capable therapeutic approach may be essential to control or protect renal damage against antibiotics adverse effects, and GM-induced nephrotoxicity is an outstanding animal model for studying pathogenesis and therapeutic approach development [12].

Rotula aquatica Lour is a member of the family Boraginaceae which is represented by about one hundred genera and two thousand species around the world. The plant is distributed throughout Peninsular and Western Ghats of India in the sandy and rocky beds of streams and rivers and are occasionally submerged in floods [13]. It is widely used as an important traditional medicine for kidney and bladder stones.

* Corresponding author.

E-mail address: mslathasbs@gmail.com (M.S. Latha).



Plasma Modified and Unmodified Polyethylene as Filler in Natural Rubber Compounds: Morphology, Cure Behavior, and Vulcanization Kinetics

Sari P. Sasidharan,* Petr Spatenka, Evgeny Anisimov, and Sabu Thomas

The present paper investigates the influence of polyethylene (PE) and plasma modified polyethylene (PPE) as fillers in natural rubber (NR) compound. The NR/PE and NR/PPE compounds were prepared through mechanical mixing using two roll mill by varying their compositions. The morphology of the compounds was analyzed in detail using field emission scanning electron microscopy (FESEM) to understand the dispersion of PE and PPE in the NR matrix as well as its interfacial adhesion. Morphological analysis revealed that unmodified polyethylene was nicely dispersed in the NR matrix whereas plasma modified polyethylene showed agglomerated structure due to the polar functional groups on the PPE surface. The vulcanization kinetics and cure characteristics of natural rubber compounds containing PE and PPE were examined using an oscillating disc rheometer. The cure behavior of the composites were studied at different temperatures (140, 160, and 180 °C) using conventional sulphur vulcanization system. The addition of polyethylene influenced the cure properties to a great extent. Theoretical modeling was done to follow the mechanism of the cure reaction. The cure reaction was kinetically controlled at the beginning followed by the diffusion mechanism. The curing reaction was found to be autocatalytic and extent of reaction increased with increasing temperature.

improves micro-hardness and roughness of the polymer surface due to the bombardment of high energy radicals and ions. This resulted in a number of scientific studies and helped in developing new materials that combine desirable properties.^[1–4] Moreover, plasma treatment can also be used for the recycling of polymers. Several studies have been reported based on plasma treatment with highlighting structural changes of selected polymeric system.^[5–7]

Polyethylene is one of the most widely used hydrocarbon polymers, which has applications in packaging, automotive, household items, medical applications, etc. Polyethylene has some disadvantages like difficult to print or paint, adhesion to metals, and polar polymers due to its non-polar nature. A good number of studies have been done in the area of plasma modification of polyethylene in the last few decades which received much attention from scientists as well as industrialists.^[8,9] Plasma modification improved the polarity of polyethylene which improves its printability,^[10] adhesion to metals,^[11,12] bonding with other polymers,^[13] and biodegradability. The anti-bacterial property and biocompatibility of polyethylene can also be improved by plasma treatment.^[14–17]

Natural rubber (NR) known for its excellent elasticity coupled with extensive availability make it suitable in a wide number of applications. NR has been modified by incorporating various types of fillers such as carbon black, clay, calcium carbonate, metal oxides, CNT, POSS, graphene, etc., and other polymers from the time immemorial.^[18] Kurian et al. investigated the morphology of tensile fractured and fatigue fractured surfaces of natural rubber vulcanizates filled with polyethylene.^[19,20] They found that the size and shape of the thermoplastic domains were varying with the thermoplastic content which enhanced their mechanical interaction with the rubber matrix. Nabil et al. used recycled polyethylene terephthalate for reinforcing natural rubber matrix.^[21]

The curing kinetics and its mechanism are very important in understanding the processing conditions of a material. It is imperative to know the effects on cure behavior of natural rubber when new materials are incorporated into it.^[22–23] Vulcanization of natural rubber has been quite extensively investigated in the

1. Introduction

The surface modification of polymers using plasma has received a lot of attention nowadays. Plasma treatment generates wide range of reactive species in the treated system such as hydroxyl, carbonyl, carboxyl, ether, peroxides, etc., which undeniably depends on the surrounding medium. Plasma modification

S. P. Sasidharan, P. Spatenka, E. Anisimov
Faculty of Mechanical Engineering, Department of Materials
Engineering, Czech Technical University in Prague
Karlovo namesti 13, CZ-12135 Prague, Czech Republic
E-mail: sarips1@gmail.com

S. P. Sasidharan, S. Thomas
International and Inter University Centre for Nanoscience and
Nanotechnology¹, Mahatma Gandhi University
Kottayam 686560 Kerala, India

S. Thomas
School of Chemical Sciences⁴
Mahatma Gandhi University
Kottayam 686560 Kerala, India

DOI: 10.1002/masy.201800135



Effect of MWCNTs on Wetting and Thermal Properties of an Immiscible Polymer Blend

A. R. Ajitha, M. K. Aswathi, Arunima Reghunadhan, Lovley Mathew, Roberto Terzano, and Sabu Thomas*

Poly (trimethylene terephthalate)/Polypropylene blend (PTT/PP) is prepared using melt mixing method and 1 wt% multiwalled carbon nanotubes (MWCNTs) are incorporated to study its effect on the thermal and wetting properties. The droplet morphology reveals the immiscibility of the neat polymers in the blend and there is a reduction in the domain size of the dispersed phase with the addition of MWCNTs due to the compatibilization effect of MWCNTs. With the addition of MWCNTs, there is a slight improvement in the melting temperatures of both PTT and PP while an increase in the crystallization temperature and glass transition temperature (T_g) is observed that may be due to the nucleation effect of MWCNTs. On blending with PP, the thermal stability of PTT matrix is increased and with the addition of MWCNTs there is not much improvement in the thermal stability of the polymer components is observed. With the addition of MWCNTs the contact angle of the blend slightly increased, may be attributed to the hydrophobic nature of MWCNTs.

are several other factors which affect the immiscibility of the polymer blends such as difference in polarity, solubility parameters, viscosity, and interfacial tension between the components. The high interfacial tension between the polymer components will lead to poor interfacial adhesion between them and blends become immiscible in nature and hence shows diminished properties than that of individual polymers.^[3] Even though immiscible polymer blends have combined attributes of single parts, due to the phase separation, poor adhesion, and sharp interface, one cannot practice them for potential applications due to inferior mechanical properties. Designing high performance products from immiscible blends are of large significance in the industrial sector. This can only be attained by the compatibilization process, where a third component (compatibilizer) is introduced so as to enhance the interaction between the blend components.^[3] Compatibilizers can stabilize the blend morphology by reducing the interfacial tension thereby improving the interfacial affinity of the polymer components by acting as surfactant or emulsifying agent. There are different types of compatibilizers with specified interactions such as polypropylene-grafted-maleic anhydride (PP-g-MAH), poly(ethylene-co-glycidyl methacrylate) (PEGMA), polypropylene-grafted-acrylic acid (PP-g-AA), polypropylene methyl polyhedral oligomeric silsesquioxanes (PP-POSS), isocyanate group etc.^[4]

1. Introduction

Polymer blending is an interesting method to produce novel materials for specific applications since it is very cost efficient and uncomplicated. By blending one can originate new material with the combined attributes of each element. Due to the negligible entropy of mixing most of the polymers are immiscible in nature.^[1,2] In addition to the entropy factor there

are several other factors which affect the immiscibility of the polymer blends such as difference in polarity, solubility parameters, viscosity, and interfacial tension between the components. The high interfacial tension between the polymer components will lead to poor interfacial adhesion between them and blends become immiscible in nature and hence shows diminished properties than that of individual polymers.^[3] Even though immiscible polymer blends have combined attributes of single parts, due to the phase separation, poor adhesion, and sharp interface, one cannot practice them for potential applications due to inferior mechanical properties. Designing high performance products from immiscible blends are of large significance in the industrial sector. This can only be attained by the compatibilization process, where a third component (compatibilizer) is introduced so as to enhance the interaction between the blend components.^[3] Compatibilizers can stabilize the blend morphology by reducing the interfacial tension thereby improving the interfacial affinity of the polymer components by acting as surfactant or emulsifying agent. There are different types of compatibilizers with specified interactions such as polypropylene-grafted-maleic anhydride (PP-g-MAH), poly(ethylene-co-glycidyl methacrylate) (PEGMA), polypropylene-grafted-acrylic acid (PP-g-AA), polypropylene methyl polyhedral oligomeric silsesquioxanes (PP-POSS), isocyanate group etc.^[4]

A. R. Ajitha, M. K. Aswathi, A. Reghunadhan, L. Mathew, S. Thomas
International and Inter University
Centre for Nanoscience and Nanotechnology
Mahatma Gandhi University
Kottayam, Kerala 686560, India
E-mail: sabupolymer@yahoo.com

L. Mathew
Viswajyothi College of Engineering and Technology
Muvattupuzha, Kerala 686670, India

R. Terzano
Department of Soil, Plant and Food Sciences
University of Bari "Aldo Moro,"
Via Amendola 165/A, Bari 70126, Italy

S. Thomas
School of Chemical Sciences
Mahatma Gandhi University
Kottayam, Kerala 686560, India

DOI: 10.1002/masy.201800103

Graft or block co-polymers are generally used as compatibilizers since they can reduce the interfacial tension between two or more immiscible polymer components which acts as a stable interface amidst the heterogeneous components of the blends. **Figure 1** shows the schematic representation of the compatibilizing mechanism of a Graft or block co-polymer within an immiscible blend to improve the interfacial adhesion. In **Figure 1**, violet part has more affinity with first polymer and blue part interacts selectively with the second polymer. Reactive compatibilization is yet another technique for the compatibilization in which the block or graft copolymers forms a stable interface by in situ reaction.^[5]

Nowadays, nanofillers have been studied for the role as effective compatibilizers due to their multi functional nature as nucleating agents, reinforcing agents, etc. For the blends with high processing temperature, unmodified solid nanoparticles



Selective Localization of MWCNT in Poly (Trimethylene Terephthalate)/Poly Ethylene Blends: Theoretical Analysis, Morphology, and Mechanical Properties

Aswathi M. Kunjappan, Ajitha A. Ramachandran, Moothetty Padmanabhan, Lovely P. Mathew, and Sabu Thomas*

Theoretical analysis is carried out to predict the nature of selective localization of multi-walled carbon nanotubes (MWCNTs) in poly-(trimethylene terephthalate/polyethylene (PTT/PE) blends. In agreement with theoretical data experimental results clearly indicate that MWCNT prefers to get associated with PTT phase than with PE. Molecular interactions responsible for such selective localization of MWCNT to PTT component can be attributed to mutual and collective π - π interactions possible between the aromatic moieties present in PTT and MWCNT. In addition, the reinforcing effect of MWCNT in the PTT/PE system was determined using tensile analysis and the morphological features of blends and blend nanocomposites are studied using scanning electron microscope (SEM). Compared to the PTT/PE blend system MWCNT incorporated blend nanocomposites show better mechanical properties. The elongation at break of the blend system is seen to rise with increasing amount of PE content. Among various blend nanocomposites, we have investigated the nanocomposites with higher PTT content show higher tensile strength and Young's modulus. The blend nanocomposite with 90/10/1 composition shows 12% increment in Young's modulus and as much as 80% increment in tensile strength compared to 90/10 blend system which signifies the role MWCNT plays in the blend system.

1. Introduction

Current environmental pollutions and waste materials in landfills bring in focus the importance of biopolymers and bioplastics. Poly trimethylene terephthalate (PTT) is a bio-based aromatic polyester which can be prepared from the polycondensation of 1,3 propane diol and terephthalic acid.^[1] In PTT about 37% of weight contribution is from its bio based content 1,3 propane diol which are produced from renewable resources.^[2] PTT is endowed with good physical and chemical properties like dimensional stability, heat resistance, good chemical stability, resistant to stretching, low moisture absorption or quick drying, easy processability, and recyclability^[3] which make all PTT-based composites very useful in diverse industrial applications.^[4] However, their low impact strength, low heat distortion temperature, and low viscosity for processing^[5] limit their applications in many ways. Polymer blending is one of the major techniques which can overcome these limitations. Through polymer blending it is possible to develop new and novel materials with attractive properties.^[6]

There are several studies which have reported substantial improvement in mechanical, thermal, and barrier properties in blends compared to their individual polymers. The property improvement and modification brought about by blending have been demonstrated well in polymer blends like poly (trimethylene terephthalate)/poly (ethylene 2,6-naphthalate) (PTT/PEN),^[7,8] polybutylene terephthalate/polyethylene terephthalate glycol (PBT/PETG),^[9] polyethylene/polypropylene (PE/PP),^[10] poly(trimethylene terephthalate)/poly-butylene terephthalate (PTT/PBT)^[11] which signify the importance of blending polymers. In addition, Chiu et al. have reported toughening mechanism shown by propylene ethylene block copolymer system when carbon black is incorporated and also by styrene-ethylene butylene-styrene triblock copolymer (SEBS). Significantly improved impact strength was observed for propylene ethylene block copolymer in their study.^[12] Wu et al. reported an improved tensile and impact strength for poly (phenylene oxide)/polyamide-6 (PPO/PA6) blend system with the addition of organo- montmorillonite.^[13] While Li et al. reported improved impact strength and reduced brittleness

A. M. Kunjappan, A. A. Ramachandran, S. Thomas
International and Interuniversity
Centre for Nanoscience and Nanotechnology
Mahatma Gandhi University
Kottayam, Kerala 686560, India
E-mail: sabuchathukulam@yahoo.co.uk

M. Padmanabhan
Department of Chemistry
Amrita Vishwa Vidyapeetham
Amritapuri Campus, Kerala 690525, India

M. Padmanabhan, S. Thomas
School of Chemical Sciences
Mahatma Gandhi University
Kottayam, Kerala 686560, India

L. P. Mathew
Viswajyothi College of Engineering and Technology
Muvattupuzha, Kerala 686670, India

DOI: 10.1002/masy.201800104



Synthesis and Activity of *Escherichia coli* on Different Chitosan Nanoparticles

Merin S. Thomas, Jiya Jose, Nandakumar K., Sabu Thomas, and Laly A. Pothen*

With a view to finding out the antimicrobial activity of nanoparticle against *E. coli*, the author prepared chitosan nanoparticles (nCHS), modified form using aloe vera (m-nCHS), hybrid nanoparticles with silver (h-nCHS) and modified, hybrid form (m,h-nCHS). The shape and uniformity of the nanoparticles are assessed by transmission electron microscopy and all the nanoparticles are found to be in the nanometer range. The physiochemical properties of the nanoparticles are determined by UV-Visible spectroscopy, zeta potential analysis, dynamic light scattering measurements, and fourier transform infrared (FTIR) spectroscopic analysis. UV – visible analysis confirms the formation of chitosan nanoparticles and hybrid Ag – chitosan nanoparticles. The stability and size of the nanoparticles are further confirmed by zeta potential and dynamic light scattering measurements. The antibacterial activity of nanoparticle against *Escherichia coli* (*E. coli*) is evaluated by calculation of minimum inhibitory concentration. The results showed that antimicrobial activity is significantly enhanced by the aloe vera modification and presence of Ag nanoparticle on chitosan nanoparticle.

deacetylation of the polymer. Chitosan is the N-deacetylated derivative of chitin.^[3]

Chitosan is a natural nontoxic biopolymer derived by the deacetylation of chitin. Chitosan and its derivatives have attracted considerable interest due to their antimicrobial and antifungal activity.^[4] Chitosan exhibits its antibacterial activity only in acidic medium because of its poor solubility p^H 6.5. Chitosan exhibits higher antibacterial activity against gram positive bacteria and gram negative bacteria. Chitosan has a number of commercial and possible biomedical uses. It can be used in agriculture for seed treatment and also as bio pesticide, helping plants to fight off fungal infections. In winemaking it can be used as a fining agent, also helping to prevent spoilage.^[5] In industry, it can be used in a self-healing polyurethane paint coating.^[6] In biomedical field, it has been found to be useful in bandages to reduce bleeding and as an antibacterial agent; it can also be used to help deliver drugs through the skin.^[7]

Chitosan nanoparticles can easily be prepared by the ionic gelation method using sodium tripolyphosphate (TPP) as a crosslinking agent. The advantage of this method was attributed to its mild conditions achieved without applying harmful organic solvent, heat or vigorous agitation that are damaging to sensitive proteins.^[8] Moreover, it could efficiently retain the bioactivity of macromolecules during preparation. The amine and –OH groups endow chitosan with many special properties, making it applicable in many areas and easily available for chemical reactions.^[9]

Chitosan nanoparticle can be formed by incorporating a polymer such as tri polyphosphate (TPP) in to a chitosan solution under constant stirring. Several research groups have studied the properties of chitosan nanoparticles with a view to using them as a drug and protein delivery agent. The biocompatibility and non-toxicity of the material makes it attractive as a neutral agent for delivery of active agents.^[10–12]

In this paper we are introducing an effective approach for developing clinically applicable chitosan by modifying the surface of the material to provide excellent bio functionality and bulk properties. We have modified chitosan nanoparticle using aloe vera, a naturally occurring medicinal plant. It is found that the modified form shows improved properties than chitosan nanoparticle. It has a high degree of antibacterial activity, wound healing etc. Another set of hybrid nanoparticles were synthesized using chitosan and silver nanoparticles. It is found that the variety hybrid has a wide range of application in medicinal field than the nonhybrid form.^[13–15]

1. Introduction

Biopolymers are polymers that degrade with the action of micro-organism, heat and moisture and are obtained from biomass. Protein, carbohydrates, ribonucleic acid (RNA), deoxy ribonucleic acid (DNA) etc. are some examples of biopolymers.^[1,2] Chitin, a natural non-toxic, biodegradable, and biocompatible polymer is a modified natural carbohydrate and the second most abundant polysaccharide in nature which is derived from crustacean shells (crabs, shrimps, and lobsters). It consists of repeating units of glucosamine and N-acetylglucosamine, the proportions of which determine the degree of

M. S. Thomas
Department of Chemistry
Mar Thoma College
Kuttapuzha P.O., Tiruvalla, Kerala 689103, India

M. S. Thomas, J. Jose, Nandakumar K., S. Thomas
International and Interuniversity Centre for Nanoscience and Nanotechnology
Mahatma Gandhi University
Priyadarsini Hills P.O., Kottayam, Kerala 686560, India

M. S. Thomas, L. A. Pothen
Department of Chemistry
C.M.S College
Kottayam, Kerala 686001, India
E-mail: lapothen@gmail.com

DOI: 10.1002/masy.201800106



Poly(ϵ -caprolactone)/Functionalized-Carbon Nanotube Electrospun Nanocomposites: Crystallization and Thermal Properties

K. Bicy, V. G. Geethamma, Nandakumar Kalarikkal, Didier Rouxel,*
and Sabu Thomas*

The interest of eco-friendly polymer nanocomposites is continuously growing because of the increased concern about environmental pollution. Polycaprolactone (PCL) is one of the extensively used bio-degradable polymers. The advantage of this biopolymer is further enhanced by the addition of nanofillers and developing nanocomposites. Carbon Nanotube (CNT) is one of the best matching nanofillers, the inclusion of CNT in PCL matrix increase the use of PCL in diverse areas. In this work PCL/CNT nanocomposites prepared by the electrospinning technique, in order to avoid CNT agglomeration, acid functionalized CNT (f-CNT) is used. Morphological properties of the electrospun nanofiber are studied by SEM and the interaction between PCL and f-CNT is studied by FT-IR. DSC and optical microscopic studies reveal the influence of f-CNT's to enhance the crystallinity and reduce the lamellar thickness and spherulite growth of PCL. The H-bonded interaction between PCL and f-CNT enhances the physical properties of bio-degradable PCL and thereby enhances its commercial application.

(PCL) is one of the widely used biodegradable polymers in various fields such as biomedical, automotive, packaging, and energy harvesting etc.^[2] Degradation of PCL occurs through the hydrolysis of its ester linkage, this enhances the usage of this polymer in diverse areas. The widespread applicability of PCL is not only because of its biodegradable nature but also its good resistance towards water, oil, solvents etc., low melting point, low viscosity, and easy processibility. Among the PCL nanocomposites Polycaprolactone/Carbon Nanotube (PCL/CNT) nanocomposite attracted the attention of research community because of its excellent properties and special structure of CNT. Low density, high aspect ratio, and high specific surface area make it into the more versatile filler.^[3,4] The incorporation of a very low concentration of CNT will dramatically improve the tensile strength, modulus, fracture toughness, thermal and

1. Introduction

Biodegradable polymer nanocomposites gained much attention in recent years because of their environmentally friendly and non-hazardous nature to the ecosystem.^[1] Polycaprolactone

electrical conductivity, sensing ability etc of the polymer.^[5,6] The role of Multiwalled Carbon Nanotube (MWCNT) on enhancing the degradation temperature of PCL was studied by Chen et al., the authors reported that low concentration of MWCNT also shows significant improvement in the degradation temperature of PCL.^[5] Goodwin et al. studied the effect of CNT's on the biodegradation of PCL, the authors reported that the addition of CNT decreases the biodegradation rate of PCL.^[7] PCL/CNT nanocomposites also find application in the biomedical field, Niezabitowska et al. prepared PCL/CNT nanocomposites and used for drug delivery.^[6] Ho et al.^[8] fabricated PCL/CNT scaffolds for cardiac tissue engineering. The property of carbon nanotubes and nanofibers on improving the mechanical, thermal, and gas barrier properties of PCL was reported by Garcia et al.^[2] In spite of the above-mentioned advantages, agglomeration of CNT is one of the major problems faced during the processing and fabrication of polymer/CNT nanocomposites. This agglomeration is due to the strong interfacial interaction between will lead to reducing the physical properties (mechanical and electrical properties) of the matrix polymer. Functionalization is an effective method to enhance CNT polymer interaction, dispersion, and alignment of CNT's. This will also improve the interfacial interaction between polymer and CNT; result in the

K. Bicy, V. G. Geethamma, N. Kalarikkal, S. Thomas
International and Inter University Center for Nanoscience and
Nanotechnology
Mahatma Gandhi University
P D Hills, Kottayam, India sabuchathukulam@yahoo.co.uk

N. Kalarikkal
School of Pure and Applied Physics
Mahatma Gandhi University
P D Hills, Kottayam, India

D. Rouxel
Institut Jean Lamour
UMR CNRS7198
Université de Lorraine
Vandoeuvre-Lès Nancy 54000, France
E-mail: didier.rouxel@univ-lorraine.fr

S. Thomas
School of Chemical Sciences
Mahatma Gandhi University
P D Hills, Kottayam, India

DOI: 10.1002/masy.201800140



Growth and synthesis of $\text{Sr}_3\text{MgSi}_2\text{O}_8:\text{Dy}^{3+}$ nanorod arrays by a solid state reaction method

Pradeep Dewangan¹ · D. P. Bisen¹ · Nameeta Brahme¹ · Raunak Kumar Tamrakar² · Shweta Sharma¹ · Kanchan Upadhyay³

Received: 21 March 2018 / Accepted: 17 September 2018 / Published online: 22 September 2018
© Springer Science+Business Media, LLC, part of Springer Nature 2018

Abstract

$\text{Sr}_3\text{MgSi}_2\text{O}_8:\text{Dy}^{3+}$ Nano-rods were synthesized by using solid state reaction method. The structural properties, morphology and band structure properties of the phosphor was studied. The structural properties were examined by X-ray diffraction, scanning electron microscopy and transmission electron microscopy. Bonding behaviour of the phosphor was also determined by recording the FTIR spectra of the phosphor. Band structure i.e. band gap of the phosphor was determined by recording the absorption spectrum. The absorption spectrum was recorded for the sample and the band gap was determined by using Tauc plot. Band gap of the phosphor was found around 5.4 eV.

Keywords $\text{Sr}_3\text{MgSi}_2\text{O}_8:\text{Dy}^{3+}$ · Nanorod · XRD · SEM · TEM · Tauc plot · SSR method

1 Introduction

Recently, nanomaterials become the boon for the optoelectronic industries. They are widely used in various detectors, computers, telephones, satellite technology etc. (Pabisch et al. 2012; Wan and Zhao 2007; Kannan et al. 2005; Presting and König 2003). The size plays an important role in its application possibilities, it enhances the use of these particles for various applications (Sanchez et al. 2005; Hong et al. 2013). The $\text{Sr}_3\text{MgSi}_2\text{O}_8:\text{Dy}^{3+}$ phosphor has wide applications in the micro and macro size also. Nowadays the nano size materials are replacing macro and micro size particles from the space and nuclear technology. As the size play very important role in its application possibilities, therefore, on the SEM and TEM devices we have studied the “adhesion” process, which can be formed in big and small size nano materials after influence of neutron flux. Moreover, we have

✉ Pradeep Dewangan
pradeep_dewangan15@rediffmail.com

¹ SoS in Physics and Astrophysics, Pt. Ravishankar Shukla University, Raipur, Chhattisgarh 492010, India

² Department of Applied Physics, Bhilai Institute of Technology (Seth Balkrishnan Memorial), Near Bhilai Power House, Durg, Chhattisgarh 49100, India

³ International and Inter University Centre for Nanoscience and Nanotechnology, Mahatma Gandhi University, Kottayam, Kerala 686560, India

Review

Self-Assembly and Applications of Amphiphilic Hybrid POSS Copolymers

Hong Chi ^{1,*} , Mingyue Wang ¹, Yiting Xiao ¹, Fuke Wang ² and Joshy K.S ³

¹ Shandong Provincial Key Laboratory of Molecular Engineering, School of Chemistry of Pharmaceutical Engineering, Qilu University of Technology (Shandong Academy of Sciences), Jinan 250353, China; Silvia9607@163.com (M.W.); Olivia9802@163.com (Y.X.)

² Polymeric Materials Department, Institute of Materials Research and Engineering, Agency for Science, Technology and Research (A*STAR), 2 Fusionopolis Way, #08-03 Innovis, Singapore 138634, Singapore; wangf@imre.a-star.edu.sg

³ International and Inter University Centre for Nanoscience and Nanotechnology, Mahatma Gandhi University, Kottayam 686 560, Kerala, India; joshyk.s@gmail.com

* Correspondence: ch9161@gmail.com; Tel.: +86-135-5319-7297

Received: 5 September 2018; Accepted: 25 September 2018; Published: 27 September 2018



Abstract: Understanding the mechanism of molecular self-assembly to form well-organized nanostructures is essential in the field of supramolecular chemistry. Particularly, amphiphilic copolymers incorporated with polyhedral oligomeric silsesquioxanes (POSSs) have been one of the most promising materials in material science, engineering, and biomedical fields. In this review, new ideas and research works which have been carried out over the last several years in this relatively new area with a main focus on their mechanism in self-assembly and applications are discussed. In addition, insights into the unique role of POSSs in synthesis, microphase separation, and confined size were encompassed. Finally, perspectives and challenges related to the further advancement of POSS-based amphiphilics are discussed, followed by the proposed design considerations to address the challenges that we may face in the future.

Keywords: self-assembly; POSS; copolymer; amphiphile

1. Introduction

Recent advances in amphiphilic copolymers have created a new surge of interest in the development of nanoscience, because many intelligent functions are directly determined by their shapes and dimensions [1–3]. Self-assembly of an amphiphilic copolymer from a single molecule to functionally architected copolymers is an efficient strategy to create competent products for applications in drug delivery [4–8], sensors [9,10], bioimaging [11–13], nanoreactors [14–16], cosmetics [17–19], and dispersant technology [20–22]. Among these new amphiphiles, the incorporation of polyhedral oligomeric silsesquioxanes (POSSs) into amphiphilic polymers to obtain improved performances has been attracting particular attention because of the unique and interesting hybrid structures of POSSs.

POSSs represent the smallest hybrid silica with the formula of $(RSiO_{1.5})_n$ ($n = 6, 8, 12$, etc.) and diameter ranging from 1 to 3 nm [23]. The size of POSSs depends on the surrounding R groups, where R could be a hydrogen atom or organic functional groups which could be precisely functionalized via the living/controlled polymerization techniques [24]. POSSs have been reported to construct hybrid polymers with well-defined structures, including telechelic-shaped [25–27] and star-shaped [28–30] polymers, dendrimers [31–33], block copolymers [34–36], and alternative copolymers [37,38]. These interesting structures and properties of POSSs make them widely used in hybrid materials [39,40], drug delivery [41,42], biomedical applications [43,44], catalytic



Exploring the mechanism of diphenylmethanol oxidation: A combined experimental and theoretical approach

Sunil Paul M. Menachery^a, Thao P. Nguyen^b, Pramod Gopinathan^c, Usha K. Aravind^d,
Charuvila T. Aravindakumar^{a,d,*}

^a School of Environmental Sciences, Mahatma Gandhi University, Kottayam, India

^b Department of Chemistry, Pohang University of Science and Technology (POSTECH), Pohang 790-784, Republic of Korea

^c Sriee Vidyadhi Raju N.S.S. College, Vazhoor, Kottayam, India

^d Advanced Centre of Environmental Studies and Sustainable Development, Mahatma Gandhi University, Kottayam, India

^e Inter University Instrumentation Centre, Mahatma Gandhi University, Kottayam, India



ARTICLE INFO

Keywords:

Diphenylmethanol
Advanced oxidation processes
Pulse radiolysis
Hydroxyl radicals
Mass Spectrometry

ABSTRACT

The mechanistic aspects of hydroxyl ($\cdot\text{OH}$) and sulfate radical ($\text{SO}_4^{\cdot-}$) induced oxidation of diphenylmethanol (DPM) in aqueous medium has been explored using a combined experimental and theoretical approach. $\cdot\text{OH}$ initiates the generation of hydroxycyclohexadienyl-type radicals (**i**) upon reaction with DPM ($\lambda_{\text{max}} = 330 \text{ nm}$; $k_2 = (1.44 \pm 0.08) \times 10^{10} \text{ dm}^3 \text{ mol}^{-1} \text{ s}^{-1}$). Time-dependent density functional theory (TDDFT) calculations revealed an *ortho*-hydroxylated adduct structure to radical **i**, which shows comparable absorbance characteristics ($\lambda_{\text{max}} = 322 \text{ nm}$). High resolution mass spectrometric (HRMS) studies reveal the existence of mono- and di-hydroxylated compounds of DPM and benzophenone as the main degradation products. Hydroxylated products were derived from the radical **i** by either a radical-radical disproportionation or a bimolecular transformation facilitated by molecular oxygen. Benzophenone (**III**) is likely originated from the radical cation (**III**), generated as a result of one electron oxidation of DPM by $\cdot\text{OH}/\text{SO}_4^{\cdot-}$, by deprotonation followed by electron and proton release.

1. Introduction

Hydroxyl radicals ($\cdot\text{OH}$), a highly reactive non-selective radical with a standard reduction potential ($E^0(\cdot\text{OH}, \text{H}^+/\text{H}_2\text{O})$) of $+2.8 \text{ V}_{\text{NHE}}$, is the most important oxidizing species formed during the radiolysis of water [1,2]. This radical has been successfully utilized by many researchers for the degradation of organic pollutants in various advanced oxidation processes (AOPs) [3–5]. $\cdot\text{OH}$ generated by Fenton and Fenton-like reactions are reportedly involved in the oxidative damage of various biomolecules including DNA and proteins [6].

Although AOPs are proven as highly efficient methodologies to degrade intractable pollutants, these techniques might produce transformation products with similar structural, chemical and toxicological characteristics to that of the parent molecule. For example, the transformation products of many organic pollutants (for example: non-ylphenol ethoxylates, chlorpyrifos, carbaryl etc.) are reported as more persistent and toxic than the parent compound [7–12]. Comprehensive investigations on the mechanism leading to the degradation of organic pollutants by $\cdot\text{OH}$ are thus very important especially in the context of

implementation of these techniques into real system. Thus, the chemical and toxicological status of all the intermediate products formed during the process needed to be monitored.

High resolution mass spectrometry (HRMS) coupled with liquid chromatography (LC), provides the highly accurate masses of the parent ion as well as the fragment ions, is regarded as an undisputed tool for the end product and metabolite profiling [3,13,14]. Some of the HRMS techniques such as Q-TOFs and Orbitraps are capable to acquire the product profile even from very complex samples without any sample purification [14–16]. Furthermore, most of the commercially available modern bench-top Q-TOF machines can achieve very low level (femtomole) sensitivity without compromising the resolving power and mass accuracy [9]. The identity of the transformation products acquired by HRMS is therefore utilized by many researchers to interpret the transient spectroscopic data recorded during their pulse radiolysis experiments [3,4,13,17]. Furthermore, structural optimizations using density functional theory (DFT) and time-dependent density functional theory (TDDFT) methods are also utilized by many authors for the accurate prediction of $\cdot\text{OH}$ reaction site, which is extremely difficult to

* Corresponding author at: School of Environmental Sciences, Mahatma Gandhi University, Kottayam, India.
E-mail address: cto@mgu.ac.in (C.T. Aravindakumar).



Differential modulation of phytoelemental composition by selected *Pseudomonas* spp.

Aswathy Jayakumar¹ · Athira Perinchery¹ · Farha M. Jaffer¹ · E. K. Radhakrishnan¹

Received: 31 January 2018 / Accepted: 7 August 2018
© Springer-Verlag GmbH Germany, part of Springer Nature 2018

Abstract

Plant growth promoting rhizobacteria (PGPR) are bioresources with potential application in ecofriendly agricultural practices. The beneficial effects of PGPR have been attributed to their ability to produce phytohormone, organic acid, siderophore, and also due to nitrogen fixation among others. In the present study, previously isolated plant growth promoting rhizospheric *Pseudomonas* spp. were evaluated for growth enhancement effect in *Vigna unguiculata* seedlings. Elemental profiling of treated plant was further carried out by inductively coupled plasma-mass spectroscopy. Results of the study showed significant increase in growth parameters such as shoot length, root length and root numbers for treated plants when compared to control. Most of the macro and micro elements were also found to get modulated by interaction with applied *Pseudomonas* spp. However, a differential modulation was observed for plants when treated with each of the *Pseudomonas* spp., which could be due to their variable interaction with the selected plant. The results of the study indicate the role of each of the associated microbial partner to specifically influence the plant nutrient mobilization along the soil plant axis. The cumulative effect of the plant microbiome hence may decide the global nutritional status of plants as per the available environmental conditions.

Keywords Rhizobacteria · ICP-MS · *V. unguiculata* · Plant growth promotion

Introduction

Plant–rhizobacterial interactions have been studied extensively for various agrological as well as environmental aspects (Chandra and Kumari 2017). Plant growth promoting rhizobacteria (PGPR) can be extracellular (*Agrobacterium*, *Arthrobacter*, *Azotobacter*, *Azospirillum*, *Bacillus*, *Burkholderia*, *Caulobacter*, *Chromobacterium*, *Erwinia*, *Flavobacterium*, *Micrococcus*, *Pseudomonas* and *Serratia*) or intracellular (*Allorhizobium*, *Bradyrhizobium*, *Mesorhizobium* and *Rhizobium*, endophytes and *Frankia*) (Gupta et al. 2015). The diverse mechanisms employed by these organisms include the production of phytohormones, ACC deaminase, siderophore, nitrogen fixation, enhanced mineral uptake and biocontrol against numerous phytopathogens (Vacheron et al. 2013). By IAA production, they have been demonstrated to modulate the cell elongation, division and differentiation in plants. Microbial population also secrete

organic acids which convert the insoluble phosphates into soluble monobasic and dibasic ions and thereby making it available to plants. Siderophore producing bacteria restrict the growth of plant pathogens due to their strong affinity towards Fe(III). The enzyme 1-aminocyclopropane-1-carboxylate (ACC) deaminase of microbial origin facilitates plant growth and development by decreasing the ethylene level, inducing salt tolerance and reducing drought stress in plants (Zahir et al. 2008). These beneficial features of rhizobacteria have significant impact on growth and yield of plants. Among the various rhizobacteria, *Pseudomonas* spp. have ubiquitous distribution and have diverse plant growth promoting as well as biocontrol mechanisms. However, the global changes introduced in plants due to rhizobacterial interaction are not fully known. The wide range of antifungal compounds produced by plant growth promoting rhizobacteria includes amphisin, 2,4-diacetylphloroglucinol (DAPG), oomycin A, phenazine, pyoluteorin, pyrrolnitrin, tensin, tropolone, and cyclic lipopeptides (Loper et al. 2007). Among these, phenazine derivatives are one of the important antifungal products of *Pseudomonas* spp.

Due to the easiness with culture handling and large-scale production, many *Pseudomonas* spp. based formulations

✉ E. K. Radhakrishnan
radhakrishnanek@mgu.ac.in

¹ School of Biosciences, Mahatma Gandhi University, PD Hills (PO), Kottayam, Kerala 686560, India



Heavy metal contamination in “chemicalized” green revolution banana fields in southern India

Nidheesh Kammadavil Sahodaran¹ · Joseph George Ray¹

Received: 13 March 2018 / Accepted: 5 July 2018 / Published online: 13 July 2018
© Springer-Verlag GmbH Germany, part of Springer Nature 2018

Abstract

The present report is a general assessment of the level of nutrient and toxic heavy metals as an impact of “chemicalized” cultivation practices for decades in banana fields in the three south Indian states, Kerala, Karnataka, and Tamilnadu. The major objective was to critically analyze the status of metallic content in green revolution fields, where chemical fertilizers or plant protective chemicals remain the major source of heavy metal contaminants. Since soil series being a soil taxonomic category that includes slightly variant soils of similar origin and common parent materials, the 286 field samples of the broad south Indian region were further grouped into composite samples representing 47 different soil series for limiting the sample analysis. The quantitative assessment of ten metals done in these soils using the Atomic Absorption Spectrophotometer included Ca, Mg, Mn, Zn, Fe, Cu, Pb, Ni, Cr, and Co. The amount of Cu observed in many fields was higher than all the previous reports of the same in the “chemicalized” fields. Similarly, the amount of Co observed in 25 fields was above its threshold levels expected for normal soils. The amount of Pb observed in all the soils appeared quite normal. The amount of Ni observed in 14 soil series was higher than its threshold levels for normal soils, except in 4 soil series, where its amount exceeded the upper limit of contamination. Cr was detected in all the samples, but found higher than its threshold level in 31 soil series. Significant positive correlations were observed between the amounts of different metals in the study. PCA results indicated that variables were correlated to four principal components, and 74.36% of the total variance was justified.

Keywords Banana · Heavy metal contamination · Southern Indian soils · Soil series · Cultivated soils · Green revolution fields

Introduction

India is the largest producer of bananas in the world, accounting for 27.8% of total banana production, which equals 33.4% of the total fruit production in India (National Horticulture Board 2016). The states of Kerala, Tamilnadu, and Karnataka are the three most important banana-producing regions in India. Since the inception of the green revolution in the 1960s (Padmavathy and Poyyamoli 2011), agriculture in India has increasingly relied on the excessive use of chemical fertilizers and pesticides. Toxic heavy metal contaminants in inorganic chemical fertilizers (Bora et al. 2015) or pesticides may accumulate in soils, which are either absorbed into the

crop or leach out into surrounding water (Singh et al. 2001). Heavy metal contaminants in field soils may possibly enter the human food chain, leading to biomagnification (Lin et al. 2010; Malan et al. 2015). Chronic environmental contamination through heavy metals occurs when metals in soils form complexes with organic matter (Efremova and Izosimova 2000) and are gradually released into ground or surface waters or cause a decrease in soil pH (Malan et al. 2015). Decrease in soil pH accelerates more dissolution and leaching out of metals into surface waters, aggravating the overall contamination issue. A large share of nutrients and metal contaminants in banana fields has the potential to cause widespread eutrophication and metal toxicities in banana-cultivating regions. The presence of heavy metals in certain banana field soils in China (Lin et al. 2010) has already been observed. In general, banana is a heavy feeder crop, but comprehensive investigation on the metal contamination in green revolution fields where banana is grown has not been conducted in India to date. To the best of our knowledge, this report is the first to describe heavy metal contamination in commercially cultivated banana fields in India.

Responsible editor: Philippe Garrigues

✉ Joseph George Ray
jgray@mgu.ac.in

¹ Laboratory of Plant Science and Ecology, School of Biosciences, Mahatma Gandhi University, Kottayam, Kerala 686560, India



Research paper

Poly(vinyl alcohol): Montmorillonite: Boiled rice water (starch) blend film reinforced with silver nanoparticles; characterization and antibacterial properties



Shiji Mathew^a, Snigdha S.^b, Jyothis Mathew^a, Radhakrishnan E.K.^{a,*}

^a School of Biosciences, Mahatma Gandhi University, P.D Hills (P.O), Kottayam, Kerala 686 560, India

^b International and Inter University Centre for Nanoscience and Nanotechnology, Mahatma Gandhi University, P.D Hills (P.O), Kottayam, Kerala 686 560, India

ARTICLE INFO

Keywords:

Nanocomposite blend
Clay mineral
Active packaging material
Boiled rice starch
Foodborne pathogens

ABSTRACT

Poly(vinyl alcohol) (PVA) is an excellent film forming polymer used for packaging applications, but it has weak barrier and mechanical properties. Hence improvement in material properties of PVA is expected to enhance its suitability as an ideal food packaging material. For the first time, this study reports the use of boiled rice starch as a blending agent to modify the physicochemical properties of PVA. The aim of the work was to develop montmorillonite (Mt)/PVA/boiled rice starch blend material reinforced with silver nanoparticles (AgNPs) for food packaging application. Highly cost effective method was used for the generation of AgNPs from AgNO₃ by using rice starch as a reducing agent. The rapid *in situ* generation of AgNPs within the polymer matrix, under the influence of direct sunlight, as conducted in this study is a novel approach. The nanocomposite films prepared by solvent casting method were characterized by SEM, XRD, FT-IR and UV-vis spectroscopy analysis. Mechanical, optical, and barrier properties of the nanocomposite films further showed its excellent properties when compared to the neat PVA film. The nanocomposite also showed promising antimicrobial activity against foodborne pathogens *Salmonella typhimurium* and *Staphylococcus aureus*. Hence the results suggest the nanocomposite blend developed in the study to be an ideal material for food packaging application.

1. Introduction

Proper packaging is in high demand to maintain the quality of food and its microbiological safety. This is highly challenging as the industry is moving towards distribution of highly processed and ready-to-eat food (Issa et al., 2017). Conventional food packaging materials have serious concern with respect to its recycling, renewability and biocompatibility (Taghizadeh et al., 2013). To tackle this, there is in need of biodegradable, low cost and eco-friendly polymer based materials.

Poly(vinyl alcohol), (PVA) is an artificial, semi-crystalline, water soluble, film forming polymer with wide range of applications. PVA has a low rate of biodegradability, poor mechanical and moisture barrier properties (Tang & Alavi, 2011). Hence many studies have been focused on the material engineering of PVA to improve its properties. One of the effective approaches for achieving this involves the incorporation of layered silicates into the polymer matrix (Purwar et al., 2015; Saha et al., 2016). Silicates such as smectite, hectorite, saponite, kaolinite, mica and montmorillonite have been used for this purpose. Among these, montmorillonite (Mt) is most commonly employed for the development of PVA based nanocomposite films (Junqueira-Gonçalves

et al., 2017; Saha et al., 2016; Yadav & Ahmad, 2015). Here, the Mt layers are considered to create a tortuous pathway (Junqueira-Gonçalves et al., 2017) for the controlled release of antimicrobial agents incorporated within the nanocomposites (Lavorgna et al., 2014). Blending of PVA with natural polymers such as starch has also been employed to get the desired properties (Guarás et al., 2016; Liu et al., 2017). Starch has been used as a better alternative for non-biodegradable and non-renewable materials in packaging industry (Pinerós-Hernández et al., 2017) due to its biocompatible (Huo et al., 2016) and excellent film forming properties (Liu et al., 2017). Starch from various sources like rice (Vargas et al., 2017), potato (Choi et al., 2017), cassava (Pinerós-Hernández et al., 2017), wheat (Bonilla et al., 2013), yam (Mali et al., 2005) and corn (Chang-Bravo et al., 2014) has been studied for film forming properties.

Nanocomposites with antimicrobial surfaces can have superior performance as packaging material. For this, different metallic nanoparticles such as silver (Ag) (Gautam & Ram, 2010), zinc oxide (ZnO) (Akhavan et al., 2017) and copper oxide (CuO) (Rao et al., 2015) have been used. Among these, silver nanoparticle (AgNPs) is the primary choice due to its broad spectrum antimicrobial effects and easiness with

* Corresponding author.

E-mail address: radhakrishnanek@mgu.ac.in (E.K. Radhakrishnan).



Biofabricated silver nanoparticles incorporated polymethyl methacrylate as a dental adhesive material with antibacterial and antibiofilm activity against *Streptococcus mutans*

Roshmi Thomas¹ · S. Snigdha² · K. B. Bhavitha^{2,3} · Seethal Babu¹ · Anjitha Ajith¹ · E. K. Radhakrishnan¹ 

Received: 21 May 2018 / Accepted: 1 September 2018
© Springer-Verlag GmbH Germany, part of Springer Nature 2018

Abstract

In this study, polymethyl methacrylate (PMMA) thin films incorporated with biofabricated silver nanoparticles were used to evaluate the in vitro antimicrobial and antibiofilm activity against the cariogenic bacterium *Streptococcus mutans*. For this, silver nanoparticles (AgNPs) were generated using *Bacillus amyloliquefaciens* SJ14 culture (MAGNPs) and extract from *Curcuma aromatica* rhizome (CAGNPs). The AgNPs were further characterized by UV–Vis spectroscopy and high-resolution transmission electron microscopy. The minimum inhibitory concentration, minimum bactericidal concentration and antibiofilm activity of AgNPs against *S. mutans* were also assessed. Here, MAGNPs were found to have superior antimicrobial activity when compared to CAGNPs. The MAGNPs and CAGNPs also demonstrated 99% and 94% inhibition of biofilm formation of *S. mutans* at concentrations of 3 µg/mL and 50 µg/mL, respectively. The AgNPs were further incorporated into PMMA thin films using solvent casting method. The thin films were also characterized by scanning electron microscopy and UV–Vis spectroscopy. Subsequently, both PMMA/MAGNPs and PMMA/CAGNPs nanocomposite thin films were subjected to antimicrobial and antibiofilm analysis. The microbicidal activity was found to be higher for the PMMA/MAGNPs thin film, which highlights the potency of microbially synthesized AgNPs as excellent agents to inhibit cariogenic bacteria from colonising dental restorative material.

Keywords Microbial AgNPs · Biofabricated AgNPs · Antibiofilm · Dental adhesive · PMMA · *Streptococcus mutans*

Introduction

Dental restorative composites mainly consist of methacrylate resins and various kinds of fillers which enhance their mechanical, antimicrobial, optical and aesthetic properties (Babu et al. 2016; Dionysopoulos et al. 2017). Dental adhesives facilitate the binding of composites to the dentin and form an interlocked interface by penetrating into the

dentin tubules. Polymethyl methacrylate (PMMA), a transparent thermoplastic has been widely used as a constituent of dental material (Takeyama et al. 1978). Its acceptance in dentistry is due to its reliability, biocompatibility, low cost, easy availability, and the ease of modification (Frazer et al. 2005; Peters et al. 2018; Lee et al. 2018). However, one of the challenges with its application is the microbial biofilm formation at the dentin–adhesive interface leading to the failure of dental restoratives (Marashdeh et al. 2018). The biofilm formation in the oral cavity is generally favored by the presence of moisture and nutrients (Saini et al. 2011; Dias et al. 2017). Due to this, cariogenic bacteria like *Streptococcus mutans* forms one of the major culprits responsible for the failure of dental restorative material. The organism has been known to have preference to grow both on tooth surfaces and on surfaces of dental implant (Loesche 1986). There is high demand to develop engineered dental restorative materials with antimicrobial potential because of the increasing antibiotic resistance among these microorganisms (Garcia et al. 2017).

Roshmi Thomas and S. Snigdha contributed equally.

✉ E. K. Radhakrishnan
radhakrishnanek@mgu.ac.in

¹ School of Biosciences, Mahatma Gandhi University, PD Hills (P.O.), Kottayam, Kerala 686 560, India

² International and Inter University Centre for Nanoscience and Nanotechnology, Mahatma Gandhi University, PD Hills (P.O.), Kottayam, Kerala 686 560, India

³ Department of Physics, St Teresas's College, Ernakulam, Kerala 682011, India



Nickel substituted cadmium ferrite as room temperature operable humidity sensor

B. Chethan^a, Y.T. Ravikiran^{b,*}, S.C. Vijayakumari^c, H.G. Rajprakash^a, S. Thomas^d

^a Department of Physics, Research center, JNN College of Engineering, Shivamogga, Karnataka, India

^b Department of PG Studies and Research in Physics, Government Science College, Chitradurga, 577 501, Karnataka, India

^c Department of Physics, SJM College of Arts, Science and Commerce, Chitradurga, Karnataka, India

^d International and Inter University Centre for Nanoscience and Nanotechnology, Mahatma Gandhi University, Kottayam, Kerala, India



ARTICLE INFO

Article history:

Received 18 May 2018

Received in revised form 8 August 2018

Accepted 10 August 2018

Available online 11 August 2018

Keywords:

Cadmium ferrite

Humidity

Porosity

Adsorption

Sensing

Response and recovery time

Stability

ABSTRACT

In this work, maximum enhancement in room temperature humidity sensing response of cadmium ferrite (CF) due to substitution of nickel ion in it, to form nickel substituted cadmium ferrite (NSCF) by sol-gel auto combustion method is presented. The shift in vibration frequency corresponding to octahedral B-site and tetrahedral A-site of NSCF as compared to those of CF were confirmed from FTIR studies and correlated with theoretical calculations of respective force constants. The higher values of porosity and surface area and lower value of crystallite size of NSCF as compared to those of CF were confirmed from XRD studies. Increase in agglomeration of small sized grains forming many pores confirmed from comparative analysis of SEM images of CF and NSCF. The NSCF recorded a maximum sensing response of 99% as against 50% of CF when measured in the range 25% RH - 95% RH. The response and recovery times of NSCF were found to be 30 s and 45 s respectively while those of CF were 123 s and 154 s respectively. The NSCF sample showed stable sensing ability over a period of two months. The sensing mechanism is discussed on the basis of chemisorption, physisorption and capillary condensation processes.

© 2018 Elsevier B.V. All rights reserved.

1. Introduction

As awareness of man is increasing to lead a more healthier and comfortable life using technological devices, need for humidity sensors has gained momentum in recent times and has found applications in wide areas such as in pharmaceutical industry, food production, electronic industries, paper and sugar industry, agriculture, food storage, climatology, meteorological studies, libraries, chemical industry, museums, nuclear power plant [1,2]. Among the many types of humidity sensors like polymer based, optical type, metal oxide based and ferrite based sensors in use [3–5], mesoporous ferrite based sensors are preferred because of their versatile micro structural properties like nanosize, large surface area, uniform grain size, because of which they readily respond to surface phenomena like adsorption which is favorable for humidity sensing [1,6,7]. Besides, the defects, vacancies and dangling bonds on their surface act as active sites for low concentration water vapor dissociation. Another interesting aspect of ferrites is the presence of more than one easily displaceable cation site thus providing

an opportunity suitable for variation in their chemical nature and oxidation state favorable for humidity sensing [6,8]. Among the ferrites, soft ferrites are very sensitive to humidity as indicated by the remarkable change in their resistance upon exposure to moisture and this property of soft ferrites has been applied by many researchers to fabricate good humidity sensing devices [9]. But nowadays, researchers are seeking to improve the efficiency of these sensors relying on the fact that increasing the porosity of the sensing surface as well as its large and disordered grain boundaries generally contribute to enhanced sensitivity and which can be achieved by tailoring their flexible chemical and physical properties either by substituting relatively varying amounts of trivalent or divalent metal ions such as chromium, nickel, copper in to it or by adopting better method of preparation [10,11].

Recently, humidity sensing properties of pellets of such soft ferrites have been studied by some of the researchers. Sasmaz Kuru et al. have reported that ferrite based Al-Cd nanoparticle synthesized by co-precipitation method has shown better humidity sensitivity of 83% in the range 15% RH - 90% RH with a response time of 5 s and a recovery time of 8 s [2]. Praseodymium doped magnesium ferrite synthesized by co-precipitation method has shown humidity sensitivity of 88% in the range 10% RH - 90% RH with a response time of 90 s and recovery time of 120 s, as reported by

* Corresponding author.

E-mail address: ytrctai@gmail.com (Y.T. Ravikiran).

Tree biomass and carbon density estimation in the tropical dry forest of Southern Western Ghats, India

Babu Padmakumar ⁽¹⁾,
Naduparambu P Sreekanth ⁽²⁾,
Viswanathan Shanthiprabha ⁽²⁾,
Joby Paul ⁽¹⁾,
Kasau Sreedharan ⁽¹⁾,
Toms Augustine ⁽¹⁾,
Kazhuthuttil K Jayasooryan ⁽¹⁾,
Mutharimettak Rameshan ⁽¹⁾,
Mahesh Mohan ⁽¹⁾,
Eswara V Ramasamy ⁽¹⁾,
Ambattu P Thomas ⁽²⁾

United Nations Framework Convention on Climate Change highlights the significance of carbon storage and emission in forests towards climate change mitigation. The aim of this study was to quantify the tree biomass and carbon density (carbon storage) in the tropical dry forest of the Chinnar Wildlife Sanctuary of Kerala located in the Southern Western Ghats, India. We investigated the species-wise contribution of carbon (C) storage, as well as the species-wise and plot-wise correlation between carbon and other dendrometric variables. We also analysed the girth (diameter) wise distribution of carbon and tree density in the study region. The study was conducted in eight selected sample plots of the region, each with an area of 0.1 hectare. Species-specific volume and specific gravity relationship coupled with suitable regression equation were used to estimate biomass. Tree carbon was assumed to be 47% of the biomass. The results showed that the average biomass and carbon density of the vegetation were 64.13 t ha⁻¹ and 30.46 t-C ha⁻¹, respectively. Among the 32 species identified, *Tamarindus indica* L. (17%), *Hardwickia binata* Roxb. (14%), *Terminalia arjuna* (Roxb. ex DC.) Wight & Arn (10%) and *Pleiospermium alatum* (Wight & Arn.) Swingle (10%) were dominant as for carbon storage. The correlation analysis showed that basal area is a good predictor of tree biomass and carbon, while the role of tree density and tree diversity remain uncertain in determining carbon storage. With respect to diametric class distribution, tree density showed a reverse J-shaped pattern indicating the sustainable regeneration of the analysed forest, where the small- (diameter at breast height 3-9 cm) to medium-sized trees (diameter at breast height 10-69 cm) were found to contribute to more than 50% of biomass and carbon in the forest. The study provides useful information for carbon mitigation strategies in a tropical dry forest in the Southern Western Ghats.

Keywords: Above Ground Tree Biomass, Carbon, Tropical Dry Forest, Kerala, Southern Western Ghats

Introduction

Forests represent a significant part of the global carbon cycle and play an important role in carbon sequestration. Forests cover 40% of the terrestrial surface though they contribute by 90% and 70% to terrestrial biomass and productivity, respectively (Korner et al. 2005). The significant role of forests in containing global carbon dioxide levels (CO₂) was acknowledged in Kyoto in December 1997. In the present climate

change scenario, the international community is increasingly made aware of the fact that the alleviation of global warming cannot be achieved without the inclusion of forests in the mitigation plan. Reducing Emissions from Deforestation and Forest Degradation and enhancing forest carbon (REDD+) is a new initiative of the United Nations Framework Convention on Climate Change (UNFCCC). It is led by developing countries with rich forest cover and calls

for economic incentives to reduce the emissions of greenhouse gases from deforestation and forest degradation in developing countries (Gibbs et al. 2007). Beyond carbon sequestration, REDD+ is also expected to play a major role in other ecosystem services and has the potential to generate benefits for indigenous and local communities. To achieve and optimize these “co-benefits”, the developing countries need to have well-established estimates of forest carbon densities or stocks for a successful implementation of mitigating policies and to take advantage of the REDD+ programme (Saatchi et al. 2011). According to Canadell & Raupach (2008), increasing the carbon density or stock of existing forests is also an important option in this regard. It is therefore vital to understand the potential role of forests, especially tropical forest, in curtailing the impact of global warming. As the climate change debate progresses, policy makers also require more scientific and reliable information on the current status of carbon storage that would benefit in effective resource management, in developing policies and setting priorities for the forest in

□ (1) School of Environmental Sciences, Mahatma Gandhi University, Kottayam 686 560 (India); (2) Advanced Centre of Environmental Studies and Sustainable Development (ACESSD), Mahatma Gandhi University, Kottayam 686 560 (India)

@ Babu Padmakumar (babupk.ktm@gmail.com)

Received: Aug 04, 2016 - Accepted: Jun 05, 2018

Citation: Padmakumar B, Sreekanth NP, Shanthiprabha V, Paul J, Sreedharan K, Augustine T, Jayasooryan KK, Rameshan M, Mohan M, Ramasamy EV, Thomas AP (2018). Tree biomass and carbon density estimation in the tropical dry forest of Southern Western Ghats, India. *iForest* 11: 534-541. - doi: 10.3832/ifor2190-011 [online 2018-08-01]

Communicated by: Tamir Klein

This site uses cookies. By continuing to use this site you agree to our use of cookies. To find out more, see our Privacy and Cookies policy. 

PAPER

Simple unmodified green silver nanoparticles as fluorescent sensor for Hg(II) ions

Maria Sebastian, Archana Aravind and Beena Mathew 

Published 25 July 2018 • © 2018 IOP Publishing Ltd

Materials Research Express, Volume 5, Number 8

beenamscs@gmail.com

School of Chemical Sciences, Mahatma Gandhi University, Kottayam-686560, Kerala, India

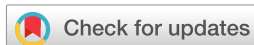
Beena Mathew  <https://orcid.org/0000-0002-2705-4901>

Received 11 June 2018

Accepted 12 July 2018

Accepted Manuscript online 12 July 2018

Published 25 July 2018



Method: Single-blind

Revisions: 2

Screened for originality? Yes

Maria Sebastian *et al* 2018 *Mater. Res. Express* **5** 085015

<https://doi.org/10.1088/2053-1591/aad317>

Buy this article in print

Abstract

A novel, simple, effective and rapid fluorescence sensing platform was fabricated using green silver nanoparticles from *Agaricus Bisporus* (AgNP-AB). AgNP-AB was synthesized by microwave reactor. The synthesized AgNPs have been used for the fluorescence

Bayesian analysis of bulk viscous matter dominated universe

Athira Sasidharan^{1,a}, N. D. Jerin Mohan^{1,b}, Moncy V. John^{2,c}, Titus K. Mathew^{1,d}

¹ Department of Physics, Cochin University of Science and Technology, Kochi, India

² School of Pure and Applied Physics, Mahatma Gandhi University, Kottayam, India

Received: 21 April 2018 / Accepted: 27 July 2018 / Published online: 7 August 2018

© The Author(s) 2018

Abstract In our previous works, we have analyzed the evolution of bulk viscous matter dominated universe with a more general form for bulk viscous coefficient, $\zeta = \zeta_0 + \zeta_1 \frac{\dot{a}}{a} + \zeta_2 \frac{\ddot{a}}{a}$ and also carried out the dynamical system analysis. We found that the model reasonably describes the evolution of the universe if the viscous coefficient is a constant. In the present work we are contrasting this model with the standard Λ CDM model of the universe using the Bayesian method. We have shown that, even though the viscous model gives a reasonable back ground evolution of the universe, the Bayes factor of the model indicates that, it is not so superior over the Λ CDM model, but have a slight advantage over it.

1 Introduction

Many observations lead to the conclusion that the present universe is accelerating [1–6]. The reason for this acceleration was attributed to the dominant presence of a new cosmic component called dark energy. The Λ CDM model came out as the most successful one for explaining this late time acceleration of the universe. In this model the cosmological constant is being considered as the dark energy. But the model is plagued with severe drawbacks. The foremost among them is the cosmological constant problem and is about the discrepancy between the observed and predicted values of the dark energy density, which is of the order of 120. The other is the coincidence problem, the mysterious coincidence between the energy densities of the dark energy and dark matter component during the current epoch of the universe in spite of their completely different evolution history. This motivates a large class of models with varying dark energy density [7–14]. Perfect fluid models like Chaplygin

gas model [15, 16] would be an alternate suggestion, due to their ability to explain both the deceleration and late acceleration by a single cosmic component, which thus effectively leads to a unification of the dark matter and dark energy sectors. There were also attempts to study this phenomenon by modifying the geometry part of the gravity theories, like $f(R)$ gravity [17–19], $f(T)$ gravity [20, 21], Gauss-Bonnet theory [22], Lovelock gravity [23], Horava-Lifshitz gravity [24], scalar–tensor theories [25], braneworld models [26] etc.

As in the case of the Chaplygin gas model, another possibility of the unified description of both dark energy and dark matter arises in the dissipative fluid models. It has been shown that the early inflationary period of the universe can be due to the presence of an imperfect fluid with bulk viscosity [27–31]. This motivates the study of the dissipative cosmologies in the context of the late acceleration of the universe [32–37]. In [33], by considering a single cosmic component, which is the dark matter with bulk viscosity, $\zeta(\rho) = \alpha\rho^m$ with α and m being constants, the authors have shown that, the universe can make a transition from a decelerating phase to a late accelerating phase and ultimately to a de Sitter epoch. In spite of this good background evolution, the model have come across with some negative aspects while analysing the structure formation. For instance, in reference [33] with $\zeta = \alpha\rho^{-0.4}$ the authors have shown that the density perturbation would rapidly be damped out, which adversely affect mainly the CMBR. It may be due to the power factor of the density -0.4 , which was obtained by constraining the model with old supernovae luminosity data by Riess et al. [1]. At around the same time, in reference [35], the authors have considered a constant bulk viscous dark matter dominated universe, with $0 < \zeta < 3$ and predicts that the universe began with a Big-Bang, followed by a decelerated expansion epoch and later transition into an accelerated epoch. Later these authors [36] extended their model by taking varying bulk viscosity of the form $\zeta = \zeta_0 + \zeta_1 H$ and found that it shows a background evolution close to that of the standard Λ CDM model. In [38], the authors have shown that the data

^a e-mail: athirasnair91@cusat.ac.in

^b e-mail: jerinmohandk@cusat.ac.in

^c e-mail: moncyjohn@yahoo.co.uk

^d e-mail: titus@cusat.ac.in

This site uses cookies. By continuing to use this site you agree to our use of cookies. To find out more, see our Privacy and Cookies policy. 

PAPER

Performance comparison of macromolecular assisted and immobilized low pressure membranes in the removal of toxic metals

Nikhil Chandra P^{1,2,4}, Kishore Kumar Nair^{3,4}  and Usha K Aravind¹

Published 20 July 2018 • © 2018 IOP Publishing Ltd

Materials Research Express, Volume 5, Number 8

pnikhilchandra@gmail.com

kknair9@gmail.com

¹ Advanced Centre of Environmental Studies and Sustainable Development, Mahatma Gandhi University, Kottayam 686560, India

² Department of Chemistry, Sree Narayana College, Kollam 691001, India

³ School of Environmental Sciences, Mahatma Gandhi University, Kottayam 686560, India

⁴ Authors to whom any correspondence should be addressed

Kishore Kumar Nair  <https://orcid.org/0000-0002-1837-5308>

Received 24 April 2018

Accepted 10 July 2018

Accepted Manuscript online 10 July 2018

Published 20 July 2018



Method: Single-blind

Revisions: 2

Screened for originality? Yes

Nikhil Chandra P *et al* 2018 *Mater. Res. Express* **5** 085504

<https://doi.org/10.1088/2053-1591/aad273>

Buy this article in print

This site uses cookies. By continuing to use this site you agree to our use of cookies. To find out more, see our Privacy and Cookies policy. 

PAPER

Augmented antimicrobial, antioxidant and catalytic activities of green synthesised silver nanoparticles

Remya Vijayan¹, Siby Joseph² and Beena Mathew¹ 

Published 25 July 2018 • © 2018 IOP Publishing Ltd

Materials Research Express, Volume 5, Number 8

beenamscs@gmail.com

¹ School of Chemical Sciences, Mahatma Gandhi University, Kottayam -686560, Kerala, India

² Department of Chemistry, St. George's College, Aruvithura, Kottayam- 686122, Kerala India

Beena Mathew  <https://orcid.org/0000-0002-2705-4901>

Received 28 December 2017

Accepted 14 February 2018

Accepted Manuscript online 14 February 2018

Published 25 July 2018



Method: Single-blind

Revisions: 1

Screened for originality? Yes

Remya Vijayan *et al* 2018 *Mater. Res. Express* **5** 085022

<https://doi.org/10.1088/2053-1591/aaaf33>

Buy this article in print

Abstract

Bayesian analysis of bulk viscous matter dominated universe

Athira Sasidharan^{1,a}, N. D. Jerin Mohan^{1,b}, Moncy V. John^{2,c}, Titus K. Mathew^{1,d}

¹ Department of Physics, Cochin University of Science and Technology, Kochi, India

² School of Pure and Applied Physics, Mahatma Gandhi University, Kottayam, India

Received: 21 April 2018 / Accepted: 27 July 2018 / Published online: 7 August 2018
© The Author(s) 2018

Abstract In our previous works, we have analyzed the evolution of bulk viscous matter dominated universe with a more general form for bulk viscous coefficient, $\zeta = \zeta_0 + \zeta_1 \frac{\dot{a}}{a} + \zeta_2 \frac{\ddot{a}}{a}$ and also carried out the dynamical system analysis. We found that the model reasonably describes the evolution of the universe if the viscous coefficient is a constant. In the present work we are contrasting this model with the standard Λ CDM model of the universe using the Bayesian method. We have shown that, even though the viscous model gives a reasonable back ground evolution of the universe, the Bayes factor of the model indicates that, it is not so superior over the Λ CDM model, but have a slight advantage over it.

1 Introduction

Many observations lead to the conclusion that the present universe is accelerating [1–6]. The reason for this acceleration was attributed to the dominant presence of a new cosmic component called dark energy. The Λ CDM model came out as the most successful one for explaining this late time acceleration of the universe. In this model the cosmological constant is being considered as the dark energy. But the model is plagued with severe drawbacks. The foremost among them is the cosmological constant problem and is about the discrepancy between the observed and predicted values of the dark energy density, which is of the order of 120. The other is the coincidence problem, the mysterious coincidence between the energy densities of the dark energy and dark matter component during the current epoch of the universe in spite of their completely different evolution history. This motivates a large class of models with varying dark energy density [7–14]. Perfect fluid models like Chaplygin

gas model [15, 16] would be an alternate suggestion, due to their ability to explain both the deceleration and late acceleration by a single cosmic component, which thus effectively leads to a unification of the dark matter and dark energy sectors. There were also attempts to study this phenomenon by modifying the geometry part of the gravity theories, like $f(R)$ gravity [17–19], $f(T)$ gravity [20, 21], Gauss-Bonnet theory [22], Lovelock gravity [23], Horava-Lifshitz gravity [24], scalar–tensor theories [25], braneworld models [26] etc.

As in the case of the Chaplygin gas model, another possibility of the unified description of both dark energy and dark matter arises in the dissipative fluid models. It has been shown that the early inflationary period of the universe can be due to the presence of an imperfect fluid with bulk viscosity [27–31]. This motivates the study of the dissipative cosmologies in the context of the late acceleration of the universe [32–37]. In [33], by considering a single cosmic component, which is the dark matter with bulk viscosity, $\zeta(\rho) = \alpha\rho^m$ with α and m being constants, the authors have shown that, the universe can make a transition from a decelerating phase to a late accelerating phase and ultimately to a de Sitter epoch. In spite of this good background evolution, the model have come across with some negative aspects while analysing the structure formation. For instance, in reference [33] with $\zeta = \alpha\rho^{-0.4}$ the authors have shown that the density perturbation would rapidly be damped out, which adversely affect mainly the CMBR. It may be due to the power factor of the density -0.4 , which was obtained by constraining the model with old supernovae luminosity data by Riess et al. [1]. At around the same time, in reference [35], the authors have considered a constant bulk viscous dark matter dominated universe, with $0 < \zeta < 3$ and predicts that the universe began with a Big-Bang, followed by a decelerated expansion epoch and later transition into an accelerated epoch. Later these authors [36] extended their model by taking varying bulk viscosity of the form $\zeta = \zeta_0 + \zeta_1 H$ and found that it shows a background evolution close to that of the standard Λ CDM model. In [38], the authors have shown that the data

^a e-mail: athirasnair91@cusat.ac.in

^b e-mail: jerinmohandk@cusat.ac.in

^c e-mail: moncyjohn@yahoo.co.uk

^d e-mail: titus@cusat.ac.in

This site uses cookies. By continuing to use this site you agree to our use of cookies. To find out more, see our [Privacy and Cookies policy](#). 

PAPER

Performance comparison of macromolecular assisted and immobilized low pressure membranes in the removal of toxic metals

Nikhil Chandra P^{1,2,4}, Kishore Kumar Nair^{3,4}  and Usha K Aravind¹

Published 20 July 2018 • © 2018 IOP Publishing Ltd

Materials Research Express, Volume 5, Number 8

pnikhilchandra@gmail.com

kknair9@gmail.com

¹ Advanced Centre of Environmental Studies and Sustainable Development, Mahatma Gandhi University, Kottayam 686560, India

² Department of Chemistry, Sree Narayana College, Kollam 691001, India

³ School of Environmental Sciences, Mahatma Gandhi University, Kottayam 686560, India

⁴ Authors to whom any correspondence should be addressed

Kishore Kumar Nair  <https://orcid.org/0000-0002-1837-5308>

Received 24 April 2018

Accepted 10 July 2018

Accepted Manuscript online 10 July 2018

Published 20 July 2018



Method: Single-blind

Revisions: 2

Screened for originality? Yes

Nikhil Chandra P *et al* 2018 *Mater. Res. Express* **5** 085504

<https://doi.org/10.1088/2053-1591/aad273>

Buy this article in print

This site uses cookies. By continuing to use this site you agree to our use of cookies. To find out more, see our Privacy and Cookies policy. 

PAPER

Augmented antimicrobial, antioxidant and catalytic activities of green synthesised silver nanoparticles

Remya Vijayan¹, Siby Joseph² and Beena Mathew¹ 

Published 25 July 2018 • © 2018 IOP Publishing Ltd

Materials Research Express, Volume 5, Number 8

beenamscs@gmail.com

¹ School of Chemical Sciences, Mahatma Gandhi University, Kottayam -686560, Kerala, India

² Department of Chemistry, St. George's College, Aruvithura, Kottayam- 686122, Kerala India

Beena Mathew  <https://orcid.org/0000-0002-2705-4901>

Received 28 December 2017

Accepted 14 February 2018

Accepted Manuscript online 14 February 2018

Published 25 July 2018



Method: Single-blind

Revisions: 1

Screened for originality? Yes

Remya Vijayan *et al* 2018 *Mater. Res. Express* **5** 085022

<https://doi.org/10.1088/2053-1591/aaaf33>

Buy this article in print

Abstract



Investigation of the mechanical, thermal and transport properties of NR/NBR blends: impact of organoclay content

Saliney Thomas¹ · Shaji Thomas² · Jiji Abraham³ · Soney C. George^{1,4} · Sabu Thomas^{1,3}

Received: 11 April 2018 / Accepted: 26 June 2018 / Published online: 4 July 2018
© Springer Nature B.V. 2018

Abstract

In the present study efforts have been made to prepare organoclay nanocomposites of NR/NBR (natural rubber/nitrile rubber) blends using 0–4 wt% cloisite 93A by mixing on a laboratory type two-roll mill as per ASTM procedure. The organoclay-filled NR/NBR blends exhibited high tensile strength due to the formation of inter-phase crosslinks. The modulus values were also found increase in line with tensile strength. The clay platelets could be aligned in the direction of stretching of the rubber sample and the strong interfacial interaction between the NR and the NBR chains and the clay platelets could support local load transfer, resulting in enhanced modulus. The results of Scanning Electron Microscopy (SEM) fractographic analysis were in agreement with the mechanical test results and support the observed changes in the NR/NBR blend properties as the clay content increases. Transmission Electron Microscopy (TEM) images showed intercalated clay layers in both phases of the blend, indicating good compatibilization. Crosslink densities of the vulcanized samples exhibited an increase in the values on the increase in dosage of the nanoclay, supporting the fact that high specific surface area of the layered silicates enhanced reinforcement of the polymer matrix.

Keywords Cloisite 93A · NBR/NR blends · Compatibilization · Morphology · Crosslink density

✉ Soney C. George
soneygeo@gmail.com

Saliney Thomas
salineythomas@gmail.com

Shaji Thomas
shajiparel@rediffmail.com

Jiji Abraham
jijiabraham02@gmail.com

Sabu Thomas
sabupolymer@yahoo.com

¹ School of Chemical Sciences, Mahatma Gandhi University, Kottayam, Kerala 686 560, India

² Department of Chemistry, Bishop Abraham Memorial College, Thuruthicadu, Mallappally, Pathanamthitta, Kerala 689597, India

³ International and Inter University Centre for Nano Science & Nanotechnology, Mahatma Gandhi University, Kottayam 686 560, India

⁴ Centre for Nano Science & Technology, Amal Jyothi Engineering College, Kanjirappally, Koovappally P.O., Kottayam Dt., Kerala 686518, India

Introduction

Since no elastomer can exhibit all the properties desired for a finished product, technologists have been attempting to incorporate the desirable properties by the process of blending. Though many reports are available on the preparation of miscible polymers, most of the blends are immiscible polymers called hetero-phase blends [1–5]. It has also been proved by many studies that certain substances with suitable structure called compatibilizers can enhance the miscibility of immiscible blends by virtue of their ability to change interfacial situation [6–9]. Compatibilizers have multifunctional roles like reducing interfacial tension between phases, thereby increasing finer dispersion, helping to increase stability against segregation, and enhancing the interfacial adhesion.

Number of compatibilizers has been applied in the preparation of elastomer blends. Sirisinha et al. [10] has been reported that for (20/80) Natural rubber (NR) / Nitrile butadiene rubber (NBR) blend, the oil resistance was higher when the size of the NR dispersed phase was smaller. Investigation by Mathai et al. [11] indicated that the equilibrium solvent uptake decreases with an increase in the concentration of NBR.



Terminalia bellirica (Gaertn.) Roxb fruit exerts anti-inflammatory effect via regulating arachidonic acid pathway and pro-inflammatory cytokines in lipopolysaccharide-induced RAW 264.7 macrophages

Kuriakose Jayesh¹ · Raj Karishma¹ · A. Vysakh¹ · Prasad Gopika¹ · M. S. Latha¹

Received: 25 April 2018 / Accepted: 3 July 2018
© Springer Nature Switzerland AG 2018

Abstract

Terminalia bellirica (Gaertn.) Roxb. (Family: Combretaceae), known as Bhibhitaki in Sanskrit and locally known as Behera in India, has been used for centuries in Ayurveda, a universal system of medicine in India. The dried fruit of *T. bellirica* is used for the treatment of several disorders. The present study aims to explore the anti-inflammatory effects of aqueous acetone extracts isolated from *T. bellirica* (AATB) in RAW 264.7 cell lines. The AATB was prepared from the fruits of *T. bellirica*. Different concentrations of AATB (6.25–100 µg/ml) were used for MTT assay. The anti-inflammatory effect of AATB was evaluated by using different assays such as total cyclooxygenase (COX), 5-lipoxygenase (5-LOX) activity, nitrate and reactive oxygen species (ROS) production. The mRNA level expression of COX-2, tumor necrosis factor alpha (TNF-α) and interleukin-6 (IL-6) were studied in LPS stimulated RAW 264.7 cells. AATB treatment significantly diminished the elevated levels of inflammatory markers. Moreover, AATB downregulated the mRNA level expression of TNF-α, IL-6 and COX-2 genes. The result of our study suggest the use of AATB and is able to reduce inflammatory conditions associated with various diseases.

Keywords *Terminalia bellirica* · Inflammation · Cytokines · Interleukin-6

Introduction

Inflammation is the response of living tissue to injury. The term “inflammation” is derived from a Latin word ‘inflammatio’ meaning to set on fire, is a significant process in the body’s defense system, which acts to eliminate and repair damaged tissue or to neutralize harmful agents (Ferrero-Miliani et al. 2007). TLR-4 is a member of the Toll-like receptor family of proteins and has been putatively identified as *Lps*, the gene essential for active responses to lipopolysaccharide (LPS) in mammals (Chow et al. 1999). Lipopolysaccharide, a component of the outer membrane of Gram-negative bacteria, is a potent activator of a variety of mammalian cell types (Schletter et al. 1995). Activation of LPS-responsive cells, such as monocytes and macrophages, occurs rapidly after LPS interacts with TLR-4 (Ulevitch and Tobias 1995). LPS

has been shown to initiate multiple intracellular signalling stages (Sweet and Hume 1996), including the activation of nuclear factor kappa B (NF-κB), which eventually leads to the synthesis and release of a number of proinflammatory mediators like IL-6, COX-2 and tumour necrosis factor-α (Schletter et al. 1995).

Arachidonic acid, the major polyunsaturated fatty acid present in mammalian systems, is the precursor for prostaglandins synthesis by cyclooxygenase pathway. COX-2 is an inducible enzyme responsible for the production of pro-inflammatory prostaglandins causing inflammation and pain (Masferrer et al. 1994). Leukotrienes (LTs) are lipid signalling molecules derived from arachidonic acid (AA) that initiate and amplify innate and adaptive immune responses by regulating the recruitment and activation of leukocytes in inflamed tissues. 5-LOX catalyse the synthesis of leukotrienes from arachidonic acid (Cho et al. 2011). With infectious and pro-inflammatory stimuli, iNOS protein is highly induced to produce NO in a micromolar range, whereas NO generation from nNOS and eNOS enzymes is constant and within the nanomolar range (Murakami and Ohigashi 2007). Myeloperoxidase (MPO), a heme protein released

✉ M. S. Latha
mslathasbs@yahoo.com

¹ School of Biosciences, Mahatma Gandhi University, Priyadarshini Hills, Kottayam, Kerala, India

by leukocytes, is one of the most widely studied molecules during the last decade; it plays a specific role in inflammation and oxidative stress at the cellular level. It has become increasingly recognized that MPO performs a very crucial role as part of the innate immune system through the formation of microbicidal reactive oxidants, while it affects the arterial endothelium (Anatoliotakis et al. 2013). The ubiquitous nuclear factor kappa B signalling pathway plays central role in regulating inflammation through transcription of pro-inflammatory genes COX-2, TNF- α and IL-6 (Tak and Firestein 2001).

Nonsteroidal anti-inflammatory drugs (NSAIDs) are the analgesics most frequently used world-wide to treat inflammatory diseases (Camu et al. 2003). NSAIDs are capable of inducing various side effects (Whelton and Hamilton 1991). Therefore, there is an urgent need to develop an anti-inflammatory drug from plants with minimal or no side effects. A large number of plants and plant-based products used in traditional medicine have now become a part of the modern world health care system (Dubey et al. 2004). *Terminalia bellirica* (Gaertn.) Roxb. (Combretaceae), known as Bhibhitaki in Sanskrit and locally called Behera in India, is a large deciduous tree found throughout India except for the dry western regions up to an elevation of 900 m (Jayesh et al. 2017a, 2018). The fruits, apart from being an integral part of Triphala, are widely used in different traditional therapeutic formulations in the indigenous system of medicine, either alone or in combination with other plant-based drugs (Meena et al. 2009). The fruits elicit various pharmacological properties like antioxidant, antidiabetic, analgesic, antipyretic, antihelminthic, hepato protective (Jayesh et al. 2017b) and antidiarrhoeal in its different extracts (Deb et al. 2016). Since tests began for these pharmacological properties, no anti-inflammatory property has yet been found, so current studies focus on anti-inflammatory properties of the plant extract AATB on RAW 264.7 murine macrophage cell lines.

Materials and methods

Chemicals and reagents

All chemicals used in this study were of analytical reagent grade. Biochemical reagents were purchased from Merck, India. Tissue culture plates were purchased from Tarson, India.

Plant material

Authenticated fruits collected during April–May 2015 from wild plants of *T. bellirica* were purchased from Kerala Forest Research Institute, Peechi, India. The specimen sample was

deposited at the institute with voucher number SBSBRL 23. After drying in shade for few days, the fruits were de-seeded, finely powdered and stored in an airtight container until used for extraction.

Preparation of extract

The fruit powder (50 g) was defatted with petroleum ether and then extracted with 70% aqueous acetone (300 ml) in a mechanical shaker for 72 h. The extracts were filtered through Whatman No. 1 filter paper, concentrated to dryness in a rotary evaporator, lyophilized and then stored at 4 °C until use. The percentage of yield was found to be 7.53%.

HPLC analysis of AATB

HPLC analysis of AATB was done using a Waters HPLC system Model 1525 equipped with dual pump and a UV detector. The mobile phase was a mixture of solvents: acetonitrile (Solvent A) and (0.05%) TFA in water (Solvent B, pH 2.25). The chromatographic separation was carried out in a linear gradient elution mode on an RP-18 column (SunFire, Waters, USA) with 5 μ m particle size, 4.6 mm internal diameter and 150 mm length as follows: 0 min 90% B, 10 min 80% B, 15 min 72% B, 20 min 65% B, 25 min 50% B and then at 26 min restoring the initial condition at 35 min. The mobile phase flow rate was 1.0 mL/min, and the injection volume was 20 μ L. The chromatographic runs were carried out at 25 °C. The photodiode array detector wavelength was set at 270 nm for the determination of different components.

Cell culture and treatments

RAW 264.7 macrophage cell line was purchased from the National Centre for Cell Sciences (NCCS), Pune, India and maintained in Dulbecco's modified Eagles medium (Gibco, Invitrogen). The lipopolysaccharide (1 μ g/mL) was used to activate the inflammatory response in RAW 264.7 cells. The different concentration (6.25, 12.5, 25, 50 and 100 μ g/mL) of the sample solution was added to the LPS stimulated RAW cells. Diclofenac sodium was used as standard drug and incubated for 24 h. After incubation, the anti-inflammatory assays were performed using the cell lysates.

Measurement of cell viability by MTT assay

The MTT assay was performed by using the procedure described by Talarico et al. (Talarico et al. 2004). Absorbance of the formazan solution was quantified by an ELISA microplate reader at 570 nm.

Measurement of total COX activity

The COX activity was analysed by the method of Shimizu et al. (Shimizu et al. 1981). COX activity was determined by reading absorbance at 632 nm.

Measurement of 5-LOX activity

The 5-LOX activity was estimated as per the method described by Axelrod et al. (1981).

Measurement of myeloperoxidase activity

Myeloperoxidase activity was assayed by the method described by Suzuki et al. (1983).

Estimation of cellular nitrate levels

The nitrate level was estimated by Greiss reaction described by (Bryan and Grisham 2007).

Measurement of inducible nitric oxide synthase

Nitric oxide synthase was determined by the method described by Salter et al. (1996).

Imaging and quantification of intracellular ROS generation

The ROS level was determined by the procedure described by Vysakh et al. and the fluorescence was measured using a fluorimeter at 470 nm excitation and emission at 635 nm (Qubit 3.0, Life technologies, USA) and expressed in arbitrary units (Vysakh et al. 2018).

Reverse transcription-polymerase chain reaction

The gene level expression of COX-2, TNF- α , IL-6 mRNA was measured by semi-quantitative Reverse Transcription-Polymerase Chain Reaction (RT-PCR) (Vysakh et al. 2018). The sequence of primers used for the study was depicted in Table 1.

Table 1 The sequence of primers used for the study

Gene	Forward primer	Reverse primer
COX -2	5'-GGAGAGACTATCAAGATAGT-3'	5'-ATGGTCAGTAGACTTTTACA-3'
IL-6	5'-GGTACATCCTCGACGGCATCT-3'	5'-GAGGATACCACTCCCAACAGACC3'
TNF- α	5'-CCCAGGCAGTCAGATCATCTTC-3'	5'-AGCTGCCCTCAGCTTGA3'
GAPDH	5'AATGCATCCTGCACCACCAACTGC-3'	5'GGAGGCCATGTAGGCCATGAGGTC3'

Statistical analysis

All the data were expressed as mean \pm standard deviation ($n = 3$) and the results were analysed by one-way ANOVA followed by Tukey's post hoc analysis using GraphPad Prism $\text{\textcircled{C}}$ version 5.03 for Windows (GraphPad Software, San Diego, CA, USA). A value of $p < 0.05$ was considered as statistically significant.

Results

HPLC analysis of AATB

HPLC analysis of AATB shows the presence of compounds like Ellagic acid, Ferulic acid and quercetin. The compounds were identified by using standards of the pure compounds. The ellagic acid standard has a retention time value of 11.08 min, ferulic acid standard has a retention time value of 11.49 min and quercetin standard has a retention time value of 13.05, respectively. AATB have retention time values of 11.09, 11.84, 13.38, respectively, which corresponds to retention time values of the standard compounds (Fig. 1).

Invitro cytotoxicity against RAW 264.7 murine macrophage cell lines

For determining the cell viability, we used MTT assay. Cell viabilities at different plant concentrations (6.25, 12.5, 25, 50 and 100 $\mu\text{g/ml}$) were studied and it was found that at 100 $\mu\text{g/ml}$ of sample concentration, 84.48% of cells were viable. From this assay we understood that, at higher concentration (100 $\mu\text{g/ml}$) the cell growth was effective; therefore, our plant extract (AATB) is non-toxic and did not show any cytotoxic effect. So 25, 50 and 100 $\mu\text{g/ml}$ doses were used for further studies (Fig. 2).

Inhibition of total COX activity by AATB plant extract

AATB extract inhibited total COX activity in a dose-dependent manner. When RAW 264.7 murine macrophage cells were induced with LPS (1 $\mu\text{g/ml}$), the total COX activity was shown to be increased. When treated with AATB extract, the total COX activity was significantly decreased ($p < 0.05$) as compared to the different concentrations of the standard

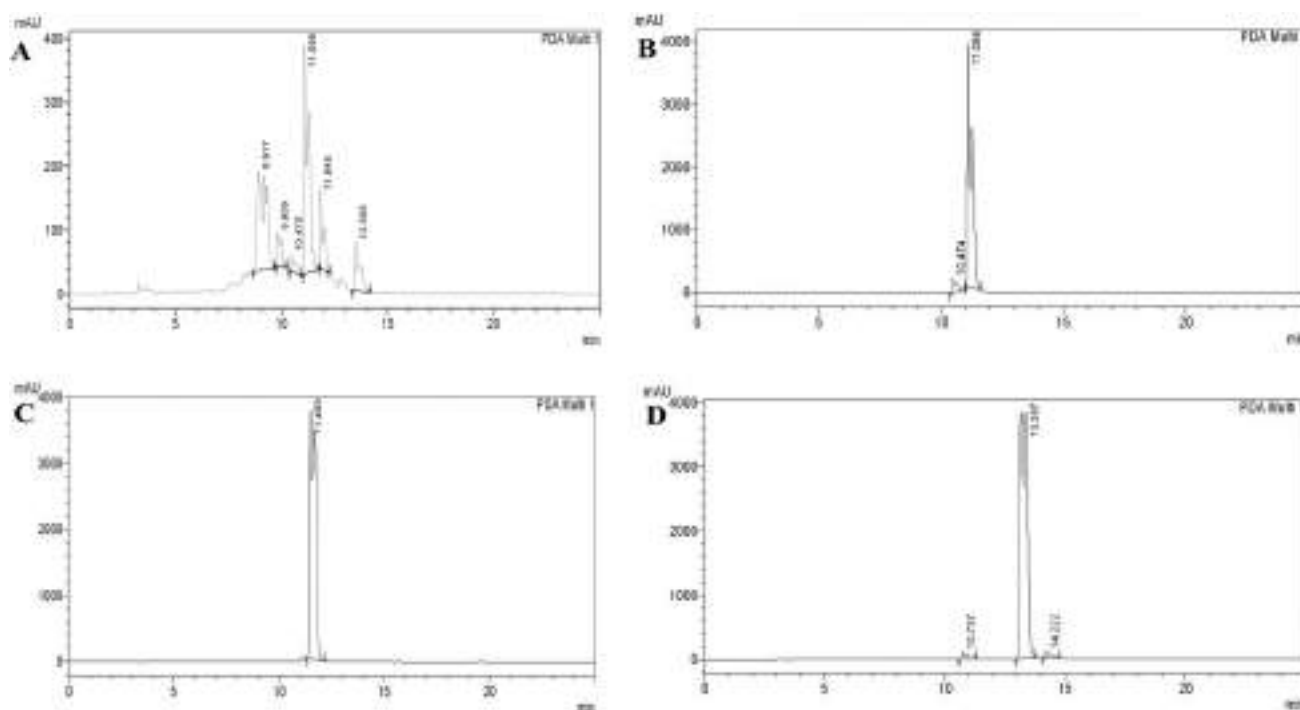
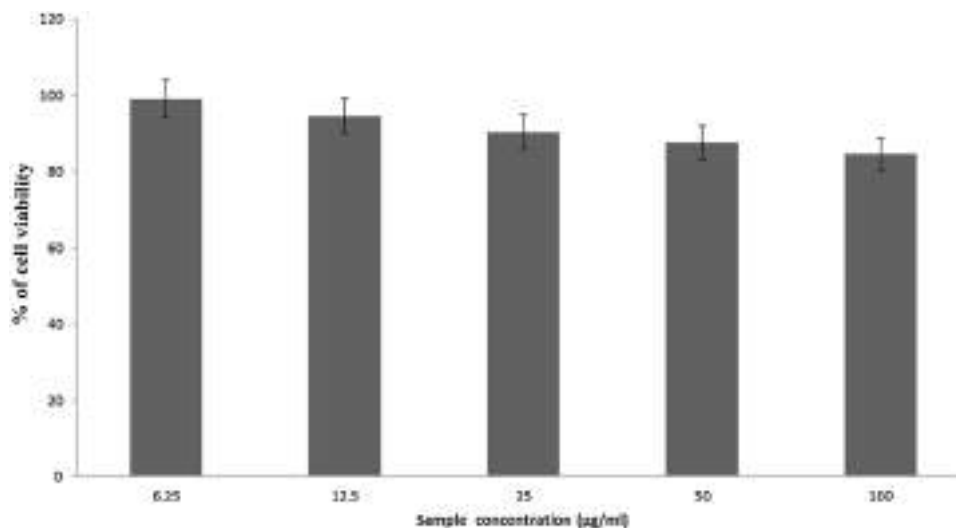


Fig. 1 HPLC analysis of AATB. **a** AATB, **b** ellagic acid standard, **c** ferulic acid standard, **d** quercetin standard

Fig. 2 Effect of AATB on cell viability in Raw 264.7 cells. The effect of AATB at various concentrations (6.25–100 $\mu\text{g}/\text{ml}$) on cell viability in RAW 264.7 cells determined using MTT assay. Values are means of three replicate determinations ($n=3$) \pm standard deviation



drug diclofenac. The total COX activity was represented as percentage of inhibition (Fig. 3).

Inhibition of total 5-LOX activity by AATB plant extract

AATB extract inhibited 5-LOX activity in a dose-dependent manner. When RAW 264.7 murine macrophage cells were induced with LPS (1 $\mu\text{g}/\text{ml}$), the total 5-LOX activity was shown to be increased. When treated with AATB extract,

the 5-LOX activity was significantly decreased ($p < 0.05$) as compared to the standard drug diclofenac. At 100 $\mu\text{g}/\text{ml}$ AATB concentration, 54.34% of 5-LOX inhibitory activity was observed (Fig. 4).

Effect of AATB on nitrate level

When RAW 264.7 murine macrophage cell lines were induced with LPS, the nitrate levels increased abruptly. Treatment with AATB extract significantly decreased

Fig. 3 Effect of AATB on total COX activity in RAW 264.7 cells: RAW 264.7 cells were pre-treated with LPS (1 µg/ml) concentration for 1 h and then incubated with AATB at various concentrations (25, 50 and 100 µg/ml) for 24 h along with the standard drug diclofenac (DIC). Values are means of three replicate determinations ($n = 3$) ± standard deviation

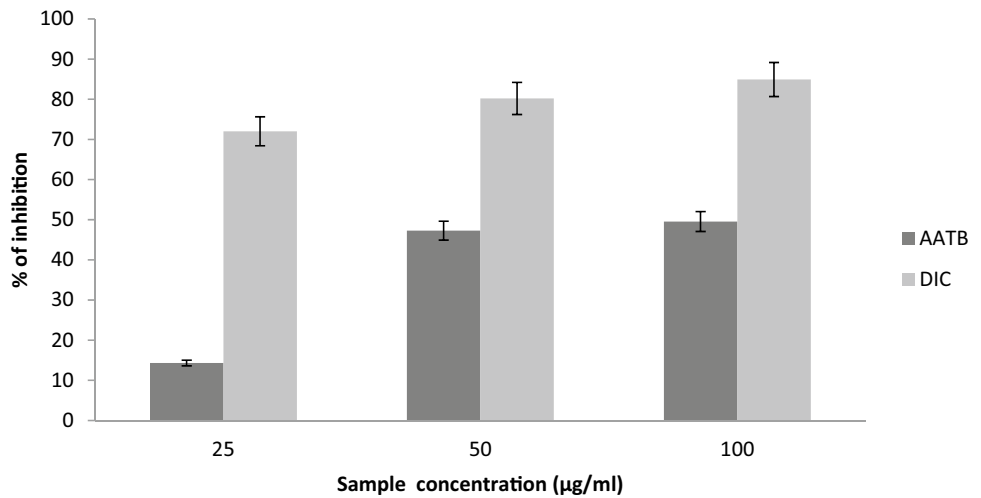
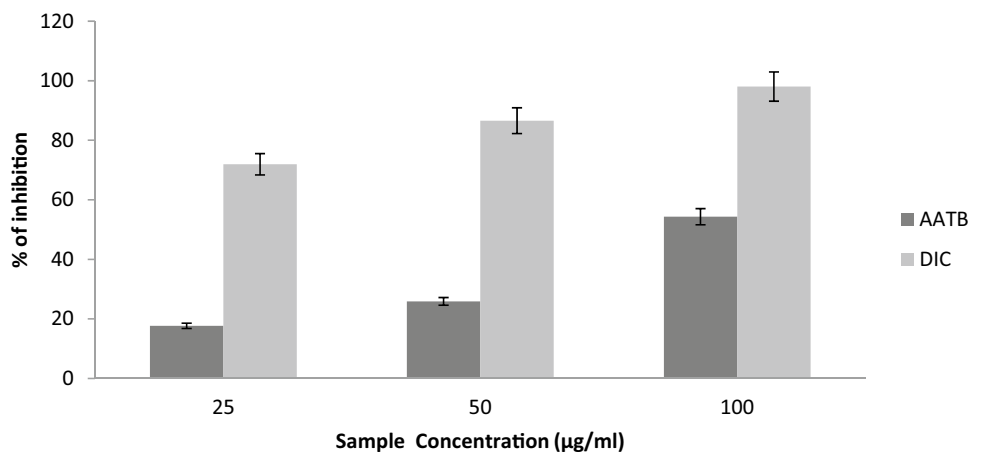


Fig. 4 Effect of AATB on 5-LOX activity in RAW 264.7 cells: RAW 264.7 cells were pre-treated with LPS (1 µg/ml) concentration for 1 h and then incubated with AATB at various concentrations (25, 50 and 100 µg/ml) for 24 h along with the standard drug diclofenac (DIC). Values are means of three replicate determinations ($n = 3$) ± standard deviation



($p < 0.05$) the nitrate level as compared to LPS control (Fig. 5).

Inhibition of myeloperoxidase activity by AATB extract

In LPS induced RAW 264.7 murine macrophage cell lines, an increase in MPO activity was observed. Treatment with AATB plant extract showed a significant decrease ($p < 0.05$) in MPO activity at 100 µg/ml sample concentration (Fig. 6).

Effect of AATB on iNOS production

iNOS is an important marker in inflammation. In LPS induced RAW 264.7 murine macrophage cell lines, a significant increase in iNOS activity was observed. The AATB plant extract treatment significantly decrease ($p < 0.05$) the iNOS activity at 100 µg/ml sample concentration when compared to the LPS control (Fig. 7).

Effect of AATB on intracellular ROS generation

The LPS stimulation increases the ROS level in RAW 264.7 murine macrophage cells. The significant reduction in ROS level was observed in AATB treated cells as compared to LPS control. Results are depicted in Fig. 8.

Gene expression studies

During LPS stimulation in RAW 264.7 murine macrophage cell lines, inflammatory cytokines such as TNF- α , IL-6 and inflammatory marker genes like COX-2 were markedly upregulated. Downregulated expression of TNF- α , IL-6 and COX-2 were seen in AATB treated group as compared to LPS treated groups (Fig. 9).

Fig. 5 Effect of AATB on nitrate level in RAW 264.7 cells: RAW 264.7 cells were pre-treated with LPS (1 $\mu\text{g}/\text{ml}$) concentration for 1 h and then incubated with AATB at various concentrations (25, 50 and 100 $\mu\text{g}/\text{ml}$) and DIC for 24 h. Values are means of three replicate determinations ($n = 3$) \pm standard deviation. ^a statistically different from LPS control

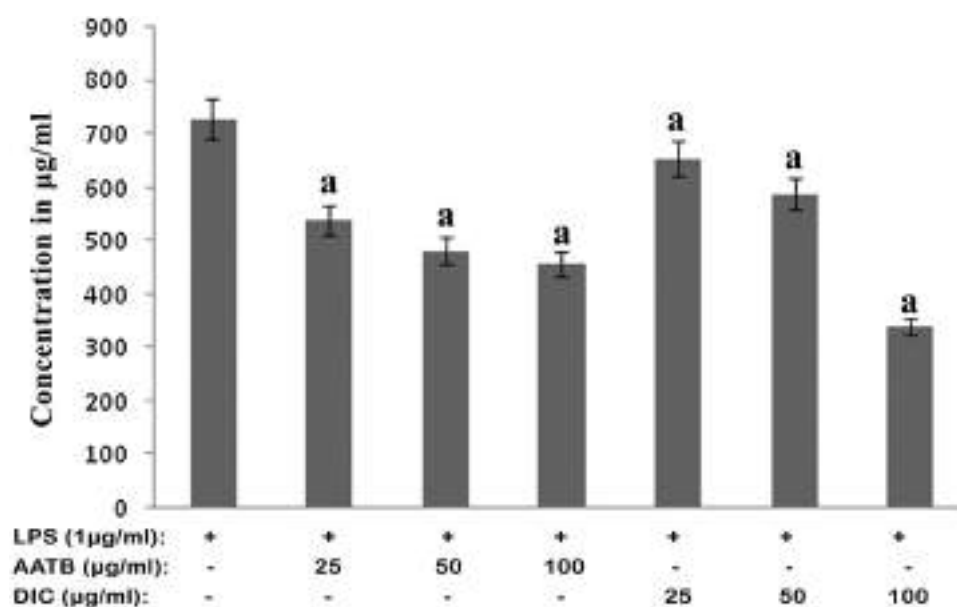
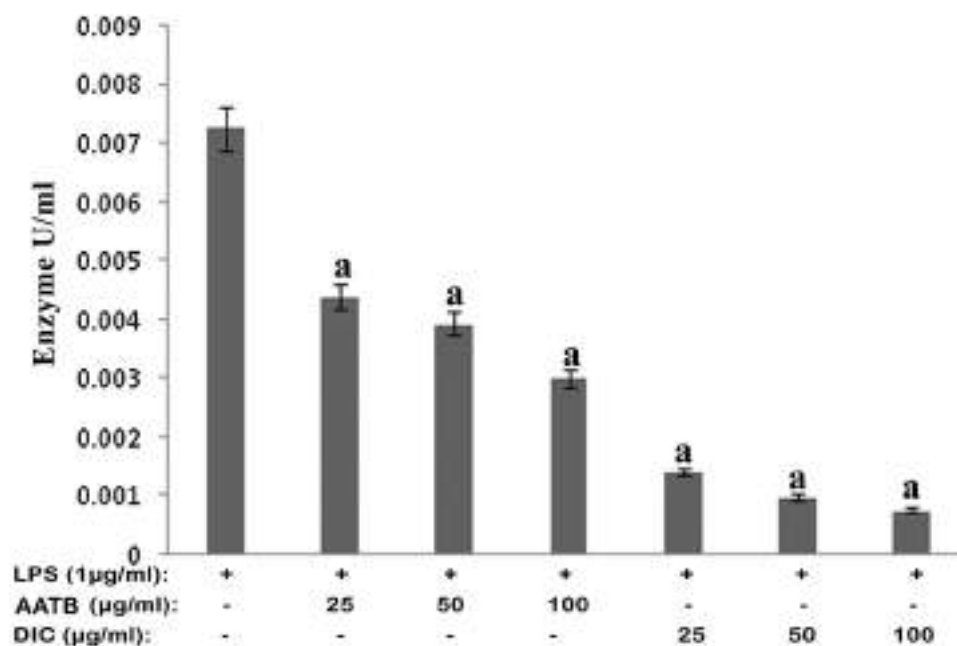


Fig. 6 Effect of AATB on MPO activity in RAW 264.7 cells. RAW 264.7 murine macrophage cells were pre-treated with LPS (1 $\mu\text{g}/\text{ml}$) concentration for 1 h and then incubated with AATB (25, 50, 100 $\mu\text{g}/\text{ml}$) and the standard drug diclofenac (DIC) at a concentration of 10 $\mu\text{g}/\text{ml}$ for 24 h. Values are means of three replicate determinations ($n = 3$) \pm standard deviation. ^astatistically different from LPS control



Discussion

Inflammation is a complex biological reaction to harmful stimuli and is associated with many pathophysiological conditions (Park et al. 2010). Macrophages play an essential role in local host defense and inflammatory responses (Park et al. 2010). In response to inflammatory stimuli, activated macrophages produce various proinflammatory factors, including COX-2, TNF- α , IL-6, iNOS and nitric oxide (NO) (Manzi and Wasiko 2000). NO is produced by mammalian cells and performs an important role in

many diseases such as inflammation, hypertension, diabetes, rheumatoid arthritis, bowel disease and atherosclerosis (Kolesov et al. 2013). LPS stimulation in RAW 264.7 murine macrophage cells reinforces the enzymatic activity of both COX and 5-LOX, which in turn activate the tremendous production of prostaglandins and leukotrienes. COX catalyzes the biosynthesis of inflammatory mediators such as prostaglandin, thromboxane and prostacyclin. Inhibition of COX was treated to be partly answerable for the anti-inflammatory activity (Zhao et al. 2009).

Traditional plant-based therapeutic agents have been getting overwhelming attention and popularity because of

Fig. 7 Effect of AATB on iNOS activity in RAW 264.7 cells: RAW 264.7 cells were pre-treated with LPS (1 µg/ml) concentration for 1 h and then incubated with AATB at various concentrations (25, 50 and 100 µg/ml) for 24 h. Values are means of three replicate determinations ($n=3$) ± standard deviation. ^a statistically different from LPS control

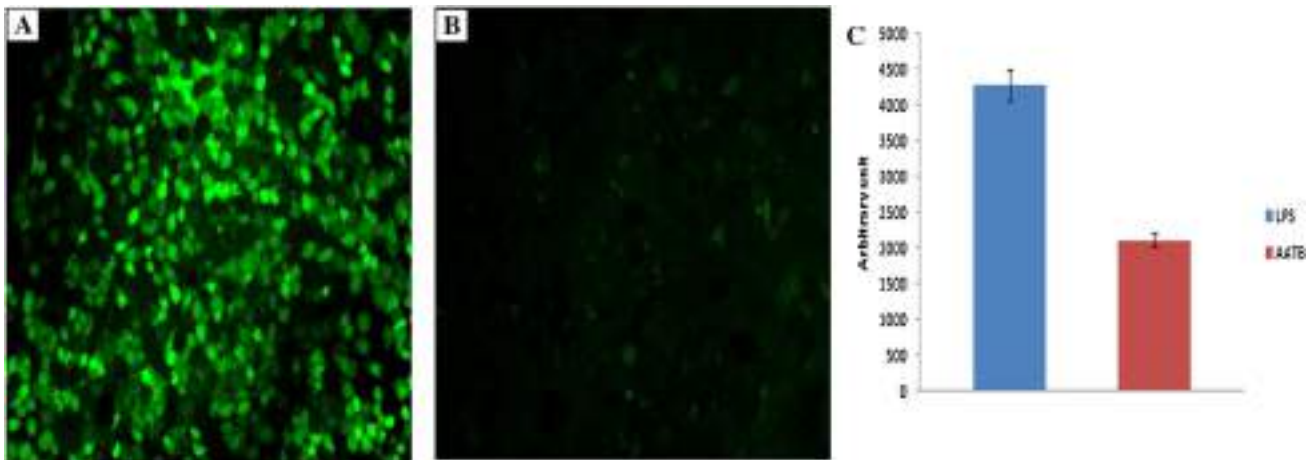
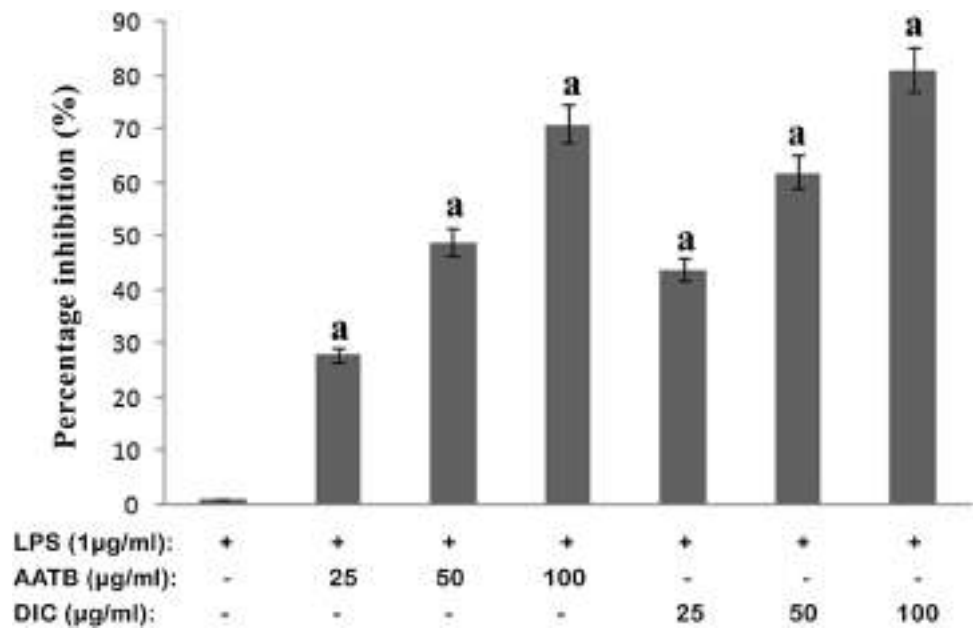


Fig. 8 Fluorescent staining of ROS generation in RAW 264.7 cells: RAW 264.7 cells treated with AATB at a concentration of 100 µg/ml. The fluorescence was measured using a fluorimeter at 470 nm excita-

tion and emission at 635 nm (Qubit 3.0, Life technologies, USA) and expressed in arbitrary units. **a** LPS; **b** LPS + AATB. Values are mean of three replicate determinations ($n=3$) ± standard deviation

the presumption that they are safe, nontoxic and effective in providing the health benefits (Manaharan et al. 2014). *T. bellirica* (Gaertn.) Roxb is a traditional medicinal plant used for diarrhoea, dyspepsia, biliousness, cough, bronchitis and upper respiratory tract infections, tropical pulmonary eosinophilia and allergic eruptions in the traditional systems of medicine (Khare 2007). Various parts of the plant have been used as a medicinal agent and there are several reports regarding the medicinal value of the plant (Desai et al. 2014). The current studies focus on the anti-inflammatory activity of RAW 264.7 murine macrophage cell line on AATB plant extract.

The AATB plant extract at higher concentration (100 µg/ml) did not show any toxicity in MTT assay. Therefore, the AATB plant extract can be used for studies on anti-inflammatory activity without any side effects.

COX-1 and COX-2 are the isoforms of cyclooxygenase enzymes and produce prostaglandins via arachidonic acid metabolic pathway (Graham et al. 2013). COX-2 is expressed in case of inflammatory stimuli and present in macrophages, leukocytes, fibroblasts and synovial cells. The treatment of AATB reduces the total COX activity in a dose-dependent manner and also helps to downregulate the COX-2 gene, one of the key markers specific for inflammation. The result

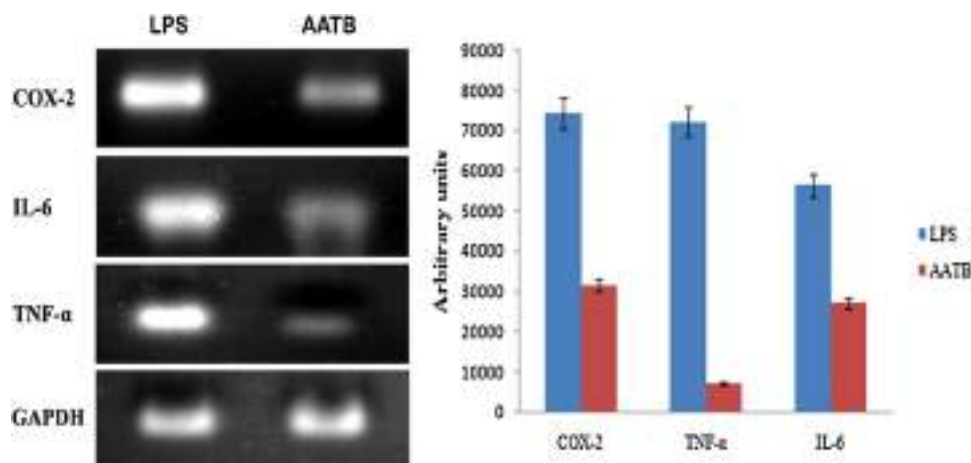


Fig. 9 RT-PCR gel of COX-2, IL-6, TNF- α mRNA in RAW 264.7 cells: Inhibitory effect of AATB on the expression of the proinflammatory markers like COX-2, and cytokines like IL-6, TNF- α was determined by reverse transcriptase-PCR. GAPDH was used as the control. The gene expression of COX-2, IL-6 and TNF- α in the LPS

stimulated group was upregulated. Downregulated expressions of COX-2, IL-6 and TNF- α were seen in the AATB treated group as compared to the LPS treated group. AATB: Aqueous Acetone fraction of *T. bellirica*

from the present study shows that AATB has the ability to suppress COX-2 expression and ameliorate the inflammation. The AATB attained this via blockage of arachidonic acid pathway of prostaglandin synthesis.

5-LOX catalyses the production of leukotrienes from arachidonic acid; it is generally produced from cell types that drive inflammatory processes like macrophages and neutrophils (Liu et al. 1991). The current study was carried out to evaluate 5-LOX activity in RAW 264.7 cells. During inflammation in LPS stimulated RAW264.7 murine macrophage cell lines, 5-LOX activity was shown to be increased (Pramod et al. 2015). This was diminished when the cells were treated with AATB plant extract. Therefore, our plant extract has the potential to inhibit the 5-LOX activity, so it can be used as a 5-LOX inhibiting drug.

Similarly, we evaluated the nitrate level and iNOS activity in LPS stimulated RAW264.7 murine macrophage cell lines. NO is a highly reactive free radical and a multifunctional gaseous molecule synthesized from L-arginine by iNOS and is related to various physiological and pathophysiological processes, including vascular functions, neurological functions and cytotoxic functions in activated inflammatory cells (Kubes and McCafferty 2000). iNOS and nitrate level activity has shown to be increased by treating with LPS, whereas treatment with AATB plant extract showed sufficient decrease in nitrate level and iNOS level as compared to the standard drug DIC.

MPO plays a central role in oxidant production by neutrophils. Also, it is the most abundant pro-inflammatory enzyme (Pulli et al. 2013; Dillingh et al. 2014) which is secreted during inflammatory response and contributes to arthritis development (Breckwoldt et al. 2008; García

et al. 2014). MPO activity was determined in LPS stimulated RAW 264.7 murine macrophage cell lines. Upon LPS stimulation, the MPO activity was shown to be increased, whereas treatment with AATB extract decreased the MPO activity. So, our plant extract can be used as a powerful drug to inhibit MPO activity in RAW 264.7 murine macrophage cell lines.

Reactive oxygen species are the key factor behind the progression of inflammatory disorders. An elevated level of ROS generation at the site of inflammation by polymorphonuclear neutrophils (PMNs) causes endothelial dysfunction and tissue injury (Mittal et al. 2014). The ROS activity within the cell was measured by using dichloro-dihydro-fluorescein diacetate (DCFH-DA) assay. The DCFH-DA diffused into the cell and was deacetylated by cellular esterases. The non-fluorescent compound produced during deacetylation was later oxidized by ROS into 2', 7' -dichlorofluorescein (DCF) which emits green fluorescence upon excitation with a blue filter (Ramachandran et al. 2014). ROS production was increased upon LPS stimulation, and was reduced to normal levels by AATB plant extract. Therefore, our plant extract has high anti-oxidant properties.

Cytokines are the important biomolecules that can act as both anti-inflammatory or pro-inflammatory in nature. The inflammatory cytokines, like tumour necrosis factor- α and IL-6, are produced by activated monocytes, macrophages, fibroblasts, mast cells and natural killer cells (Chandrasenan et al. 2016). Blocking of these cytokines is considered an effective therapeutic approach to treat inflammatory diseases (Esposito and Cuzzocrea 2009; Tanaka et al. 2012). Besides inflammatory cytokines, prostaglandin E2 also plays a vital role in inflammatory response.

Cyclooxygenase-2 is the key enzyme behind the production of PGE₂ and is stimulated by cytokines, endotoxin, or growth factors (Kang et al. 2007). Nuclear factor kappa-B also plays an important role in the production of these pro-inflammatory mediators (Saklatvala et al. 2003). The LPS treatment in RAW 264.7 macrophages initiates the upregulation of proinflammatory cytokines such as tumour necrosis factor-alpha, interleukin-6 and proinflammatory mediator enzyme COX-2. The upregulated expressions of these genes were suppressed by the treatment of AATB at a concentration of 100 µg/ml. This result showed the potential effect of AATB in curing inflammatory mediators generated during inflammation via various pathways.

Conclusion

In conclusion, our findings indicate that AATB was able to attenuate the chronic inflammatory response by suppressing many inflammatory mediators including COX-2, 5-LOX, MPO, NO, iNOS level and ROS in RAW 264.7 murine macrophage cells stimulated with LPS. Furthermore, AATB suppressed the mRNA expressions of genes like COX-2, TNF-α and IL-6, so our plant extract has high anti-inflammatory and antioxidant properties, and hence may be used as a potent natural anti-inflammatory therapeutic agent.

Acknowledgements The authors are grateful to School of Biosciences, Mahatma Gandhi University and Biogenix Research Center, Poojapura, Thiruvananthapuram, India for providing the excellent research support.

Compliance with ethical standards

Conflict of interest The authors declare that they have no conflict of interest.

Ethical approval This article does not contain any studies with human participants or animals performed by any of the authors.

References

Anatoliotakis N, Deftereos S, Bouras G et al (2013) Myeloperoxidase: expressing inflammation and oxidative stress in cardiovascular disease. *Curr Top Med Chem* 13:115–138

Axelrod B, Cheesbrough TM, Laakso S (1981) [53] Lipoygenase from soybeans. EC 1.13.11.12 Linoleate:oxygen oxidoreductase. *Methods Enzymol* 71:441–451. [https://doi.org/10.1016/0076-6879\(81\)71055-3](https://doi.org/10.1016/0076-6879(81)71055-3)

Breckwoldt MO, Chen JW, Stangenberg L et al (2008) Tracking the inflammatory response in stroke in vivo by sensing the enzyme myeloperoxidase. *Proc Natl Acad Sci USA* 105:18584–18589. <https://doi.org/10.1073/pnas.0803945105>

Bryan NS, Grisham MB (2007) Methods to detect nitric oxide and its metabolites in biological samples. *Free Radic Biol Med* 43:645–657. <https://doi.org/10.1016/j.freeradbiomed.2007.04.026>

Camu F, Shi L, Vanlersberghe C (2003) The role of COX-2 inhibitors in pain modulation. *Drugs* 63(Suppl 1):1–7

Chandrasenan P, Anjumol V, Neethu M et al (2016) Cytoprotective and antiinflammatory effect of polyphenolic fraction from red cabbage (*Brassica oleracea* Linn var. capitata f rubra) in experimentally induced ulcerative colitis. *J Appl Pharm Sci*. <https://doi.org/10.7324/japs.2016.600122>

Cho K-J, Seo J-M, Kim J-H (2011) Bioactive lipoygenase metabolites stimulation of NADPH oxidases and reactive oxygen species. *Mol Cells* 32:1–5. <https://doi.org/10.1007/s10059-011-1021-7>

Chow JC, Young DW, Golenbock DT et al (1999) Toll-like receptor-4 mediates lipopolysaccharide-induced signal transduction. *J Biol Chem* 274:10689–10692

Deb A, Barua S, Das B (2016) Pharmacological activities of Baheda (*Terminalia bellirica*): a review. *Jpp* 5:194–197

Desai JS, Chaudhari S, Adam A, Chaudhari H (2014) Effect of alcoholic extract of *Terminalia Bellirica* Roxb. in dextran sulfate sodium induced colitis. *World J Pharm Pharm Sci* 3:2121–2133

Dillingh MR, van Poelgeest EP, Malone KE et al (2014) Characterization of inflammation and immune cell modulation induced by low-dose LPS administration to healthy volunteers. *J Inflamm* 11:28. <https://doi.org/10.1186/s12950-014-0028-1>

Dubey NK, Kumar R, Tripathi P (2004) Global promotion of herbal medicine: India's opportunity. *Curr Sci* 86:37–41

Esposito E, Cuzzocrea S (2009) TNF-alpha as a therapeutic target in inflammatory diseases, ischemia-reperfusion injury and trauma. *Curr Med Chem* 16:3152–3167

Ferrero-Miliani L, Nielsen OH, Andersen PS, Girardin SE (2007) Chronic inflammation: importance of NOD2 and NALP3 in interleukin-1β generation. *Clin Exp Immunol* 147:227–235

García JJ, López-Pingarrón L, Almeida-Souza P et al (2014) Protective effects of melatonin in reducing oxidative stress and in preserving the fluidity of biological membranes: a review. *J Pineal Res* 56:225–237. <https://doi.org/10.1111/jpi.12128>

Graham GG, Davies MJ, Day RO et al (2013) The modern pharmacology of paracetamol: therapeutic actions, mechanism of action, metabolism, toxicity and recent pharmacological findings. *Inflammopharmacology* 21:201–232. <https://doi.org/10.1007/s10787-013-0172-x>

Jayesh K, Helen LR, Vysakh A et al (2017a) In vivo toxicity evaluation of aqueous acetone extract of *Terminalia bellirica* (Gaertn.) Roxb. fruit. *Regul Toxicol Pharmacol* 86:349–355. <https://doi.org/10.1016/j.yrtph.2017.04.002>

Jayesh K, Raisa HL, Vysakh A et al (2017b) *Terminalia bellirica* (Gaertn.) Roxb. fruit mitigates CCl₄ induced oxidative stress and hepatotoxicity in rats. *Biomed Pharmacother* 93:327–333. <https://doi.org/10.1016/j.biopha.2017.06.080>

Jayesh K, Helen LR, Vysakh A et al (2018) Protective role of *Terminalia bellirica* (Gaertn.) roxb fruits against CCl₄ induced oxidative stress and liver injury in rodent model. *Indian J Clin Biochem*. <https://doi.org/10.1007/s12291-017-0732-8>

Kang Y-J, Mbonye UR, DeLong CJ et al (2007) Regulation of intracellular cyclooxygenase levels by gene transcription and protein degradation. *Prog Lipid Res* 46:108–125. <https://doi.org/10.1016/j.plipres.2007.01.001>

Khare C (2007) *Indian medicinal plants*. Springer, New York

Kolesov SA, Korkotashvili LV, Yazykova AB et al (2013) S-nitrosothiols, nitric oxide and proinflammatory cytokines in children with inflammatory bowel disease. *Clin Lab* 59:953–957

Kubes P, McCafferty DM (2000) Nitric oxide and intestinal inflammation. *Am J Med* 109:150–158

Liu MC, Hubbard WC, Proud D et al (1991) Immediate and late inflammatory responses to ragweed antigen challenge of the peripheral airways in allergic asthmatics: cellular, mediator, and permeability changes. *Am Rev Respir Dis* 144:51–58. <https://doi.org/10.1164/ajrccm/144.1.51>

- Manaharan T, Chakravarthi S, Radhakrishnan AK, Palanisamy UD (2014) In vivo toxicity evaluation of a standardized extract of *Syzygium aqueum* leaf. *Toxicol Reports* 1:718–725. <https://doi.org/10.1016/j.toxrep.2014.09.006>
- Manzi S, Wasko MC (2000) Inflammation-mediated rheumatic diseases and atherosclerosis. *Ann Rheum Dis* 59:321–325
- Masferrer JL, Zweifel BS, Manning PT et al (1994) Selective inhibition of inducible cyclooxygenase 2 in vivo is antiinflammatory and nonulcerogenic. *Proc Natl Acad Sci USA* 91:3228–3232
- Meena AK, Bansal P, Kumar S (2009) Plants-herbal wealth as a potential source of ayurvedic drugs. *Asian J Tradit Med* 4:152–170
- Mittal M, Siddiqui MR, Tran K et al (2014) Reactive oxygen species in inflammation and tissue injury. *Antioxid Redox Signal* 20:1126–1167. <https://doi.org/10.1089/ars.2012.5149>
- Murakami A, Ohigashi H (2007) Targeting NOX, INOS and COX-2 in inflammatory cells: chemoprevention using food phytochemicals. *Int J Cancer* 121:2357–2363. <https://doi.org/10.1002/ijc.23161>
- Park S-B, Kim M-S, Lee HS et al (2010) 1,2,3,6-tetra-*O*-galloyl-beta-D-allopyranose gallotannin isolated, from *Euphorbia jolkini*, attenuates LPS-induced nitric oxide production in macrophages. *Phytother Res* 24:1329–1333. <https://doi.org/10.1002/ptr.3110>
- Pramod C, Neethu M, Anjumol V et al (2015) Triterpenoids isolated from *Euphorbia tirucalli* Linn. inhibit lipopolysaccharide-mediated inflammatory response in RAW264.7 murine macrophage cell line. *Int J Adv Res* 3:1091–1099
- Pulli B, Ali M, Forghani R et al (2013) Measuring myeloperoxidase activity in biological samples. *PLoS One* 8:e67976. <https://doi.org/10.1371/journal.pone.0067976>
- Ramachandran R, Saraswathy M, Marques PE et al (2014) Up-regulation of nuclear related factor 2 (NRF2) and antioxidant responsive elements by metformin protects hepatocytes against the acetaminophen toxicity. *Toxicol Res (Camb)* 3:350. <https://doi.org/10.1039/C4TX00032C>
- Saklatvala J, Dean J, Clark A (2003) Control of the expression of inflammatory response genes. *Biochem Soc Symp* 70:95–106
- Salter M, Duffy C, Garthwaite J, Strijbos PJ (1996) Ex vivo measurement of brain tissue nitrite and nitrate accurately reflects nitric oxide synthase activity in vivo. *J Neurochem* 66:1683–1690
- Schletter J, Heine H, Ulmer AJ, Rietschel ET (1995) Molecular mechanisms of endotoxin activity. *Arch Microbiol* 164:383–389
- Shimizu T, Kondo K, Hayaishi O (1981) Role of prostaglandin endoperoxides in the serum thiobarbituric acid reaction. *Arch Biochem Biophys* 206:271–276. [https://doi.org/10.1016/0003-9861\(81\)90091-6](https://doi.org/10.1016/0003-9861(81)90091-6)
- Suzuki K, Ota H, Sasagawa S et al (1983) Assay method for myeloperoxidase in human polymorphonuclear leukocytes. *Anal Biochem* 132:345–352
- Sweet MJ, Hume DA (1996) Endotoxin signal transduction in macrophages. *J Leukoc Biol* 60:8–26
- Tak PP, Firestein GS (2001) NF-kappaB: a key role in inflammatory diseases. *J Clin Invest* 107:7–11. <https://doi.org/10.1172/JCI11830>
- Talarico LB, Zibetti RGM, Faria PCS et al (2004) Anti-herpes simplex virus activity of sulfated galactans from the red seaweeds *Gymnogongrus griffithsiae* and *Cryptonemia crenulata*. *Int J Biol Macromol* 34:63–71. <https://doi.org/10.1016/j.ijbiomac.2004.03.002>
- Tanaka T, Narazaki M, Kishimoto T (2012) Therapeutic targeting of the interleukin-6 receptor. *Annu Rev Pharmacol Toxicol* 52:199–219. <https://doi.org/10.1146/annurev-pharmtox-010611-134715>
- Ulevitch RJ, Tobias PS (1995) Receptor-dependent mechanisms of cell stimulation by bacterial endotoxin. *Annu Rev Immunol* 13:437–457. <https://doi.org/10.1146/annurev.iy.13.040195.002253>
- Vysakh A, Gopika P, Jayesh K et al (2018) *Rotula aquatica* Lour attenuates secretion of proinflammatory mediators and cytokines in lipopolysaccharide-induced inflammatory responses in murine RAW 264.7 macrophages. *Inflammopharmacology* 26(1):29–38
- Whelton A, Hamilton CW (1991) Nonsteroidal anti-inflammatory drugs: effects on kidney function. *J Clin Pharmacol* 31:588–598. <https://doi.org/10.1002/j.1552-4604.1991.tb03743.x>
- Zhao F, Wang L, Liu K (2009) In vitro anti-inflammatory effects of arctigenin, a lignan from *Arctium lappa* L., through inhibition on iNOS pathway. *J Ethnopharmacol* 122:457–462. <https://doi.org/10.1016/j.jep.2009.01.038>



Metal oxide nanoparticles in electrochemical sensing and biosensing: a review

Jaise Mariya George¹ · Arun Antony¹ · Beena Mathew¹

Received: 19 April 2018 / Accepted: 26 June 2018 / Published online: 4 July 2018
© Springer-Verlag GmbH Austria, part of Springer Nature 2018

Abstract

This review (with (318) refs) describes progress made in the design and synthesis of morphologically different metal oxide nanoparticles made from iron, manganese, titanium, copper, zinc, zirconium, cobalt, nickel, tungsten, silver, and vanadium. It also covers respective composites and their function and application in the field of electrochemical and photoelectrochemical sensing of chemical and biochemical species. The proper incorporation of chemical functionalities into these nanomaterials warrants effective detection of target molecules including DNA hybridization and sensing of DNA or the formation of antigen/antibody complexes. Significant data are summarized in tables. The review concludes with a discussion on current challenge and future perspectives.

Keywords Electrochemical sensing · Graphene · MWCNT · MCO_2O_4 · Nickel hydroxide electrodes · Electrocatalysis · Molecular imprinted polymer sensor · Sensitivity · Modified electrode · Amperometry

Introduction

Highly sensitive novel electroanalytical devices fabricated on nanostructured metal oxides are cost-effective and improve selectivity when coupled to biorecognition molecules [1]. Metal oxide nanoparticles (MO NPs) with different morphologies have been made through versatile methods. These MO NPs exhibit various types of electrical and photochemical properties due to their size, stability, and high surface area. The main functions of metal nanoparticles in electroanalysis involve the toughening of the conductive sensing interface, the catalytic properties of nanoparticles allowing their expansion with metals and the electrical contact of redox-centers in proteins with the surface of the transducers [2].

The fast electron transfer between the transducer and analyte molecule in presence of metal nanoparticles considered them as “electronic wires” and “electrocatalysts” because of its nanosize and structure [3]. The biocompatible MO NPs are generally used to immobilize biomolecules for the fabrication of immunosensors, enzyme sensors, and DNA sensors, while semiconducting nanoparticles are mainly used as markers and

tracers in the electrochemical study [4]. The strong affinity of MO NPs to the surface of the working electrode can be achieved by various techniques including physical adsorption, electrodeposition, chemical covalent bonding and electropolymerization [5].

Major transition MO NPs included in this review are oxides of iron, copper, cobalt, nickel, manganese, titanium, silver, vanadium, zirconium, zinc, and tungsten. Some disadvantages of these MO NPs are, they have wide band gap making them as semiconductors or even insulators, poor ion transport kinetics [6] and the pulverization of electrode film resulting from the pronounced volume expansion and contraction during the charging/discharging processes [7]. These unpleasant difficulties can be overcome by the hybridization with carbonaceous materials, other metal nanoparticles, and polymers (Fig. 1). This review emphasizes the significance of MO NPs in biological and chemical sensors. Nevertheless, as far as we know, no broad review based on MO NPs in electrochemical sensing has been reported so far.

Iron oxide nanoparticles

Hematite (Fe_2O_3) and magnetite (Fe_3O_4) nanoparticles impart a novel area in electrochemical sensing. The oxidation state is Fe^{3+} in Fe_2O_3 and two oxidation states such as Fe^{2+} and Fe^{3+} in Fe_3O_4 . The higher electrical conductivity of Fe_3O_4 at room temperature is due to the electron hopping processes between

✉ Beena Mathew
beenamathew@mgu.ac.in

¹ School of Chemical Sciences, Mahatma Gandhi University, Kottayam 686560, Kerala, India



From the journal:

Catalysis Science & Technology

Cobalt-catalyzed C–H activation: recent progress in heterocyclic chemistry

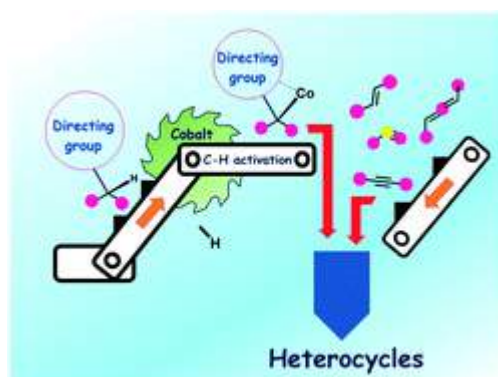


[Sankuviruthiyil M. Ujwaldev,^a](#) [Nissy Ann Harry,^a](#) [Mathiyazhagan Arun Divakar^a](#) and [Gopinathan Anilkumar^{ab}](#)

[Author affiliations](#)

Abstract

Cobalt-catalyzed C–H activation has gone through some major advancements in the past couple of decades. These reactions have proven to be highly efficient, selective, and atom-economical transformations without the requirement for pre-functionalization. These methodologies have found wide applications in heterocyclic chemistry for the synthesis and functionalization of heterocycles. This review focuses on the recent contributions made by cobalt-catalyzed C–H activation protocols toward heterocyclic chemistry from 2016 to 2018.



About

Cited by

Related

Buy this article

£42.50*

* Exclusive of taxes

This article contains 36 page(s)

Other ways to access this content

Log in

Using your institution credentials

Sign in

With your membership or subscriber account

Publication details

The article was received on 07 Jul 2018, accepted on 22 Oct 2018 and first published on 23 Oct 2018

Tweet

Share

Article type:

Minireview

DOI:

10.1039/C8CY01418C

Citation:

Catal. Sci. Technol., 2018, **8**, 5983-6018

BibTex



Go

[Request permissions](#)

Issue 18, 2018

[Previous](#)[Next](#)

From the journal:

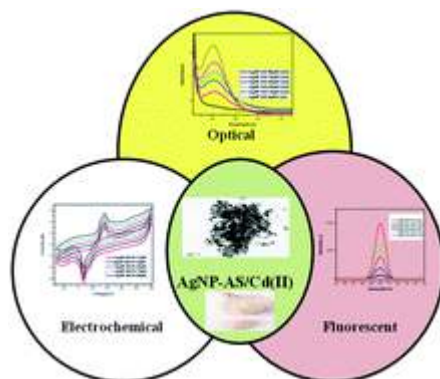
New Journal of Chemistry

Green silver nanoparticles as a multifunctional sensor for toxic Cd(II) ions

[Archana Aravind^a](#), [Maria Sebastian^a](#) and [Beena Mathew^{id} *^a](#)[Author affiliations](#)

Abstract

A highly sensitive and selective technique was developed for the detection of Cd(II) ions using green synthesized silver nanoparticles (AgNPs) from *Allium sativum* (AS) extract without any surface functionalization. The synthesized AgNP-AS was characterized by various analytical techniques. The aggregation of Cd(II) ions with AgNP-AS produces a color change from brown to golden yellow. The Cd(II) ion aggregation with AgNP-AS was studied by UV-vis spectroscopy, fluorescence spectroscopy, and electrochemical techniques. The limit of detection of the system was calculated by differential pulse voltammetry (DPV) and it was found to be 0.277 μM . The synthesized AgNP-AS shows high selectivity towards Cd(II) ions compared with various metal ions such as Ni(II), Cu(II), Zn(II), Cr(III), Fe(II), Pb(II), Co(II) and Hg(II) ions. Furthermore, AgNP-AS was applied for the sensing of Cd(II) ions in real samples collected from a lake, pigment, cosmetic product, and fertilizer industries. The synthesized AgNP-AS also exhibited antibacterial properties against waterborne bacteria like *Escherichia coli* and *Staphylococcus aureus* extracted from the lake water sample collected from the Ashtamudi lake, Kollam, Kerala.



About

Cited by

Related

Buy this article

£42.50*

* Exclusive of taxes

This article contains 10 page(s)

Other ways to access this content

Log in

Using your institution credentials

Sign in

With your membership or subscriber account

Publication details

The article was received on 25 Jul 2018, accepted on 06 Aug 2018 and first published on 08 Aug 2018

Tweet

Share



Network access provided by: Mahatma Gandhi University

Issue 40, 2018

[Previous](#)

[Next](#)



From the journal:

Physical Chemistry Chemical Physics

Halogen bond shortens and strengthens the bridge bond of [1.1.1]propellane and the open form of [2.2.2]propellane†



[Jyothish Joy](#),  ^a [Edakkandy Akhil](#)^b and [Eluvathingal D. Jemmis](#)  ^{*a}

[Author affiliations](#)

Abstract

Detailed electronic structural analysis of [1.1.1]propellane and the open form of [2.2.2]propellane, especially their highest occupied molecular orbital (HOMO), shows the existence of significant electronic congestion at their bridge bond. The HOMO of [1.1.1]propellane is a spread-out orbital of its inverted tetrahedral bridgehead atoms. The HOMO of the open form of [2.2.2]propellane is an anti-bonding combination of its bridgehead atoms due to the stabilizing through-bond interaction. This unique spatial disposition of the HOMO enables a high electron density at the bridgehead atoms. Herein, we utilize the electron scavenging power of halogen bond donors to extract a fraction of destabilizing electrons from the bridge bond with the aim to alleviate its electronic congestion, which results in shortening and strengthening of the bridge bond with a reduction in the bond order. This result answers the seminal question raised by K. B. Wiberg in 1983, "how can one have a relatively 'strong bond' without much bonding character?"

The article was received on 11 Aug 2018, accepted on 19 Sep 2018 and first published on 20 Sep 2018

Tweet

Share

Article type:

Paper

DOI:

10.1039/C8CP05125A

Citation:

Phys. Chem. Chem. Phys., 2018, 20, 25792-25798

BibTex

Go

[Request permissions](#)

Search articles by author

- Jyothish Joy
- Edakkandy Akhil
- Eluvathingal D. Jemmis

Go

Spotlight



Cite this: *New J. Chem.*, 2018, 42, 17138

Correction: An effective EMI shielding material based on poly(trimethylene terephthalate) blend nanocomposites with multiwalled carbon nanotubes

Ajitha A. R,^a Mohammed Arif P,^a Aswathi M. K,^a Lovely P. Mathew,^{ab} Geethamma V. G,^a Nandakumar Kalarikkal,^{ac} Sabu Thomas^{*ade} and Tatiana Volova^e

DOI: 10.1039/c8nj90098a

rsc.li/njc

Correction for 'An effective EMI shielding material based on poly(trimethylene terephthalate) blend nanocomposites with multiwalled carbon nanotubes' by Ajitha A. R *et al.*, *New J. Chem.*, 2018, **42**, 13915–13926.

The authors would like to correct the Acknowledgements section. The Acknowledgements section should read:

The authors would like to thank UGC, New Delhi, India (JRF scheme, ref. no. 17-06/2012(i) EU-V) for JRF research fellowship and Nanomission DST for the support. This study was financially supported by Project "Agropreparations of the new generation: a strategy of construction and realization" (Agreement No. 074-02-2018-328) in accordance with Resolution No. 220 of the Government of the Russian Federation of April 9, 2010, "On measures designed to attract leading scientists to the Russian institutions of higher learning".

The Royal Society of Chemistry apologises for these errors and any consequent inconvenience to authors and readers.

^a International and Inter University Centre for Nanoscience and Nanotechnology, Mahatma Gandhi University, Kottayam, Kerala 686 560, India.

E-mail: sabupolymer@yahoo.com, sabuthomas@mgu.ac.in

^b Viswajyothi College of Engineering and Technology, Muvattupuzha, Kerala 686 670, India

^c School of Pure and Applied Physics, Mahatma Gandhi University, Kottayam, Kerala 686 560, India

^d School of Chemical Sciences, Mahatma Gandhi University, Kottayam, Kerala 686 560, India

^e Siberian Federal University, 79 Svobodnyi Av., Krasnoyarsk, 660041, Russia





Log in / register

[All chapters](#)

[Previous](#)

[Next](#)



From the book:

Biobased Aerogels: Polysaccharide and Protein-based Materials

Chapter 1

Polysaccharide and Protein Based Aerogels: An Introductory Outlook

Rubie Mavelil-Sam, Laly A. Pothan and Sabu Thomas

Since the conception of aerogels in 1931 by Steven Kistler, they have become an advanced material of interest to scientists around the globe. Over recent years, as with other emerging materials, aerogels have taken a paradigm shift to more bio-based precursors. The underlying theme in this chapter, and in this book in general, comprises of a useful summary of the current progress and topical developments in the study of such bio-based aerogels composed of polysaccharides and proteins.

This content is free to download. Please choose one of the options below to gain access.

Log in

Using your FREE account

[Register for a FREE account](#)

Other ways to access this content

Log in

Using your institution credentials

Sign in

With your membership or subscriber account

Publication details

<https://doi.org/10.1039/9781782629979-00001>

Print publication date: 29 Aug 2018

Copyright year: 2018

Print ISBN: 978-1-78262-765-4

PDF eISBN: 978-1-78262-997-9

ePub eISBN: 978-1-78801-519-6

Citation:

BibTex

Go

From the book series:

[Green Chemistry Series](#)

» Journals, books & databases



Home

About us

Membership & professional community

Campaigning & outreach

Journals, books & databases

Teaching & learning



[Log in / register](#)

[All chapters](#)

[Previous](#)

[Next](#)



From the book:

Biobased Aerogels: Polysaccharide and Protein-based Materials

Chapter 13

Applications of Aerogels in Aerospace and Packaging

Cintil Jose Chirayil, Jithin Joy, Lovely Mathew and Sabu Thomas

Polysaccharides and proteins are regarded as the key ingredients for the production of bio-based materials in life sciences (e.g. food, cosmetics, medical devices, pharmaceuticals, aerospace materials, and packaging, etc.). The biodegradability and biocompatibility of these biopolymers, coupled to the large variety of chemical functionalities they encompass, make them promising candidates for aerospace and packaging applications. Case studies on polysaccharide-based aerogels from several sources and our own results, as well as their behaviour regarding packaging and aerospace applications, are described. This chapter focuses on the state of the art of the evolution of aerogels in general, with an emphasis on their functions and significance in previous astronomical applications. Future outer-space applications have been proposed in line with the current research trend.

Buy this chapter

£30.00*

* Exclusive of taxes

This chapter contains 8 page(s)

Other ways to access this content

Log in

Using your institution credentials

Sign in

With your membership or subscriber account

Publication details

<https://doi.org/10.1039/9781782629979-00220>

Print publication date: 29 Aug 2018

Copyright year: 2018

Print ISBN: 978-1-78262-765-4

PDF eISBN: 978-1-78262-997-9

ePub eISBN: 978-1-78801-519-6

Citation:

BibTex

Go

From the book series:

Green Chemistry Series

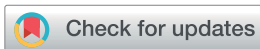
» Journals, books & databases



Home

About us

Membership & professional community



Cite this: *RSC Adv.*, 2018, 8, 30412

Green and facile approach to prepare polypropylene/*in situ* reduced graphene oxide nanocomposites with excellent electromagnetic interference shielding properties†

Gejo George,^a Sanu Mathew Simon,^a Prakashan V. P.,^a Sajna M. S.,^a Muhammad Faisal,^b Runcy Wilson,^c Anoop Chandran,^d Biju P. R.,^a Cyriac Joseph ^a and N. V. Unnikrishnan ^{*a}

The present work discloses the admirable electromagnetic interference shielding effectiveness (~50 dB at X and Ku Bands) realized by means of excellent dispersion state of reduced graphene oxide (rGO) in a polypropylene (PP) matrix, even at high concentrations (20 wt%). This was achieved by means of a latex method (polymer matrix; here PP in the aqueous emulsion state) combined with *in situ* reduction of graphene oxide using L-ascorbic acid as the reducing agent (green approach). A probable reaction mechanism between the maleic acid anhydride part of the PP matrix with the remaining –OH groups of rGO which may further assist in the better dispersion of graphene is also suggested. The prepared PP/rGO nanocomposites showed a percolation threshold in between that of 1.5 and 3 wt% rGO content. The microcapacitor and the conductive pathway formation in the system are explained nicely with the help of a schematic diagram. The electromagnetic interference shielding effectiveness (EMI SE) of 50 and 48 dB achieved for the X and Ku-bands for the 20 wt% rGO filled sample is one of the best among current works based on GO as the filler. The thermal stability of the samples increased marginally due to the addition of thermally stable rGO. The crystallization temperature increased with increasing rGO content owing to its good nucleating ability, whereas the melting characteristics shifted from double to single melting behavior possibly due to the ability of rGO to explicitly nucleate a particular polymorph of PP. A simple, cost efficient, green and promising approach to prepare non-polar polymer/graphene nanocomposites with a good dispersion state of graphene and excellent properties is reported in the present work.

Received 11th June 2018
 Accepted 13th August 2018

DOI: 10.1039/c8ra05007d

rsc.li/rsc-advances

1. Introduction

Shielding of electromagnetic (EM) waves in the microwave frequency region has become an important necessity for the proper functioning of electronic devices.^{1–5} Previously there has been extensive use of metal based composites for potential EMI shielding applications due to their very high conductivity and hence capability to reflect the incident EM waves. However, their properties such as high weight, low rigidity, high environmental sensitivity *etc.* have limited their use.^{1,6} The current trend is the use of polymer based composites for EMI shielding

applications owing to advantageous characteristics such as better compatibility, good flexibility, light weight nature, low cost *etc.*^{1,7}

The distinctive properties of carbon based nanofillers (carbon nanotubes (CNTs), carbon nanofibers (CNFs), graphene oxide (GO) *etc.*) such as excellent conductivity and huge aspect ratio have helped scientists/researchers universally to manufacture nanocomposites with enhanced electrical conductivity and low percolation thresholds.^{5,8–10} Researchers have reported that if a nanocomposite has a resistivity below 10 Ω sq^{–1} it can be used as efficient electromagnetic interference (EMI) shields.^{5,11}

Researchers have stated that such resistivity values (high conductivity) can be achieved by the formation of interconnected conductive networks by the incorporation of nanofillers far beyond the electrical percolation threshold of the material.^{12–15} It has been reported that even in the case of one atom thick graphene which is supposed to be highly conductive, a very high graphene content is required to make a polymer

^aSchool of Pure & Applied Physics, Mahatma Gandhi University, Kottayam, Kerala, India – 686 560. E-mail: nvu100@yahoo.com

^bResearch Center – Physics, Department of Physics, PES University – South Campus, Bangalore, Karnataka, India – 560 100

^cDepartment of Chemistry, St. Cyrils College, Adoor, Kerala, India – 691 529

^dDepartment of Physics, St. Cyrils College, Adoor, Kerala, India – 691 529

† Electronic supplementary information (ESI) available. See DOI: 10.1039/c8ra05007d



nanocomposite be conducting in nature.¹² Liang *et al.* in 2009 reported an electromagnetic interference shielding efficiency (EMI SE) of ~21 dB for graphene/epoxy composites.¹⁶ An EMI SE of 20 dB was achieved by Ling *et al.* even after decreasing the graphene content to 10 wt% for the polyetherimide graphene system.^{12,17} Yan *et al.* however, incorporated a very high loading (30 wt%) of graphene into a polystyrene matrix and reported EMI SE values of 29.3 dB.^{12,18} Researchers have reported several graphene based composite systems involving matrices like polymethyl methacrylate,¹⁹ water borne polyurethane,²⁰ phenolic²¹ *etc.* for potential EMI shielding applications. However, the general consensus is that for a composite material to show reasonable EMI SE (greater than or equal to 20 dB) properties copious amounts of nanofillers are to be added to the matrix.¹² The incorporation of high nanofillers (graphene, CNT *etc.*) however, may lead to very high cost of production and processing difficulties.¹² The significance of conductivity and percolation threshold on the EMI shielding ability of a given material is still not well understood.²²

Polypropylene is one of the most common thermoplastics which has been reinforced with different types of fibres and fillers over the past decades to yield composites with superior properties.²³ Researchers have recently showed the potential of graphene based PP nanocomposites as an appealing material for a number of practical applications owing to the enhanced mechanical, electrical, thermal and barrier properties due to the addition of graphene filler.^{23–31} Fabrication of materials with good strength and EMI shielding properties can be realized by the addition of graphene into PP matrix.^{32,33} However, careful analysis of the literature reveals that studies pertaining to the dielectric properties of PP/graphene system is very scarce.²⁷

One of the major challenges in the preparation of PP/rGO or GO composites is to achieve a homogenous and uniformly dispersed graphene oxide in the PP matrix which is rather difficult owing to the weak interactions between these two.²³ Melt mixing technique is one of the most common methods for the preparation of such materials and has been utilized by several researchers for the preparation of PP/graphene composites.^{23,24,28,29,31} Melt mixing process has however, several disadvantages such as poor dispersion of graphene in the PP matrix at very high loadings, risk of degradation of the polymer chains during the process *etc.* In order to overcome these shortcomings researchers have utilized the solution mixing process to fabricate PP/graphene composites.^{26,34} However, solution mixing process has a major drawback in the form of using toxic solvents (xylene, in the case of PP matrix) which is harmful to both the user and environment and also limits the use of this technology to a very small scale.²³ In recent times several researchers have utilized a simple and environment friendly latex technology to produce polymeric nanocomposites based on carbon nanotubes and graphene.^{23,31,35} It has been claimed by these researchers that the mixing of carbon nanotube/graphene dispersion in water with a polymer emulsion will lead to composites with excellent filler distribution and dispersion.^{23,31,35} Hsiao *et al.*³⁶ reported nanocomposites based on graphene nanosheets with high electrical conductivity and EMI shielding performance fabricated using a waterborne polyurethane as the matrix. Similarly Song *et al.*³¹

reported the preparation of graphene/PP masterbatch using PP latex technology and later mixed this masterbatch with a PP matrix to improve its mechanical and thermal stability. More recently, Wang *et al.*²³ manufactured PP latex/*in situ* reduced graphene oxide composites and studied their dielectric properties. However, in most of the works where GO was reduced *in situ*, hydrazine hydrate was used as the reducing agent which is highly toxic and flammable in nature thereby presenting danger to both the user and the environment.^{31,37,38} Vitamin C or L-ascorbic acid is non toxic in nature and is naturally used as a reducing agent in living beings^{39–42} and also as a mild reductant in the laboratories.^{39,43–46} Researchers like Zhang *et al.*³⁹ and Andrijanto *et al.*⁴⁷ have already reported the use of L-ascorbic acid as a reducing agent to reduce graphene oxide to rGO at room temperature and 70 °C respectively. Zhang *et al.*³⁹ reported that the use of L-ascorbic acid to reduce GO has the added benefit of L-ascorbic acid acting out as a capping agent to reduce the agglomeration tendency of reduced GO. Merino *et al.*⁴⁸ had reported that among the various reducing agents available only ascorbic acid can compete with the conventional but toxic hydrazine hydrate in terms of reducing ability to reduce GO to rGO.

In this article, the major objective is to *in situ* reduce GO via a facile, cost efficient and green approach involving L-ascorbic acid as the reducing agent with in PP latex matrix (aqueous emulsion of PP); thus facilitating the efficient dispersion of rGO in PP matrix even at high concentration which is rather difficult in normal methods leading to PP/*in situ* reduced graphene oxide nanocomposites with excellent EMI shielding and conductivity. A careful study was done on the effect of rGO content on the EMI shielding and dielectric properties of these composites. Furthermore, this study also explored the effect of rGO content on the thermal properties of the composite specimens.

2. Experimental

2.1 Materials

An aqueous non-ionically modified polypropylene (PP) emulsion (Trade name: AQUACER 1868) stabilized by several SDS (sodium dodecyl sulfate) like anionic surfactants and possessing a maleic acid anhydride grafted PP content of 40 wt%, ~40 mPa s viscosity and a pH level of 9 was used as the polymer matrix during this study and was supplied by BYK Additives & Instruments. Graphene oxide was procured from United Nanotech Innovations Pvt. Ltd, Bangalore, India with a purity of >98%, average sheet thickness of around 0.8–2 nm and average number of layers ranging from 3–10. L-Ascorbic acid was delivered by Sigma Aldrich (A92902). All the dispersions were prepared using distilled water.

2.2 Preparation of *in situ* reduced graphene oxide incorporated polypropylene composites

Graphene oxide was dispersed in water with a weight concentration of 30 wt% using magnetic stirrer (speed 500 rpm and time 10 minutes) at room temperature. In order to attain uniformly mixed PP/GO dispersion the above mentioned GO dispersed in water was mixed with PP latex thoroughly using



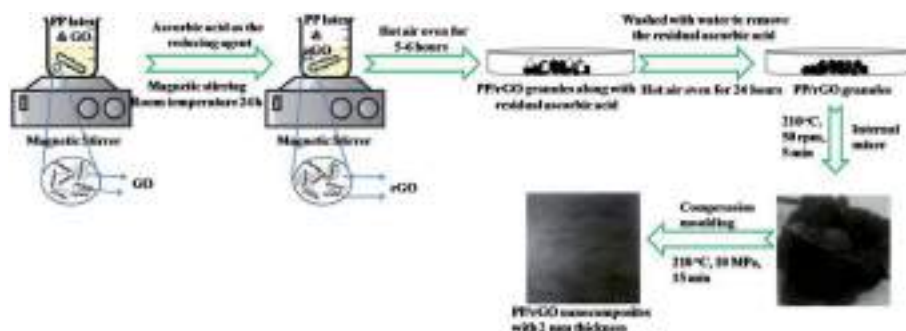


Fig. 1 Schematic representation of the processing stages in the preparation of *in situ* reduced graphene oxide/PP nanocomposites. Part of the image was drawn using <https://www.chemix.org/>.

a magnetic stirrer (speed 1000 rpm for 10 minutes) at room temperature. To this mixture *L*-ascorbic acid dissolved in water was added and stirred for 24 h at room temperature. In a typical experimental setup to reduce (*in situ*) GO within the PP latex emulsion, a 2 : 1 concentration of *L*-ascorbic acid was taken with respect to the GO concentration. The mixture was then stirred for 24 h at room temperature. The rGO concentration was varied from 0–20 wt% (0–12 vol%) (0–0.12 V_f). A control reduction experiment was performed to demonstrate the reduction capability of *L*-ascorbic acid. In this experiment all the chemicals except PP latex was taken as mentioned above and reduction process was performed for 24 h under the same conditions. The rGO sheets precipitated out from the dispersion as the reduction process continued and finally after 24 h the black solids were collected after centrifuging, dried and later analyzed using FT-IR, UV-Vis, XPS, Raman, FE-SEM and TEM analysis.

The PP/rGO dispersion was then poured into a Petri dish and kept in an air oven at 70 °C for 6 h to remove the water and other volatiles. The dried PP/rGO granules were then washed several times using distilled water to remove the ascorbic acid present in the system. The wet PP/rGO grains on a Petri dish were then kept in an air oven at 70 °C for 24 h to remove the water. To further enhance the uniform dispersion of rGO in the PP matrix and to wipe out any remaining moisture presence, the dried and moisture free PP/rGO grains were passed through an internal mixer (operating at 210 °C and 50 rpm speed for 5 minutes). Compression moulding at 210 °C, 10 MPa pressure and 15 min holding time was then utilized to prepare PP/rGO nanocomposites (2 mm thick) from the obtained PP/rGO lumps. The preparation scheme for the PP/*in situ* reduced rGO nanocomposite is shown in Fig. 1.

2.3 Characterization of reduced graphene oxide and PP/rGO composites

Perkin Elmer Spectrum 400 FTIR spectrometer was used to record the Fourier Transform Infra Red Spectra (FT-IR) of the samples from 400 to 4000 cm^{-1} . An Agilent Technologies Cary Series UV-Vis-NIR Spectrophotometer was used to record the absorption spectra of the samples. Field Emission Scanning Electron Microscopy (FE-SEM) and Transmission Electron Microscopy (TEM) analysis was used to characterize the reduced graphene oxide and its corresponding composites. A Nova

NanoSEM 450 operating at 10–20 kV was used for the FE-SEM analysis of the samples. For FE-SEM analysis, rGO was taken as such, however in order to understand the interfacial adhesion between the matrix (PP) and reinforcement (rGO), a tiny piece of the composite specimen was dipped in liquid nitrogen and then fractured and used for FE-SEM analysis. A JEOL JEM-2010 at 200 kV was used to perform the TEM analysis of the samples. The rGO sample was dispersed in water, casted on a standard TEM grid and later dried for the TEM analysis. The composite sample on the other hand, was cryomicrotomed to cut the sample and cast on a TEM grid. Hioki 3532-50 LCR Hitester was used to study the dielectric properties (dielectric constant, ac conductivity *etc.*) of the samples (10 mm diameter and 2 mm thickness, coated with silver paste) with two probe method from 50 Hz to 5 MHz. The EMI SE values of rGO/PP nanocomposites (2 mm thick) in the X and Ku band regions of the microwave frequency was carried out using a Vector Network Analyser (Agilent Model PNA E8362B) employing the wave guide transmission technique. The EMI SE values by means of absorption, reflection and total shielding can be estimated using the scattering parameters. A TGA Perkin Elmer TGA 4000 was used to perform the thermogravimetric analysis of the samples in nitrogen atmosphere over a temperature range of 0–800 °C (heating rate 5 °C min^{-1}). DSC Netzsch DSC204F1 equipment was used to study the crystallization and melting behavior of the composites using Differential Scanning Calorimetry (temperature range: –30 to 250 °C and heating rate 10 °C min^{-1}). Raman spectra of the samples were recorded using a Horiba Jobin Yvon LABRAM-HR 800 spectrograph employing a 632 nm Helium neon laser. X-ray photoelectron spectroscopy (XPS) of the samples was measured using a Thermo Fisher Scientific ESCALAB X-ray Photoelectron Spectrometer employing a twin-crystal; micro-focused monochromator with a 500 mm Rowland circle. X-ray diffraction (XRD) studies were done using a PANalytical X'Pert PRO X-ray diffractometer from 2θ values ranging from 05–60°.

3. Results and discussion

3.1 FT-IR, UV-visible, XPS, Raman spectroscopic and XRD analysis

The FT-IR spectrum of graphene oxide and reduced graphene oxide (ascorbic acid as the reducing agent) is shown as Fig. 2a.



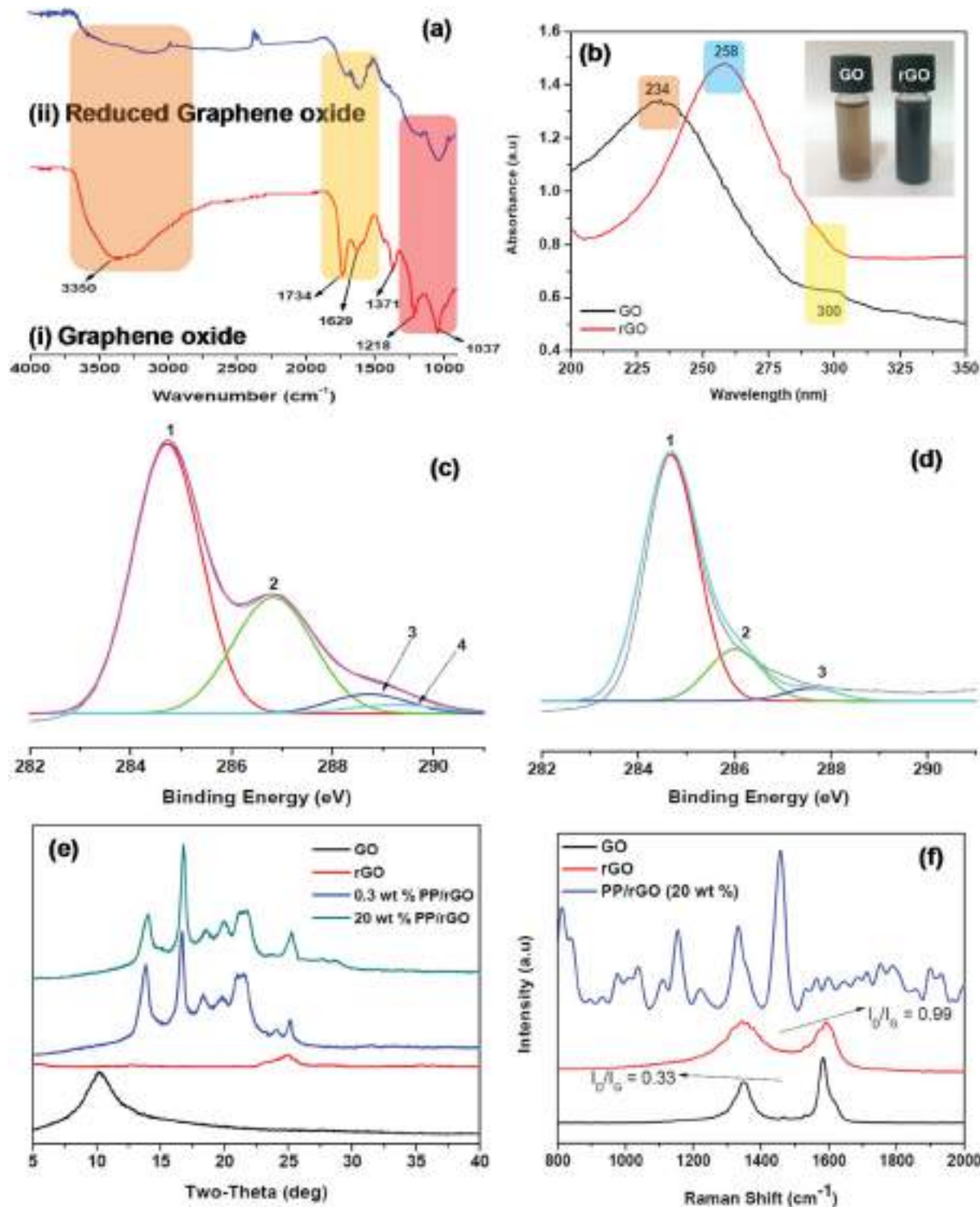


Fig. 2 (a) FT-IR, (b) UV-Vis absorption and (c) and (d) XPS spectra of GO and rGO respectively. (e) XRD and (f) Raman spectra of GO, rGO and rGO/PP nanocomposites. Inset of (b) shows GO and rGO suspensions with 0.2 mg ml^{-1} concentration.

The spectrum of GO (Fig. 2ai) clearly shows all the characteristic peaks of graphene oxide *viz.* the C–O stretching at 1037 cm^{-1} , C–O–C bending at 1218 cm^{-1} , C=O stretching at 1734 cm^{-1} and most importantly the broad peak at 3350 and small peak at 1371 cm^{-1} corresponding to the –OH stretching vibration and

deformation respectively due to the C–OH groups in the material.

The graphene oxide is then reduced using L-ascorbic acid (mentioned in the experimental section) for 24 h and the FT-IR spectrum is recorded (Fig. 2aii). The reduction of GO to rGO is confirmed by the complete removal and reduction in intensities



of different peaks. The peaks centered at 1037, 1218, 1734 and 3350 cm^{-1} either disappeared completely or decreased in intensity significantly due to the elimination of oxygen containing functional groups as a result of the reduction process. A considerable decrease in the $-\text{OH}$ peak (3350 cm^{-1}) intensity is observed due to the removal or conversion of oxygen containing functional groups. However, it should be noted that $-\text{OH}$ peak has not completely disappeared indicating that some left over oxygen functionalities still stay behind in the reduced graphene oxide. The recovery of sp^2 lattice structure is confirmed by a strong band at 1629 cm^{-1} .^{39,47} The reduction of GO to rGO was also confirmed using UV-Vis spectroscopy (Fig. 2b). Graphene oxide shows two characteristic peaks at 234 and 300 nm in the absorption spectrum, both of which on reduction gradually decays and vanishes after 24 hours of reaction. A new absorption peak centered at 258 nm shows up in the rGO absorption spectrum. The absorption intensity enhances for the reduced sample considerably and based on previous reports might be the indication of GO being reduced to rGO and the slow reinstatement of aromatic structure in the system.^{39,49} The GO and rGO aqueous solutions are shown in Fig. 2b inset and the change in colour from brown (GO) to black (rGO) is also clearly evident. Zhang *et al.*³⁹ have stated that L-ascorbic acid has the added advantage of stabilizing the aqueous rGO dispersion without the help of other capping agents or surfactants. This additional benefit of L-ascorbic acid may assist in properly dispersing the rGO sheets throughout the aqueous PP latex emulsion. The photos of PP latex and PP/*in situ* reduced GO mixture are shown as Fig. S1 (ESI†).

The conversion of GO to rGO was further evidenced by XPS, XRD and Raman analysis. The C 1s XPS spectra of graphene oxide (Fig. 2c) shows the characteristic peaks at 284.74, 286.86, 288.71 and 289.32 eV respectively corresponding to $\text{C}=\text{C}/\text{C}-\text{C}$ in aromatic rings, epoxy and alkoxy $\text{C}-\text{O}$, $\text{C}=\text{O}$ and COOH groups. However, after reduction (Fig. 2d) the C 1s peak intensities of all the carbons bound to oxygen especially the $\text{C}-\text{O}$ (epoxy and alkoxy), $\text{C}=\text{O}$ and COOH peaks clearly diminish. This reduction in intensity and disappearance of peak discloses the fact that most of the oxygen containing functionalities in GO were removed after the reduction process.³⁹ The X-ray diffractograms of GO, rGO and PP/rGO nanocomposites are shown in Fig. 2e. The XRD of GO reveals the presence of a peak at around 10° ($0\ 0\ 2$ plane) clearly indicating the oxidized state of graphene affecting the crystal structure.⁵⁰ However, upon reduction the sample reveals a broad peak centered at around 25° indicating the reduction of GO leading to reduced graphene oxide nano-sheets which may begin to stack up due to the strong van der Waals forces.⁵⁰ For PP latex, diffraction peaks at 14, 16, 17, 21.5, 26° has been reported by researchers like Song *et al.*³¹ and Fu *et al.*³⁷ The incorporation of rGO into PP latex matrix leads to nanocomposites showing only the crystalline diffraction peaks of PP matrix in the XRD spectra indicating that the rGO sheets dispersed in the PP matrix is well distributed.³¹ Fu *et al.*³⁷ have stated that the absence of characteristic intense peaks at 10° or 27° corresponding to GO and graphite suggests that the dispersion state of graphene is good in the matrix. However, the peak shape and intensity change at 13.7, 16.8 and 18.0°

corresponding to (110), (040) and (130) planes respectively in the presence of rGO denote that the existence of rGO affects the crystallization behavior of the matrix to some extent.³¹ This effect of rGO concentration on the crystallization of PP matrix is later investigated using DSC analysis. Raman spectroscopy was also used to further confirm the reduction of GO to rGO and to evaluate the change in characteristic peak reflections from graphite to GO and finally to rGO. Graphite exhibits two characteristic peaks namely the G band at around 1580 cm^{-1} and the weaker of the two bands known as the D band at 1350 cm^{-1} which is also referred to as the defect band.³¹ The G band is due to the sp^2 hybridized graphitic domains whereas, the presence of sp^3 hybridized carbon and defects are the reason for the D band in graphite.^{51,52} However, as evident from Fig. 2f GO on the other hand has two bands (G and D) broadened and shifted to the higher wavenumber regions (1593 and 1356 cm^{-1}) respectively which is also accompanied by increased $I_{\text{D}}/I_{\text{G}}$ values (0.33). This has been reported to be due to the increase in defect like amorphous domains and also to the seclusion of carbon double bonds as a result of oxidation.^{31,53} The reduction of GO to rGO leads to the G and D bands remaining broader than those of pristine graphite however, the $I_{\text{D}}/I_{\text{G}}$ values increases dramatically to around 0.99. This increment in $I_{\text{D}}/I_{\text{G}}$ values for rGO compared to GO has been attributed to increased number of aromatic domains of overall smaller size or due to the presence of defects in the crystal lattice as a result of reduction process.^{31,54-56}

The FT-IR spectrum of neat polypropylene and 20 wt% PP/graphene oxide sample (before and after reduction) is shown as Fig. 3. For neat polypropylene (Fig. 3a) the characteristic peaks of polypropylene are clearly visible. The symmetrical $-\text{CH}$ stretching from methyl group is the reason for the peak at 2951 cm^{-1} whereas, the peaks at 2917, 1456 and 1367 are due to the asymmetrical $-\text{CH}$ stretching, asymmetrical and symmetrical bending modes of methyl $-\text{CH}$ bonds respectively. The peak at 1251 cm^{-1} is ascribed to the various bending modes (scissoring, rocking, wagging and twisting) of methylene group. The FT-IR spectrum of unreduced PP/GO composite sample is shown as Fig. 3c and contains the characteristic peaks of both PP and graphene oxide. The broad peak at 3293 cm^{-1} is due to the $-\text{OH}$ stretching vibration of $\text{C}-\text{OH}$ groups present in the graphene oxide. Similarly, as a result of the addition of unreduced graphene oxide into PP matrix, the presence of carbonyl groups ($\text{C}=\text{O}$ stretching) and the presence of $\text{C}-\text{OH}$ bending modes is validated by the peaks at 1636 and 1546 cm^{-1} respectively.⁴⁷

However, on *in situ* reduction of graphene oxide using L-ascorbic acid to fabricate PP/rGO nanocomposites the reduction in oxygen containing groups is clearly observable (Fig. 3b). The peaks at 1636 and 1546 cm^{-1} clearly diminish in the case of reduced sample demonstrating the elimination of oxygen containing functionalities present in GO. Most importantly the intense broad peak at 3293 cm^{-1} due to $-\text{OH}$ stretching vibration clearly decreases in intensity pinpointing the removal of oxygen functionalities. It should however, be noted that the broad $-\text{OH}$ peak has not totally vanished (only reduced in intensity) indicating that some residual oxygen



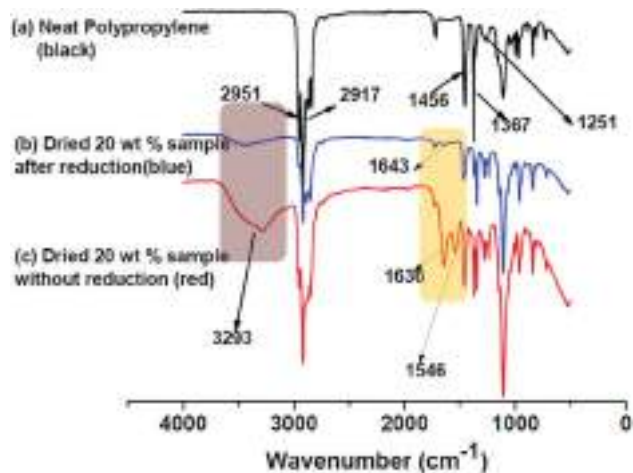


Fig. 3 FT-IR spectra of (a) neat PP, (b) PP/rGO sample after 24 h reduction and (c) unreduced PP/GO sample.

functionalities still remain on the surface of GO even after reduction.

The PP latex utilized during this study is maleic acid anhydride grafted PP and hence has the minute possibility of maleic acid anhydride part of the PP matrix reacting with the remaining $-OH$ groups of the rGO. The proposed reaction mechanism is shown in Fig. 4. The FT-IR spectrum of 20 wt% rGO filled PP composite after reduction shows a small peak at 1643 cm^{-1} . This might be due to the anhydride and carboxylic acid functionalities produced as a result of the hydrolysis of esterification product of the reaction between the residual $-OH$ groups in rGO with maleic

anhydride. This minute possibility of bonding between the maleic anhydride parts of PP with rGO may lead to better and efficient dispersion of graphene sheets between the PP chains.

3.2 Morphological characterization

FE-SEM analysis was employed to get a peek into the morphology of rGO and PP/rGO composites. The FE-SEM images of rGO and PP/rGO samples are shown in Fig. 5.

Fig. 5a depicts the FE-SEM image of rGO sample and clearly shows sheets of rGO stacked together with each other. Fig. 5b on the other hand shows the FE-SEM image of neat polypropylene where the voids and pores on the surface are clearly visible. However, on the addition of reduced graphene oxide to this PP matrix a realistic uniform distribution of graphene in the PP matrix can be observed clearly with extremely low concentration of aggregation (Fig. 5c and d). This uniform distribution of graphene throughout the PP matrix even at high concentrations (20 wt%) of rGO leads us to believe that there is some degree of interaction taking place between rGO and PP matrix. Fig. 5(e) and (f) are the FE SEM images of PP/rGO composites with 5 and 20 wt% rGO respectively at higher magnification. Well dispersed sheet like structures of rGO is clearly visible in both the images. Since both the matrix and filler are being mixed in the solvent form itself, uniform mixing of rGO within the PP matrix will be achieved, possibly leading to reduction of voids and pores in the nanocomposites.

3.3 Distribution of rGO in PP matrix

The distribution of rGO in the PP matrix was analyzed using TEM (Fig. 6). The TEM image of rGO (Fig. 6a) clearly reveals thin

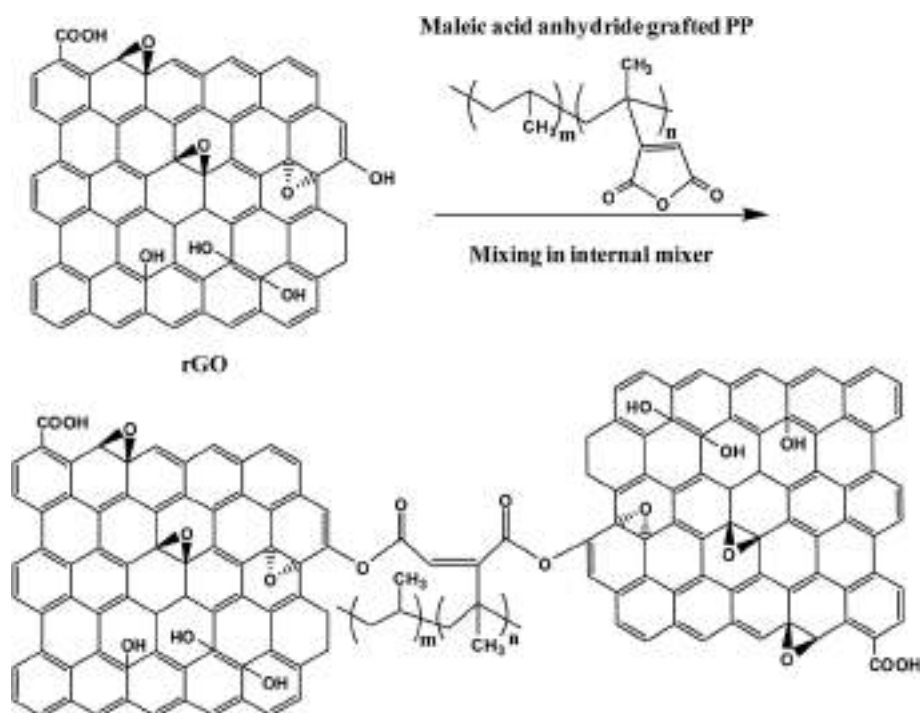


Fig. 4 Proposed reaction between maleic acid anhydride grafted PP and rGO.



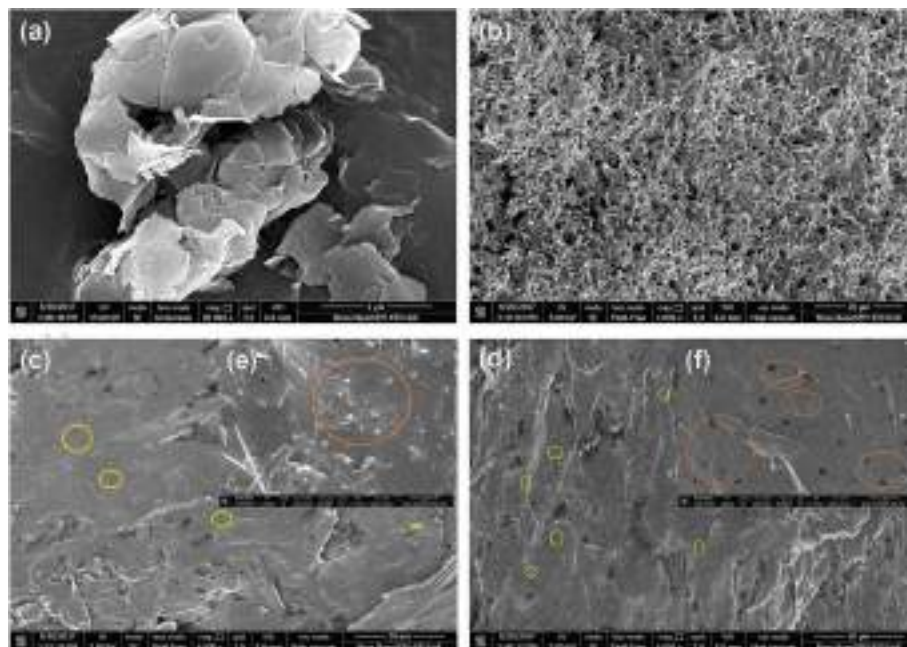


Fig. 5 FE-SEM images of (a) reduced graphene oxide, (b) neat PP, (c) and (e) 5 wt% rGO filled PP composite and (d) and (f) 20 wt% rGO filled PP composite.

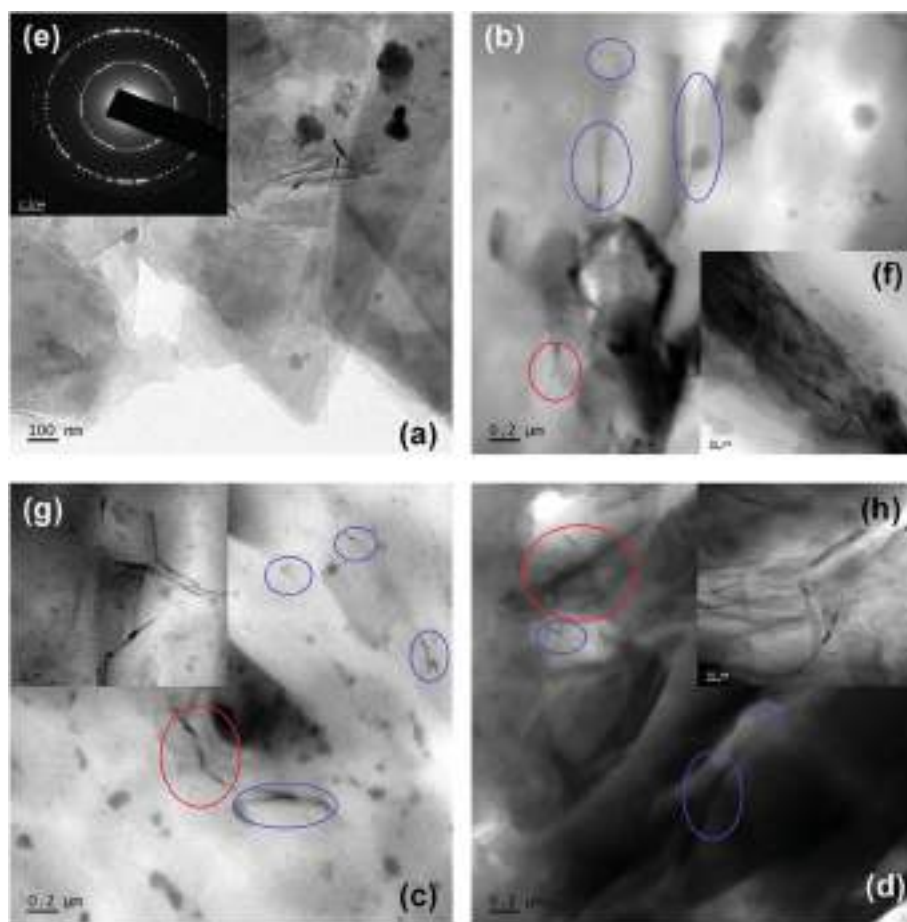


Fig. 6 TEM images of (a) rGO and (e) SAED pattern of rGO, (b) and (f) 5 wt% rGO filled PP composite, (c) and (g) 10 wt% rGO filled PP composite and (d) and (h) 20 wt% rGO filled PP composite. Images (f), (g) and (h) are HR-TEM images of the red circles in (b), (c) and (d) respectively.



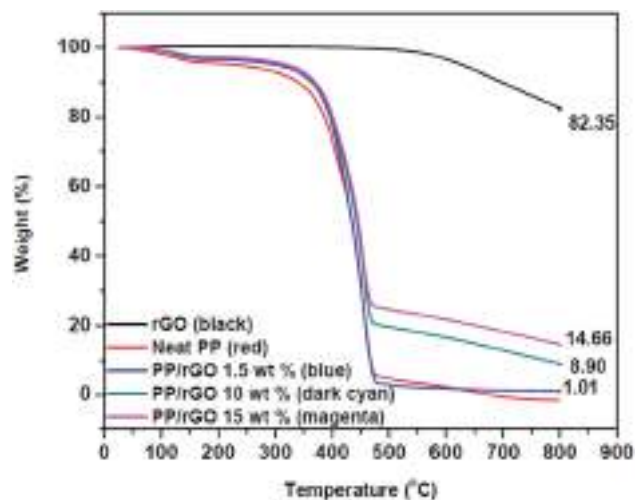


Fig. 7 TGA thermograms of reduced graphene oxide and rGO/PP nanocomposites with varying rGO content.

rGO sheets dispersed across the grid. The sheets at some places appear to be folded, irregular and entangled with each other. The SAED (selected area electron diffraction) pattern (Fig. 6e) of rGO shows well defined diffraction spots which leads us to conclude that the crystalline state of GO was re-established to some extent.³⁹ The TEM images of 5, 10 and 20 wt% rGO filled PP latex composites are shown in Fig. 6(b), (c) and (d) respectively. The low viscosity of PP latex (~40 mPa s) aids in the formation of well dispersed rGO sheets throughout the PP matrix as evidenced by the TEM images. Fig. 6(b)–(d) clearly show the distribution of few layers rGO (blue circles) in the PP matrix. The distribution of rGO in the PP matrix increases with increasing rGO concentration and is clearly observable in the TEM images. The magnification of the TEM images reveal rGO sheets [Fig. 6(f)–(h)] with thickness of ~10–20 nm distributed uniformly throughout the PP matrix. This uniform distribution of rGO throughout the PP matrix may facilitate the formation of conductive networks or pathways in the composite. At very high rGO concentration (20 wt%) extensive networks of closely packed rGO sheets are clearly visible (Fig. 6h). The SEM and TEM analysis of the rGO filled PP latex composites conclusively showcases the uniform distribution of rGO sheets throughout the PP matrix with good homogeneity. This uniform distribution of rGO sheets in the PP matrix is attained due to three possible rationales: (a) PP dispersion/latex has a low viscosity of ~40 mPa s and hence the nanoparticle dispersion can be uniformly and efficiently distributed using simple magnetic stirring owing to kinetic factors,⁵⁷ (b) the PP emulsion employed in the current work is a water-based suspension of maleic anhydride-grafted isotactic polypropylene and has low tendency for nanoparticle aggregation and facilitates uniform dispersion and (c) the proposed reaction between rGO and maleic anhydride part of PP may also facilitate the uniform distribution of rGO in the PP matrix. It has been reported that the polarity of maleic anhydride will most likely assist in uniform and efficient dispersion of graphene oxide in the PP matrix.^{57,58}

Table 1 T_i , T_{max} and residue left for neat PP and different composite samples

Sample	Initial degradation temperature (T_i) (°C)	Maximum loss temperature (T_{max}) (°C)	Residue left (%) at 800 °C
PP latex	338	473	0.00
1.5 wt% rGO/PP	358	476	1.01
10 wt% rGO/PP	367	473	8.90
15 wt% rGO/PP	368	473	14.6

3.4 Thermal properties of PP/rGO nanocomposites

The thermogravimetric data of reduced graphene oxide and rGO/PP composites with varying rGO content are shown in Fig. 7. Reduced graphene oxide has good thermal stability and shows only a small degradation peak at around 500 °C, and may be due to the presence of small quantities of residual oxygen groups present even after reduction and other small defects. The residue after 800 °C is around 83% which depicts the good thermal stability of rGO in nitrogen atmosphere. The degradation of polypropylene latex shows two stage decomposition with the initial degradation probably due to moisture/water removal followed by the major degradation point at around 400 °C and is primarily attributed to the scission of saturated and unsaturated carbon bonds present in the PP system.⁵⁹ This degradation leads to the residue remaining for PP latex after 800 °C close to 0%. However, on incorporating thermally stable rGO into PP latex, a part of the good inherent thermal stability of rGO is transferred to the as prepared composites also, thereby PP latex/rGO composites showcasing marginally improved stability compared to that of neat PP latex. The residue remaining for each sample depicts increasing residue % with increasing rGO content. For 1.5 wt% PP/rGO sample the residue is 1.01%, whereas for the 10 and 15 wt% samples the residue remaining is 8.9 and 14.6% respectively. This provides us with ample confirmation for the incorporation of rGO into PP latex matrix. Several earlier reports on graphene based polymeric nanocomposites have suggested that the incorporation of graphene into polymeric matrices enhances the thermal stability of the polymers to some extent only.^{31,60,61} The marginally enhanced thermal stability of PP/rGO nanocomposites imparted by the addition of thermally stable rGO into PP latex, is clearly evidenced by the monotonous rise in initial degradation (T_i) and marginal increment in maximum mass loss temperatures (T_{max}). The values of T_i , T_{max} and residue left for PP latex and PP latex/rGO composites are tabulated in Table 1.

This marginal increment in thermal stability for rGO filled PP composites may be credited to the barrier effects of graphene sheets just like that of clay planets.³¹ The increase of 20 °C in initial degradation temperature between PP latex and 1.5 wt% rGO/PP is similar to that of the increase reported by Song *et al.*³¹ wherein hydrazine hydrate was used as the reducing agent rather than ascorbic acid. The differential scanning calorimetric curves of crystallization and melting of *in situ* reduced rGO/PP composites are shown in Fig. 8.



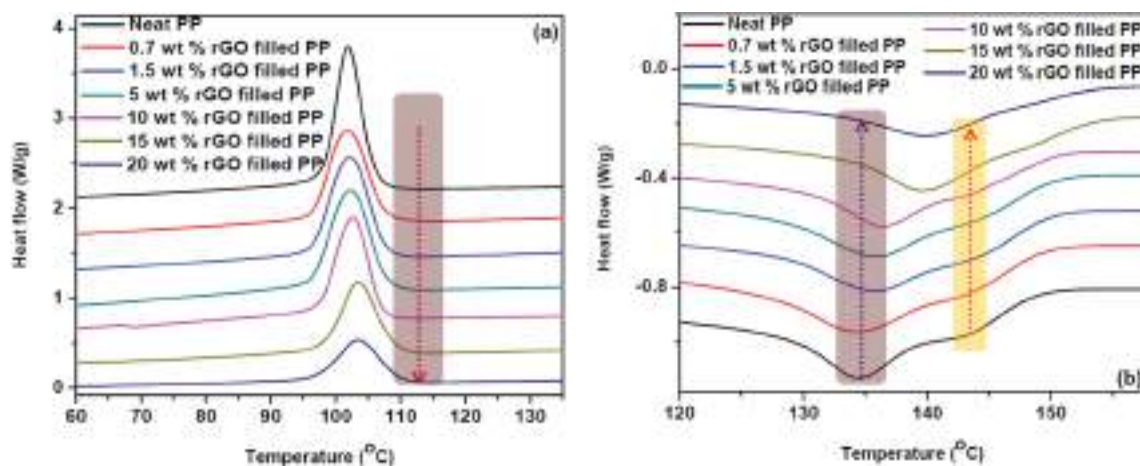


Fig. 8 Differential scanning calorimetric curves of (a) crystallization and (b) melting of PP/rGO nanocomposites with different rGO contents. The arrow direction indicates increasing rGO content.

Table 2 Onset crystallization, crystallization, T_{M1} and T_{M2} temperatures for neat PP and rGO/PP composites

Sample	Crystallization temperature (°C)	Onset crystallization temperature (°C)	T_{M1} (°C)	T_{M2} (°C)
Neat polypropylene	102.0	110.2	134.4	143.7
0.7 wt% rGO/PP	102.0	111.1	134.4	144.0
1.5 wt% rGO/PP	102.1	111.0	136.0	145.0
5 wt% rGO/PP	102.3	111.7	136.1	145.2
10 wt% rGO/PP	102.5	111.0	135.2	Peak not visible
15 wt% rGO/PP	103.6	112.4	140.0	Peak not visible
20 wt% rGO/PP	103.6	112.4	140.0	Peak not visible

The crystallization temperatures of the rGO filled composites are found to increase with increasing graphene concentration (Fig. 8a). In all the samples both the onset crystallization and crystallization temperatures followed an ascending trend with increasing rGO content. For instance, the crystallization temperature of PP filled with 20 wt% *in situ* reduced GO was found to be 1.6 °C higher than that of neat polypropylene. The effect of graphene content on crystallization is more obvious in the case of onset crystallization temperature, wherein the sample with 20 wt% rGO shows 2.2 °C increment compared to that of neat PP. Zhao *et al.*⁶² have credited this improvement in crystallization properties of PP with the addition of graphene to the strong heterogeneous nucleation effect of graphene sheets. The effect of graphene concentration on the onset crystallization and crystallization temperatures of PP/rGO composites are tabulated in Table 2. Nano materials are known to be efficient nucleating agents and Fig. 8a evidently points to the capability of graphene oxide sheets to speed up the crystallization process of PP by making available abundant nucleation sites. The vertical dashed line denotes the onset of crystallization temperature for 20 wt% rGO filled PP composite and is compared with the other samples in Table 2. It can also be observed from Fig. 8a that with increasing rGO content the crystallization (exothermic) curves became wider and shallower in accordance with the work of Wakabayashi *et al.*⁶³ where graphite was used as the filler for PP matrix. This change in

peak shape may point to the conservative rather than progressive increase in the crystallization rate. This finding is however, contradictory to the findings of Song *et al.*³¹ where PP latex/rGO composite did not show such an effect. This discrepancy in the crystallization behavior might be due to the difference in processing methods. Song *et al.*³¹ used PP latex and employed hydrazine hydrate for reducing GO followed by using this as a master batch and adding to PP granules (matrix) for the fabrication of composites. Whereas, in the present work PP latex is used as the matrix and utilizes ascorbic acid as the reducing agent to reduce GO.

The endothermic (melting behavior) of *in situ* reduced rGO/PP latex nanocomposites is shown in Fig. 8b. The melting curve of PP unmistakably exposes the double melting behavior ($T_{M1} = 134.4$ °C and $T_{M2} = 143.7$ °C). This double melting behavior however, slowly and steadily proceeds in the path of single melting behavior with the addition of reduced graphene oxide. The melting temperature 1 (T_{M1}) gradually swings to higher temperatures and finally overlaps with the second melting peak (T_{M2}) which is not clearly visible above 5 wt% rGO content. The values of T_{M1} and T_{M2} for different samples are tabulated in Table 2.

The obvious diminishing of double melting behavior for PP/rGO system is clearly noticeable above 5 wt% rGO filled composite and changes completely to a single peak at high rGO concentrations of 15 and 20 wt%. Miltner *et al.*³⁵ have reported



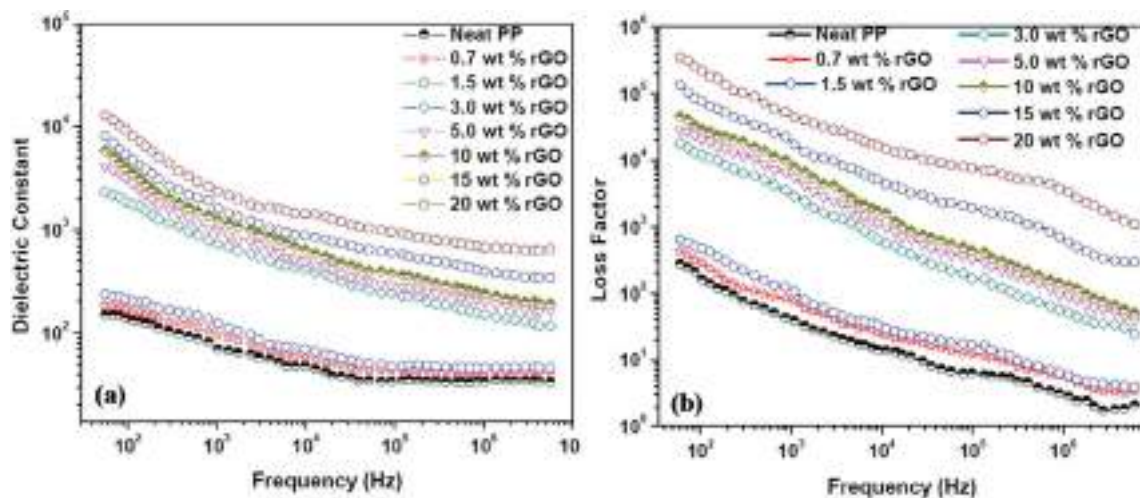


Fig. 9 Effect of different rGO contents on the (a) dielectric constant and (b) loss factor of PP/rGO composites at room temperature as a function of frequency.

that materials with polymorphism (a materials ability to exist in more than one form or crystal structure) generally display multiple melting point behavior. The change in equilibrium between the two forms of PP (hexagonal and monoclinic) might be the reason for this shift of T_{M1} to higher temperature region and consequent vanishing of T_{M2} with increasing rGO content. Hence it can also be concluded that rGO has the unique potential to specifically nucleate a particular polymorph of PP than its counterpart, leading to the equilibrium shift. It is well reported that shear induced crystallization or the presence of nanoparticles can favour the crystallization of β form (hexagonal) of PP.^{64,65} Among these different types of nanoparticles graphene and its derivatives have already been reported to favour the β form (hexagonal) of PP during crystallization. Xu *et al.*²⁸ reported that even at very low concentrations of GO (0.5 and 1 wt%) the crystallization of β form was favoured by means of shear amplification effect. Similarly Yuan *et al.*⁶⁶ also accounted that at 1 wt% addition of functionalized graphene sheets the β form of PP was obtained. Hence, in the present

work it is quite understandable that at high concentrations of rGO (20 wt%) the equilibrium between α (monoclinic) and β (hexagonal) forms of PP shifts to the β form predominantly.

3.5 Electrical conductivity studies of the composites

The dielectric constant (dielectric permittivity) and loss factor values of PP/rGO nanocomposites at room temperature are shown in Fig. 9 as a function of frequency with respect to varying graphene content.

The real part of the complex dielectric permittivity is more commonly referred to as dielectric constant or dielectric permittivity (ϵ') whereas the loss factor can be defined as the amount of energy dissipated in a dielectric material.²³ The composite or any given material should have high dielectric properties and conductivity in order to showcase good EMI shielding behavior.⁵⁷ Fig. 9a and b clearly depict that both the dielectric constant and loss factor of PP/rGO composites increases with increasing weight % of rGO content. For neat PP, the dielectric constant at 10^2 Hz frequency is ~ 150 which

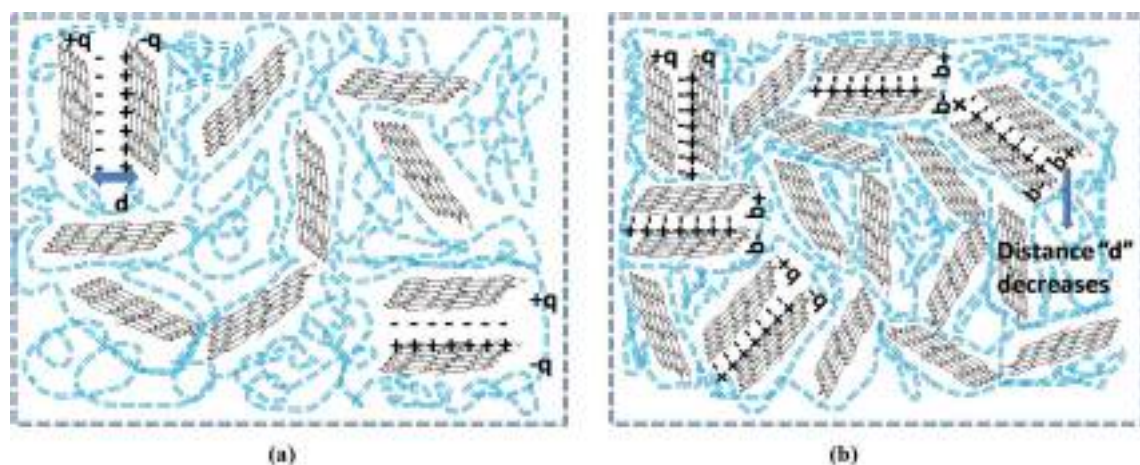


Fig. 10 Schematic representation of microcapacitor formation in PP/rGO nanocomposites at (a) low rGO content and (b) high rGO content. Blue dotted lines represent PP chains.



decrease to around 34 at 10^7 Hz. However, in the case of 20 wt% rGO incorporated PP composites the samples exhibit a dielectric constant of around 10 219 at low frequency (10^2 Hz) which decreases to ~ 680 at higher frequencies (10^7 Hz). The very high dielectric constant values for the PP/rGO composites indicate that the dielectric permittivity of PP composites can be significantly enhanced by blending it with reduced graphene oxide. The TEM images (Fig. 6) has shown that the conducting filler (reduced graphene oxide) is well distributed throughout the PP matrix. The exfoliated rGO layers predominantly appear to be secluded by the insulating PP matrix leading to the creation of large number of microcapacitor structures (Fig. 10) throughout the PP/rGO composite, which in turn may give rise to increased intensity of local electric field.

Researchers have already conclusively reported that the formation of large number of microcapacitor structures in a given material will lead to a remarkable enhancement in the dielectric constant of conducting filler/polymer composites at the percolation threshold.^{23,67–69} The increased intensity of local electric field as a result of improved presence of microcapacitors paves the way for enhanced migration and buildup of charge carriers at the PP/rGO interface.²³ During the microcapacitor formation the few layers thick rGO sheets act as the electrode material which is isolated by polypropylene which is an insulator material. The formation of such microcapacitors increases with increasing rGO content and results in increased dielectric constant. The presence of large quantities of rGO in the PP matrix leads to decreased space between the electrodes (Fig. 10) in the microcapacitor thus aiding the total dielectric constant value of the sample. The brisk decrease of dielectric constant with increasing frequency (at low frequency regions) can be explained on the basis of incapability of dipoles with huge relaxation time to trail the quickly changing external field. However, when it comes to the MHz range this peculiar behavior is halted due to the fact that the relaxation times of dipoles in this regime is much lower compared to the applied frequency.

The substantial increase in dielectric constant with increasing rGO content can also be attributed to the polarization at the matrix (polymer) and filler (rGO) interface.^{57,70} This type of polarization is referred to as Maxwell–Wagner Sillar effect or interfacial polarization.⁵⁷ A sharp increase (few orders magnitude) in dielectric constant is observed above 1.5 wt% rGO content, thus leading to the conclusion that for the present system the percolation threshold is in between 1.5 and 3 wt%. On attaining the percolation threshold the number of PP (matrix) – rGO (filler) interfaces increases dramatically along with increment in accumulation of charges at the interface thus leading to very high interfacial polarization and hence showing few orders magnitude increment in dielectric constant. Fig. 9a also reveals that above the percolation threshold the dielectric constant values of the samples more or less becomes frequency dependent mainly at lower frequencies. The dielectric constant values of 10, 15 and 20 wt% rGO filled samples clearly shows a sharp decreasing tendency with frequency compared to that of the samples with lower rGO contents. However, at very high frequencies (at or above 10^6 Hz) this reliance on frequency

diminishes. The charge carriers present at the interface undergoes constant motion at higher frequencies and is the reason why at higher frequencies it remains more or less same.^{71,72} This trend of dielectric constant with frequency can also be attributed to two other factors namely, (a) lagging effect of interfacial and orientational polarization with applied external electric field and (b) charge and molecular re-orientation hindering the rapid change in applied external field direction.^{70,73}

The dielectric loss (Fig. 9b) of PP/rGO composites also showed the same tendency as that of the dielectric constant, the loss values increased with increasing rGO content but decreased with increasing frequency for all the samples. Above the percolation threshold (*i.e.* between 1.5 and 3 wt%) dielectric loss also showed a jump of few orders of magnitude for the composites. The leakage current is the major factor that controls the dielectric loss or loss factor of highly conducting polymeric composites.²³ With increasing conducting filler content in polymer matrix based composite, once the percolation threshold is reached the formation of conductive networks/pathways takes place resulting in enhanced leakage current and thereby dielectric loss. The formation of such conductive networks/pathways in polymer composites due to the addition of highly conducting filler contributes to higher dielectric loss which in turn might aid the dissipation of electromagnetic waves by absorption mechanism.⁵⁷ The effect of rGO content on the ac conductivity of PP/rGO composite systems as a function of frequency with respect to different rGO content is shown as Fig. 11.

The values increased with increasing rGO content with the highest values being observed for 20 wt% rGO filled samples. Neat PP and composite specimens with 0.7 and 1.5 wt% rGO respectively demonstrated conductivity values in between that of 10^{-7} to 10^{-6} S m^{-1} (insulating behavior) at 50 Hz frequency and more importantly for all these samples the conductivity increased with increasing frequency which is characteristic of dielectric materials.^{22,74} On the other hand the sample with 3 wt% rGO content illustrated conductivity values in the range of 10^{-4} S m^{-1} whereas the samples with 10, 15 and 20 wt% rGO content showed conductivity values in the range of 10^{-2} and 10^{-1} S m^{-1} respectively. The important observation nonetheless is that, in the samples with 3 and 5 wt% rGO the conductivity was found to be independent of frequency until a frequency of 10^3 and 10^4 Hz respectively and after which the values increased with frequency. The DC conductivity values on the other hand are dominated by the polarization of dipoles and a characteristic feature of such polarization is this frequency independent behavior.^{22,75} Composite specimens with 15 and 20 wt% rGO content displayed frequency independent behavior throughout the entire frequency range. It has been reported that the onset of frequency independent performance is believed to be the transition of a material from insulating to conducting nature.^{22,76} Hence, this study reveals that for the present system (PP latex/*in situ* reduced rGO composite) the percolation threshold is in between 1.5 and 3 wt% of rGO. The dramatic increase in conductivity above the percolation threshold can be explained on the basis of formation of conductive pathways/



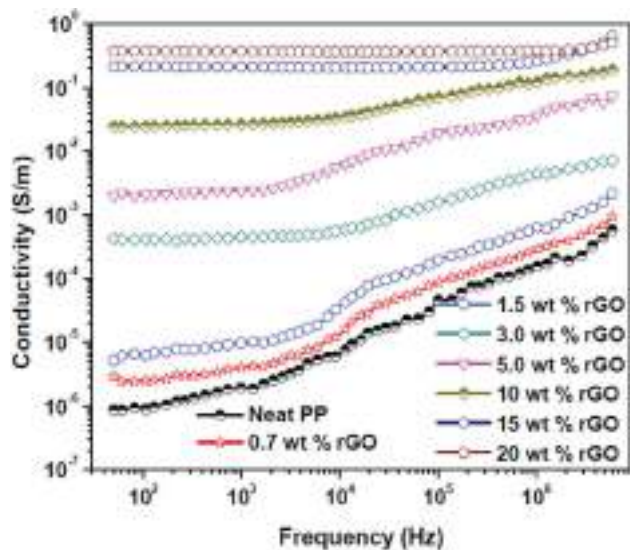


Fig. 11 AC conductivity variation of PP/rGO composites with varying rGO content as a function of frequency.

networks throughout the system thus facilitating the current transfer. It has already been reported that composites filled with conductive fillers show huge increase in conductivity values above the percolation threshold due to the formation of conductive networks and also due to the hopping mechanism induced charge transfer.⁷⁰ The different conducting mechanisms taking place inside a heterogeneous composite material before and after the percolation threshold can be depicted as shown in Fig. 12.

Polypropylene is an insulator and such materials show hopping of electrons as the major charge transport mechanism in it. On the addition of conducting filler like rGO with its concentration below the percolation threshold, the formation of narrow conductive islands in the matrix along with hopping contributes to the total conductivity (Fig. 12a). However, the addition of rGO above the percolation threshold results in the formation of extensive conductive networks or pathways (Fig. 12b) throughout the system and supports the conduction process for extended distances and contributes

sufficiently to the total conductivity. The conductivity above the percolation threshold is also aided by inter-island hopping mechanism. Below the percolation threshold the scarcity of long range conductive pathways or networks restricts the charge flow to only short distances and hence the conductivity will be low. The formation of conductive pathways or networks however, leads to long range metal like conduction thereby increasing the conductivity values to a few orders of magnitude above the percolation threshold.

Size, shape, concentration, distribution *etc.* of the filler are the major factors that govern the formation of conductive networks/pathways in a given composite material.⁷⁰ A significant advantage of graphene reported by scientists is that, being a two dimensional material it assists in the process of connecting with each other more effortlessly compared to other conducting nanofillers due to its huge aspect ratio and hence the use of graphene based materials helps in attaining low percolation thresholds for composites.^{23,77} However, it has also been reported that on comparison, at the same filler content CNT based composites have higher conductivity than the graphene based counterparts due to the individual CNT showing very low contact resistance.⁵ They also claim that compared to 2D geometry of graphene sheets, the 1D geometry of CNTs are more favorable towards the formation of conductive networks.⁵ Al-Saleh, however has experimentally proven that the intrinsic conductivity of graphene conductive pathways or networks at high filler content is superior to that of the CNT networks.⁵ A low percolation threshold of conductivity can provide composites with many advantages such as maintenance of its mechanical properties at low filler loading, reduction in weight, low cost of production *etc.* However, percolation threshold of conductivity only means the amount of filler (wt% or vol%) required for the formation of conductive networks wherein the conductivity values show few order magnitude increment (For *e.g.* say from 10^{-7} to 10^{-4}). Even so, it has been extensively reported that for a material to behave as an EMI shield it should possess even higher conductivity values.^{78,79} Hence, for practical EMI shielding applications the addition of rGO above the percolation threshold may be required.

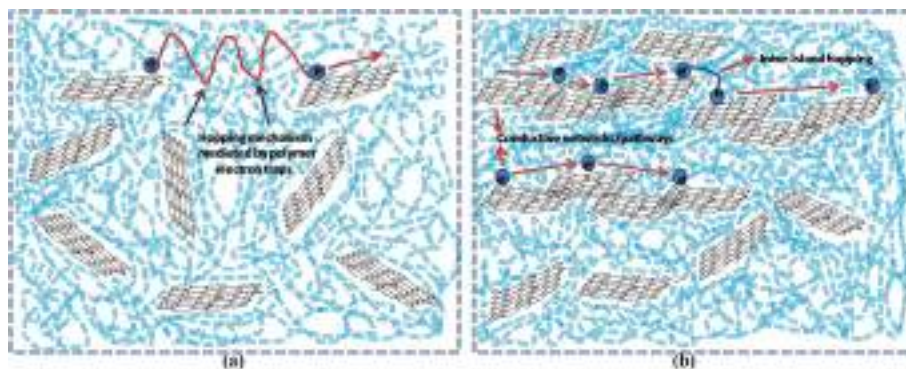


Fig. 12 Proposed conducting mechanisms taking place in PP/rGO composites at (a) below percolation threshold and (b) above percolation threshold.



3.6 Electromagnetic interference shielding effectiveness of *in situ* reduced rGO/PP composites

Conductivity, dielectric properties, dispersion state of the filler in the matrix, aspect ratio and loading of the incorporated fillers are some of the major aspects that govern the electromagnetic interference shielding effectiveness (EMI SE) of a given composite/nanocomposite. Good dielectric behavior and conductivity can be accomplished by means of incorporating highly conducting filler.^{57,80} The EMI SE of a given material can be determined using the *S* parameters (S_{11} , S_{12} , S_{22} , S_{21}). In materials with an EMI SE value of ~ 10 dB, researchers have claimed that the major mechanism in such a system consists of absorption and reflection and in such cases multiple reflections can be neglected. The *S* parameters can be utilized to calculate the SE_R and SE_A values using the following equations:⁵

$$SE_A = 10 \log_{10} \left[\frac{1 - |S_{11}|^2}{|S_{12}|^2} \right] \quad (1)$$

$$SE_R = 10 \log_{10} \left[\frac{1}{(1 - |S_{11}|^2)} \right] \quad (2)$$

where SE_A and SE_R are the shielding effectiveness due to absorption and reflection respectively. On estimating EMI SE of a material using vector network analyzer the scattering parameters S_{11} and S_{12} are referred to as forward reflection and reverse transmission coefficient respectively.⁵⁷ In addition to the above mentioned calculations the *S* parameters S_{11} and S_{12} can also be used to calculate the reflected, absorbed and transmitted powers using the following equations:⁵

$$R = |S_{11}|^2 = |S_{22}|^2 \quad (3)$$

$$T = |S_{12}|^2 = |S_{21}|^2 \quad (4)$$

$$A = 1 - R - T$$

where *R*, *T* and *A* are the reflected, transmitted and absorbed powers respectively.

Electromagnetic interference shielding effectiveness (EMI SE) is a thickness dependent property^{22,81} and throughout the course of this work samples with thickness of 2 mm was prepared and studied. The EMI SE values of *in situ* reduced rGO/PP nanocomposites with respect to rGO content over the X and Ku band regions are presented in Fig. 13.

The EMI SE values of PP/rGO composites clearly expose its frequency independent behavior over a broad frequency range (8–18 GHz). For neat PP the EMI SE value over X band was approximately 0.5 dB whereas over Ku band it was ~ 0.3 dB. However, on addition of conducting filler like rGO the EMI SE values increased considerably over both the X and Ku band regions. The highest EMI SE values were shown by 20 wt% rGO filled samples (~ 50 dB over X band and ~ 48 dB over the Ku band respectively). The substantial increase in the EMI SE values of rGO filled PP samples may be the result of extensive conductive networks/pathways being formed with increasing rGO content. It can be observed that for the same sample the EMI SE values at two different bands (X and Ku) are dissimilar, this peculiarity has been reported by several researchers wherein the same sample will show different EMI SE values at different bands.²² The increased EMI SE values with increasing rGO content can also be attributed to (a) the continuity of the conductive networks/pathways being formed in the system increases with increasing rGO content and (b) the chance of formation of thick conductive interfaces between the PP multifacets facilitating the enhanced EMI SE as a result of strong interaction with the EM waves.¹² For practical commercial applications an EMI SE value of 20 dB equivalent to 1% of transmittance is required and can be achieved by conductivity

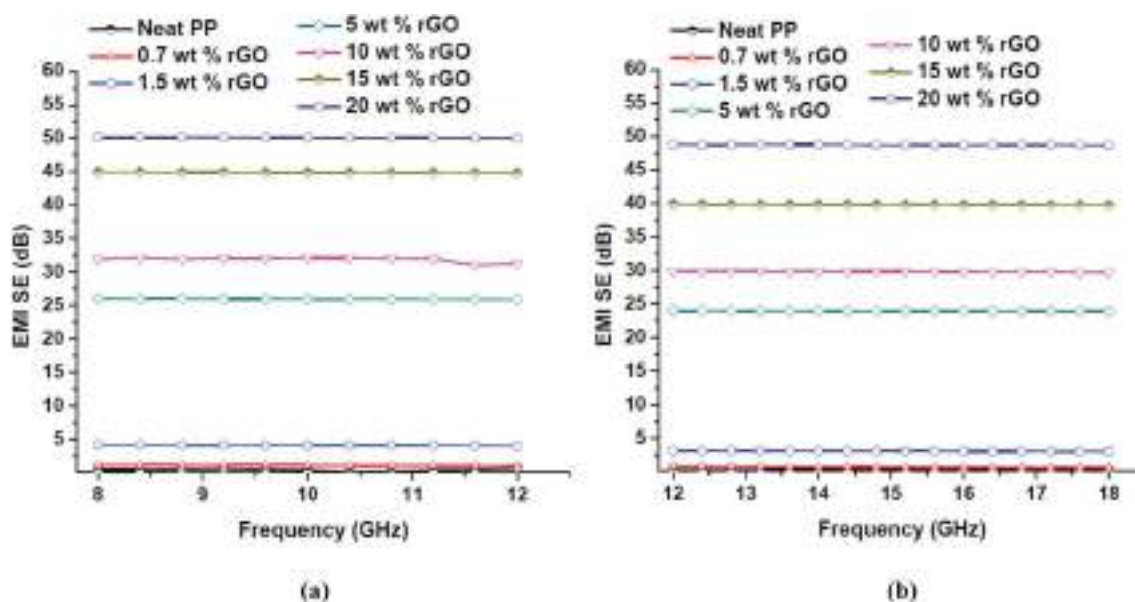


Fig. 13 EMI SE values of PP/rGO composites with different rGO content over (a) X and (b) Ku bands of the microwave frequency region.



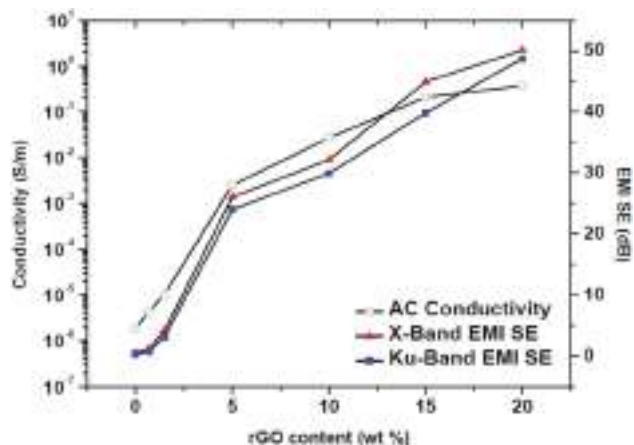


Fig. 14 EMI SE values at X and Ku bands plotted together with ac conductivity at 1.2 kHz against different rGO contents.

of around 1 S m^{-1} .^{57,70} This 20 dB EMI SE value was achieved using 5 wt% rGO itself. The present study without a doubt divulges that PP latex/*in situ* reduced rGO composites have the ability to meet the stringent conditions for its possible commercial applications. In order to show a relationship between the electrical conductivity and EMI shielding of a material the conductivity values at 1200 Hz and the EMI SE values of the samples at X (10 GHz) and Ku (15 GHz) bands are plotted against rGO content and is shown in Fig. 14.

The EMI SE and conductivity values do not show any significant improvement upto 1.5 wt% rGO content. However, above 1.5 wt% rGO content which is the percolation threshold in this case, both the conductivity and EMI SE values showcase noteworthy improvement. Hence it can be concluded that a major criterion to achieve good EMI shielding behavior for polymer composites is that the conducting filler content should be well above the percolation threshold. Numerous conducting pathways and microcapacitors will be created above the percolation threshold which may aid in attenuating the EM waves properly.²² Kumar *et al.*²² have also claimed that a minimum conductivity of $10^{-4} \text{ S cm}^{-1}$ for a given material will yield good EMI shielding behavior. Increased conductive pathways and

microcapacitors above percolation threshold will lead to large number of nomadic charge carriers and/or electric or magnetic dipoles that can interact with EM waves²⁴ thereby increasing the EMI shielding efficiency.^{22,82} Table 3 shows a comparative analysis of recently reported EMI SE values of graphene filled polymer composites. The values in Table 3 evidently demonstrate that the present method to *in situ* reduce graphene oxide within the PP latex matrix during the mixing stages itself yields excellent properties to the resulting composite. Moreover, the current work proposes a green and economical route for the preparation of PP/rGO composites wherein ascorbic acid (vitamin C) is used as the reducing agent and aqueous medium is used during the entire processing stages.

3.7 Electromagnetic interference shielding effectiveness mechanism

The contribution of absorption and reflection towards total shielding effectiveness at two different frequencies for both X and Ku bands was plotted against the rGO content (Fig. 15) to understand the EMI shielding mechanism of the prepared PP/rGO composites. It can be clearly observed that in both the X and Ku bands the absorption contribution is much higher compared to that of the reflection counterpart, in spite of varying rGO concentration. For *e.g.* at 9.2 GHz (X-band) the absorption contribution is ~ 43 dB whereas, the reflection contribution is only ~ 8 dB for 20 wt% rGO filled sample. In general the average contribution of absorption and reflection towards total shielding effectiveness in the X and Ku bands are ~ 80 – 85 and ~ 15 – 20 respectively. The above mentioned results clearly point to the fact that in PP/rGO system the primary shielding mechanism is absorption with not so little contribution from reflection also. It can be inferred that the present composites can be utilized as effective EM absorbers. Scientists have already established that for an EMI shielding material to showcase good EM absorption property it should possess high conductivity and high permeability.²² It has also been stated that changes in absorption contribution to total EMI SE will be more distinct than the reflection contribution with increasing electrical conductivity.²² This point is evident from our study wherein the samples with high conductivity demonstrate very

Table 3 Recent trends in the area of EMI SE of polymer/graphene composites

Composite	Filler content wt (%) [vol%] $\{V_f\}$	Thickness (mm)	EMI SE (dB)	Ref.
PP/rGO	20.0 [12] $\{0.12\}$	2.0	50 (X band) 48 (Ku band)	Present work
PP/graphene nanosheets	20.0	0.5	13.0 (S band)	83
PP/graphene nanoplatelets	10.0	1.0	19.0 (X band)	33
PU/graphene nanosheets	0.12 V_f	0.05	14 (X band)	84
Epoxy/functionalized graphene	15	—	21 (X band)	16
PS/rGO	3.47 vol%	2.5	45 (X band)	12
PVDF/graphene decorated with graphene quantum dots	2	—	37 (X band)	85
PS/sulfur doped rGO	7.5 vol%	2.0	24.5 (Ku band)	86
PEI/graphene	10	2.3	20 (X band)	17
PS/functionalized graphene sheets	30	2.5	29 (X band)	18



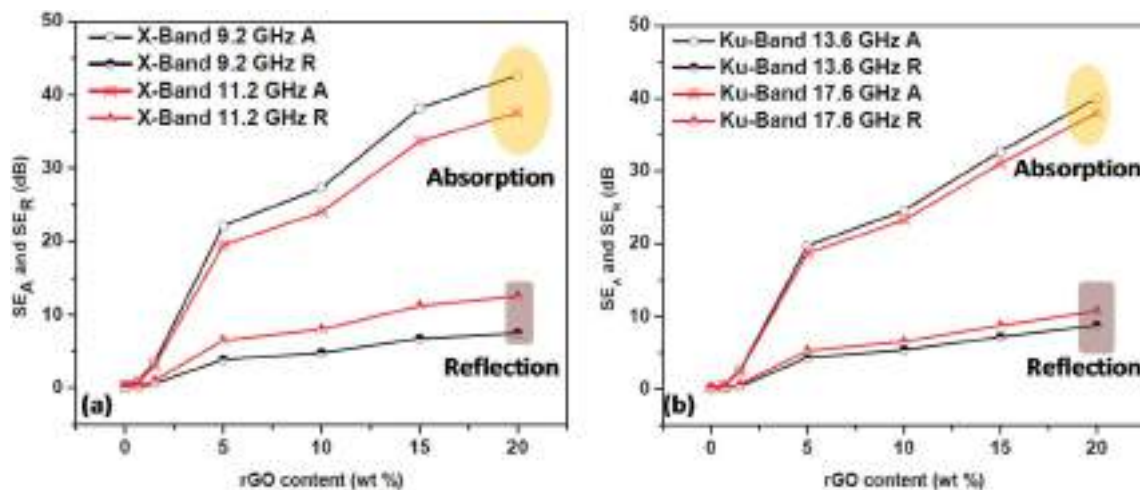


Fig. 15 Absorption and reflection contributions to the total EMI shielding effectiveness of PP/rGO composites at two different frequencies of (a) X-Band and (b) Ku-Band.

high absorption contributions to total EMI SE. EMI shielding materials with good absorption contribution has the potential for applications in stealth by attenuating the EM waves to heat which is then dissipated by the shielding material possessing good thermal conductivity.²² In short, a simple green approach was utilized to fabricate PP/*in situ* reduced graphene oxide nanocomposites with the potential to be employed as effective EM absorbers.

4. Conclusions

PP/*in situ* reduced rGO nanocomposites was successfully fabricated with exceptional rGO dispersion state *via* latex technology by means of simple magnetic stirring and L-ascorbic acid as the green reducing agent. The reduction of GO to rGO was confirmed using FT-IR, UV-visible, Raman and XPS spectroscopy. XRD was utilized to gain insight into the exfoliation state of rGO within the PP matrix. FE-SEM and TEM analysis was used to analyze the morphology and dispersion state of rGO in the PP matrix and were found to be uniformly distributed throughout the matrix. These results obviously point to the fact that the employed latex method (matrix in liquid form) combined with the *in situ* reduction *via* a green approach has an important part in homogeneously dispersing the rGO sheets in the PP matrix which is otherwise rather very difficult to achieve at high filler loadings. The as prepared nanocomposites showcase excellent electrical properties (dielectric constant and ac conductivity) with a percolation threshold in between 1.5 and 3 wt%. The enhanced ac conductivity of the composites with increasing rGO content leads them to display excellent EMI shielding capability. The obtained EMI SE values of 50 and 48 dB for X and Ku bands respectively for the PP/rGO composites (2 mm thick) are one of the best among contemporary works where GO was used as the filler. The present PP/rGO system can be utilized as efficient EM absorbers because of the absorption mechanism dominating the reflection part. The prepared nanocomposites exhibited marginally improved thermal

stability with increasing rGO content. The nanocomposites also exhibited increment in crystallization and onset crystallization temperatures due to the nucleating ability of rGO. The melting behavior on the other hand, changed from double melting performance to single melting due to the ability of rGO to specifically nucleate a particular polymorph of PP (β or hexagonal form). A green, low cost and effective approach to prepare rGO filled polymer composites with outstanding dispersion state of graphene nanosheets in the polymer matrix is proposed in this work. These prepared nanocomposites can be used as master batches which can be efficiently mixed with other polymers to prepare blends or can be mixed with PP granules itself. The as prepared polymer/rGO nanocomposites will have the potential to be used as novel dielectric and EMI shielding materials.

Conflicts of interest

There are no conflicts to declare.

Acknowledgements

Gejo George thankfully acknowledges the financial support by UGC in the form of Dr D. S. Kothari Postdoctoral Fellowship (No. F.4-2/2006(BSR)/CH/15-16/0211). Gejo George also gratefully acknowledges BYK Additives & Instruments for supplying us with the AQUACER 1868 samples for research purpose. Gejo George would also like to thank Mr Jacob K. Chacko, Research Scholar, SB College, Changanacherry, Kerala, India for his valuable suggestions and fruitful discussions. Gejo George would also like to thank <https://www.chemix.org/> website for the help in drawing of certain parts in Fig. 1. Sanu Mathew Simon acknowledges the support in the form of DST PURSE PII (SR.417 & SR.416 dated 27.02.2017). The authors would like to also thank Sophisticated Instrumentation and Computation Centre (SICC), University of Kerala for performing XPS analysis.



Notes and references

- P. Yadav, S. Rattan, A. Tripathi and S. Kumar, *Mater. Res. Express*, 2017, **4**, 65601.
- S. L. Shi and J. Liang, *Nanotechnology*, 2008, **19**, 255707.
- R. K. Goyal, *Mater. Chem. Phys.*, 2013, **142**, 195–198.
- S. Abbas, A. Dixit, R. Chatterjee and T. Goel, *J. Nanosci. Nanotechnol.*, 2007, **7**, 2129–2133.
- M. H. Al-Saleh, *J. Phys. D: Appl. Phys.*, 2016, **49**, 195302.
- W. L. Song, M. S. Cao, M. M. Lu, J. Yang, H. F. Ju, Z. L. Hou, J. Liu, J. Yuan and L. Z. Fan, *Nanotechnology*, 2013, **24**, 115708.
- G. P. Kar, S. Biswas and S. Bose, *Mater. Res. Express*, 2016, **3**, 64002.
- G. Mittal, V. Dhand, K. Y. Rhee, S. J. Park and W. R. Lee, *J. Ind. Eng. Chem.*, 2015, **21**, 11–25.
- C. Kingston, R. Zepp, A. Andrady, D. Boverhof, R. Fehir, D. Hawkins, J. Roberts, P. Sayre, B. Shelton, Y. Sultan, V. Vejins and W. Wohlleben, *Carbon*, 2014, **68**, 33–57.
- M. S. Cao, X. X. Wang, W. Q. Cao and J. Yuan, *J. Mater. Chem. C*, 2015, **3**, 6589–6599.
- M. H. Al-Saleh and U. Sundararaj, *Carbon*, 2009, **47**, 2–22.
- D. X. Yan, H. Pang, B. Li, R. Vajtai, L. Xu, P. G. Ren, J. H. Wang and Z. M. Li, *Adv. Funct. Mater.*, 2015, **25**, 559–566.
- Z. Chen, W. Ren, L. Gao, B. Liu, S. Pei and H.-M. Cheng, *Nat. Mater.*, 2011, **10**, 424–428.
- X. Gui, H. Li, L. Zhang, Y. Jia, L. Liu, Z. Li, J. Wei, K. Wang, H. Zhu, Z. Tang, D. Wu and A. Cao, *ACS Nano*, 2011, **5**, 4276–4283.
- X. Sun, H. Sun, H. Li and H. Peng, *Adv. Mater.*, 2013, **25**, 5153–5176.
- J. Liang, Y. Wang, Y. Huang, Y. Ma, Z. Liu, J. Cai, C. Zhang, H. Gao and Y. Chen, *Carbon*, 2009, **47**, 922–925.
- J. Ling, W. Zhai, W. Feng, B. Shen, J. Zhang and W. ge Zheng, *ACS Appl. Mater. Interfaces*, 2013, **5**, 2677–2684.
- D. X. Yan, P. G. Ren, H. Pang, Q. Fu, M. B. Yang and Z. M. Li, *J. Mater. Chem.*, 2012, **22**, 18772–18774.
- H. B. Zhang, W. G. Zheng, Q. Yan, Z. G. Jiang and Z. Z. Yu, *Carbon*, 2012, **50**, 5117–5125.
- S. T. Hsiao, C. C. M. Ma, H. W. Tien, W. H. Liao, Y. S. Wang, S. M. Li and Y. C. Huang, *Carbon*, 2013, **60**, 57–66.
- A. P. Singh, P. Garg, F. Alam, K. Singh, R. B. Mathur, R. P. Tandon, A. Chandra and S. K. Dhawan, *Carbon*, 2012, **50**, 3868–3875.
- G. S. Kumar, D. Vishnupriya, A. Joshi, S. Datar and T. U. Patro, *Phys. Chem. Chem. Phys.*, 2015, **17**, 20347–20360.
- D. Wang, X. Zhang, J. W. Zha, J. Zhao, Z. M. Dang and G. H. Hu, *Polymer*, 2013, **54**, 1916–1922.
- K. Kalaitzidou, H. Fukushima and L. T. Drzal, *Composites, Part A*, 2007, **38**, 1675–1682.
- Y. Huang, Y. Qin, Y. Zhou, H. Niu, Z. Z. Yu and J. Y. Dong, *Chem. Mater.*, 2010, **22**, 4096–4102.
- M. C. Hsiao, S. H. Liao, Y. F. Lin, C. A. Wang, N. W. Pu, H. M. Tsai and C. C. M. Ma, *Nanoscale*, 2011, **3**, 1516.
- Y. Li, J. Zhu, S. Wei, J. Ryu, L. Sun and Z. Guo, *Macromol. Chem. Phys.*, 2011, **212**, 1951–1959.
- J. Z. Xu, C. Chen, Y. Wang, H. Tang, Z. M. Li and B. S. Hsiao, *Macromolecules*, 2011, **44**, 2808–2818.
- J. E. An, G. W. Jeon and Y. G. Jeong, *Fibers Polym.*, 2012, **13**, 507–514.
- M. El Achaby, F. E. Arrakhiz, S. Vaudreuil, A. el Kacem Qaiss, M. Bousmina and O. Fassi-Fehri, *Polym. Compos.*, 2012, **33**, 733–744.
- P. Song, Z. Cao, Y. Cai, L. Zhao, Z. Fang and S. Fu, *Polymer*, 2011, **52**, 4001–4010.
- T. T. Li, A. P. Chen, P. W. Hwang, Y. J. Pan, W. H. Hsing, C. W. Lou, Y.-S. Chen and J. H. Lin, *Mater. Manuf. Processes*, 2017, 1–7.
- F. E. Alam, J. Yu, D. Shen, W. Dai, H. Li, X. Zeng, Y. Yao, S. Du, N. Jiang and C. Te Lin, *Polymer*, 2017, **9**, 662–672.
- Y. S. Yun, Y. H. Bae, D. H. Kim, J. Y. Lee, I. J. Chin and H. J. Jin, *Carbon*, 2011, **49**, 3553–3559.
- H. E. Miltner, N. Grossiord, K. Lu, J. Loos, C. E. Koning and B. Van Mele, *Macromolecules*, 2008, **41**, 5753–5762.
- S. T. Hsiao, C. C. M. Ma, H. W. Tien, W. H. Liao, Y. S. Wang, S. M. Li, C. Y. Yang, S. C. Lin and R. B. Yang, *ACS Appl. Mater. Interfaces*, 2015, **7**, 2817–2826.
- S. Fu, N. Li, K. Wang, Q. Zhang and Q. Fu, *Colloid Polym. Sci.*, 2015, **293**, 1495–1503.
- D. Wang, X. Zhang, J. W. Zha, J. Zhao, Z. M. Dang and G. H. Hu, *Polymer*, 2013, **54**, 1916–1922.
- J. Zhang, H. Yang, G. Shen, P. Cheng, J. Zhang and S. Guo, *Chem. Commun.*, 2010, **46**, 1112–1114.
- P. Karrer, *Chem. Rev.*, 1934, **14**, 17–30.
- H. J. Loeffler and J. D. Ponting, *Ind. Eng. Chem., Anal. Ed.*, 1942, **14**, 846–849.
- M. B. Davies, D. A. Partridge and J. A. Austin, *Vitamin C*, The Royal Society of Chemistry, 1991.
- M. Ambrosi, E. Fratini, V. Alfredsson, B. W. Ninham, R. Giorgi, P. Lo Nostro and P. Baglioni, *J. Am. Chem. Soc.*, 2006, **128**, 7209–7214.
- L. Lu, A. Kobayashi, K. Tawa and Y. Ozaki, *Chem. Mater.*, 2006, **18**, 4894–4901.
- G. S. Métraux, Y. C. Cao, R. Jin and C. A. Mirkin, *Nano Lett.*, 2003, **3**, 519–522.
- Y. Wang, P. H. C. Camargo, S. E. Skrabalak, H. Gu and Y. Xia, *Langmuir*, 2008, **24**, 12042–12046.
- E. Andrijanto, S. Shoelarta, G. Subiyanto and S. Rifki, *AIP Conf. Proc.*, 2016, **1725**, 020003.
- M. J. Fernández-Merino, L. Guardia, J. I. Paredes, S. Villar-Rodil, P. Solís-Fernández, A. Martínez-Alonso and J. M. D. Tascón, *J. Phys. Chem. C*, 2010, **114**, 6426–6432.
- D. Li, M. B. Müller, S. Gilje, R. B. Kaner and G. G. Wallace, *Nat. Nanotechnol.*, 2008, **3**, 101–105.
- S. K. Mishra, S. N. Tripathi, V. Choudhary and B. D. Gupta, *Sens. Actuators, B*, 2014, **199**, 190–200.
- M. S. Dresselhaus, G. Dresselhaus, A. Jorio, A. G. Souza Filho and R. Saito, *Carbon*, 2002, **40**, 2043–2061.
- K. N. Kudin, B. Ozbas, H. C. Schniepp, R. K. Prud'homme, I. A. Aksay and R. Car, *Nano Lett.*, 2008, **8**, 36–41.



- 53 F. Tuinstra and J. L. Koenig, *J. Chem. Phys.*, 1970, **53**, 1126–1130.
- 54 X. Zhao, Q. Zhang, D. Chen and P. Lu, *Macromolecules*, 2010, **43**, 2357–2363.
- 55 W. S. Hummers and R. E. Offeman, *J. Am. Chem. Soc.*, 1958, **80**, 1339.
- 56 J. I. Paredes, S. Villar-Rodil, P. Solís-Fernández, A. Martínez-Alonso and J. M. D. Tascón, *Langmuir*, 2009, **25**, 5957–5968.
- 57 M. A. Poothanari, J. Abraham, N. Kalarikkal and S. Thomas, *Ind. Eng. Chem. Res.*, 2018, **57**, 4287–4297.
- 58 R. A. Khare, A. R. Bhattacharyya and A. R. Kulkarni, *J. Appl. Polym. Sci.*, 2011, **120**, 2663–2672.
- 59 S. M. Luz, J. Del Tio, G. J. M. Rocha, A. R. Gonçalves and A. P. Del'Arco, *Composites, Part A*, 2008, **39**, 1362–1369.
- 60 Y. Xu, W. Hong, H. Bai, C. Li and G. Shi, *Carbon*, 2009, **47**, 3538–3543.
- 61 J. Liang, Y. Huang, L. Zhang, Y. Wang, Y. Ma, T. Cuo and Y. Chen, *Adv. Funct. Mater.*, 2009, **19**, 2297–2302.
- 62 S. Zhao, F. Chen, C. Zhao, Y. Huang, J. Y. Dong and C. C. Han, *Polymer*, 2013, **54**, 3680–3690.
- 63 K. Wakabayashi, P. J. Brunner, J. Masuda, S. A. Hewlett and J. M. Torkelson, *Polymer*, 2010, **51**, 5525–5531.
- 64 M. Aliofkhazraei, N. Ali, W. I. Milne, C. S. Ozkan, S. Mitura and J. L. Gervasoni, *Graphene Science Handbook: Nanostructure and Atomic Arrangement*, 2016.
- 65 F. Navarro-Pardo, J. Laria, T. Lozano, A. B. Morales-Cepeda, P. G. Lafleur, S. Sánchez-Valdés and F. Rodríguez-González, *J. Appl. Polym. Sci.*, 2013, **130**, 2932–2937.
- 66 B. Yuan, C. Bao, L. Song, N. Hong, K. M. Liew and Y. Hu, *Chem. Eng. J.*, 2014, **237**, 411–420.
- 67 Z. M. Dang, Y. H. Lin and C. W. Nan, *Adv. Mater.*, 2003, **15**, 1625–1629.
- 68 Z. M. Dang, L. Wang, Y. Yin, Q. Zhang and Q. Q. Lei, *Adv. Mater.*, 2007, **19**, 852–857.
- 69 Z. M. Dang, J. K. Yuan, J. W. Zha, T. Zhou, S. T. Li and G. H. Hu, *Prog. Mater. Sci.*, 2012, **57**, 660–723.
- 70 J. Abraham, M. Arif P, P. Xavier, S. Bose, S. C. George, N. Kalarikkal and S. Thomas, *Polymer*, 2017, **112**, 102–115.
- 71 K. Prashantha, J. Soulestin, M. F. Lacrampe, P. Krawczak, G. Dupin, M. Claes and A. Tewari, *Polym. Polym. Compos.*, 2010, **18**, 489–494.
- 72 G. George, S. M. Simon, V. P. Prakashan, M. S. Sajna, M. Faisal, A. Chandran, R. Wilson, P. R. Biju, C. Joseph and N. V. Unnikrishnan, *Polym. Compos.*, 2018, **39**, E1169–E1183.
- 73 P. Xu, H. Gui, Y. Hu, A. Bahader and Y. Ding, *J. Electron. Mater.*, 2014, **43**, 2754–2758.
- 74 E. El Shafee, M. El Gamal and M. Isa, *J. Polym. Res.*, 2012, **19**, 9805–9812.
- 75 R. V. Barde, K. R. Nemade and S. A. Waghuley, *J. Australas. Ceram. Soc.*, 2015, **3**, 116–122.
- 76 P. Saini, V. Choudhary, B. P. Singh, R. B. Mathur and S. K. Dhawan, *Synth. Met.*, 2011, **161**, 1522–1526.
- 77 C. W. Nan, Y. Shen and J. Ma, *Annu. Rev. Mater. Res.*, 2010, **40**, 131–151.
- 78 J. M. Thomassin, C. Jérôme, T. Pardoën, C. Bailly, I. Huynen and C. Detrembleur, *Mater. Sci. Eng., R*, 2013, **74**, 211–232.
- 79 L. C. Jia, D. X. Yan, C. H. Cui, X. Jiang, X. Ji and Z. M. Li, *J. Mater. Chem. C*, 2015, **3**, 9369–9378.
- 80 S. R. Dhakate, K. M. Subhedar and B. P. Singh, *RSC Adv.*, 2015, **5**, 43036–43057.
- 81 C. S. Zhang, Q. Q. Ni, S. Y. Fu and K. Kurashiki, *Compos. Sci. Technol.*, 2007, **67**, 2973–2980.
- 82 M. Chen, L. Zhang, S. Duan, S. Jing, H. Jiang, M. Luo and C. Li, *Nanoscale*, 2014, **6**, 3796–3803.
- 83 C. L. Huang, C. W. Lou, C. F. Liu, C. H. Huang, X. M. Song and J. H. Lin, *Appl. Sci.*, 2015, **5**, 1196–1210.
- 84 R. Jan, A. Habib, M. A. Akram, I. Ahmad, A. Shah, M. Sadiq and A. Hussain, *Mater. Res. Express*, 2017, **4**, 35605.
- 85 N. V. Lakshmi and P. Tambe, *Compos. Interfaces*, 2017, **24**, 861–882.
- 86 F. Shahzad, S. Yu, P. Kumar, J. W. Lee, Y. H. Kim, S. M. Hong and C. M. Koo, *Compos. Struct.*, 2015, **133**, 1267–1275.





Network access provided by: Mahatma Gandhi University

Issue 24, 2018

[Previous](#)[Next](#)

From the journal:

New Journal of Chemistry

Highly lithium ion conductive, Al₂O₃ decorated electrospun P(VDF-TrFE) membranes for lithium ion battery separators



[Bicy K.](#)^a [Shruti Suriyakumar](#)^b [Anu Paul P.](#)^a [Anu A. S.](#)^a [Nandakumar Kalarikkal](#) ^{ac} [Arul Manuel Stephen](#)^b [Geethamma V. G.](#)^a
[Didier Rouxel](#)^{*d} and [Sabu Thomas](#) ^{*ae}

[Author affiliations](#)

Abstract

Electrospun battery separators have drawn considerable attention due to their high porosity, surface area, and electrochemical performance. In this paper, a novel Al₂O₃ nanoparticle decorated poly(vinylidene fluoride-trifluoroethylene) (P(VDF-TrFE)) membrane was fabricated by the electrospinning technique. Both P(VDF-TrFE) and Al₂O₃ are well known for their excellent properties, like mechanical strength, piezoelectric nature, thermal stability *etc.*, and the electrospun membrane was prepared by combining the excellence of these two materials. The physical properties of P(VDF-TrFE) and the influence of nanoparticles on the physical properties were evaluated by morphological, thermal, XRD and FT-IR analysis. SEM and TEM analysis shows that the nanoparticles increase the fiber diameter and are located on the surface as well as in the bulk of the fiber. XRD studies reveal that the nanoparticles were localized at the inter-planar spacing of the polymer chains. The melting temperature of P(VDF-TrFE) is increased by the addition of Al₂O₃ nanoparticles, and all the prepared membranes exhibit superior thermal and dimensional stability compared to the Celgard 2320 separator. The prepared membranes were explored as a lithium-ion battery separator by characterizing their wettability, electrolyte uptake, % porosity, ionic conductivity and charge–discharge performance. The high porosity (>80%) of

The article was received on 19 Apr 2018, accepted on 08 Oct 2018 and first published on 10 Oct 2018

[Tweet](#)[Share](#)

Article type: Paper

DOI: 10.1039/C8NJ01907J

Citation: *New J. Chem.*, 2018, **42**, 19505-19520

[Request permissions](#)

Search articles by author

- Bicy K.
- Shruti Suriyakumar
- Anu Paul P.
- Anu A. S.
- Nandakumar Kalarikkal
- Arul Manuel Stephen
- Geethamma V. G.
- Didier Rouxel
- Sabu Thomas

Spotlight



Network access provided by: Mahatma Gandhi University

Issue 19, 2018

Previous

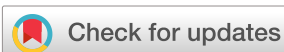
Next



From the journal:

New Journal of Chemistry

In situ dose dependent gamma ray irradiated synthesis of PMMA–Ag nanocomposite films for multifunctional applications†



[K. B. Bhavitha](#),^{ab} [Anju K. Nair](#),^{ab} [Hanna Mariya](#),^b [Jiya Jose](#),^b [Anshida Mayeen](#),^c [Kala M. S.](#),^a [Abhijit Saha](#),^{id d} [Sabu Thomas](#),^{be}
[Oluwatobi S. Oluwafemi](#)^{id *fg} and [Nandakumar Kalarikkal](#)^{id *bc}

Author affiliations

* Corresponding authors

^a Department of Physics, St Teresas's College, Ernakulam-682011, Kerala, India

^b International and Inter University Centre for Nanoscience and Nanotechnology, Mahatma Gandhi University, Kottayam-686 560, Kerala, India

E-mail: nkkalarikkal@mgu.ac.in

^c School of Pure and Applied Physics, Mahatma Gandhi University, Kottayam-686 560, Kerala, India

^d UGC DAE CSR, Kolkata Centre, Kolkata-700098, West Bengal, India

^e School of Chemical Sciences, Mahatma Gandhi University, Kottayam-686 560, Kerala, India

^f Department of Applied Chemistry, University of Johannesburg, P.O. Box 17011, Doornfontein, Johannesburg 2028, South Africa

E-mail: oluwafemi.oluwatobi@gmail.com

^g Centre for Nanomaterials Sciences Research, University of Johannesburg, Johannesburg, South Africa

* Exclusive of taxes

This article contains 12 page(s)

Other ways to access this content

Log in

Using your institution credentials

Sign in

With your membership or subscriber account

Supplementary files

Supplementary information

PDF (623K)

Publication details

The article was received on 30 May 2018, accepted on 08 Aug 2018 and first published on 10 Aug 2018

Tweet

Share

Article type:

Paper

DOI:

10.1039/C8NJ02684J

Citation:

New J. Chem., 2018, **42**, 15750-15761

BibTex



Go

[Request permissions](#)

Search articles by author

K. B. Bhavitha



Network access provided by: Mahatma Gandhi University

[All chapters](#)[Previous](#)[Next](#)

From the book:

Electrospinning: From Basic Research to Commercialization

CHAPTER 1

Electrical Spinning to Electrospinning: a Brief History

K. Ghosal, C. Agatemor, N. Tucker, E. Kny and S. Thomas

Fine fibers made by electrostatic force have been discussed, investigated, and patented since the late 18th century. However, until the 1980s, potential applications for such fibers were restricted by various technological limitations. In 1995, Doshi and Reneker reworked and simplified the electrical spinning process. This book begins with this journey, and describes how the invention fueled applications. It also presents a short account of the current status of electrospinning in diverse fields of application.

Download this chapter

PDF format

[Chapter HTML](#)[ePub](#)

Publication details

<https://doi.org/10.1039/9781788012942-00001>**Print publication date:** 16 Aug 2018**Copyright year:** 2018

Issue 11, 2018

[Previous](#)[Next](#)

From the journal:

MedChemComm

Selected aryl thiosemicarbazones as a new class of multi-targeted monoamine oxidase inhibitors†



[Bijo Mathew](#), ^{†*}^a [Seung Cheol Baek](#), [†]^b [Della Grace Thomas Parambi](#), ^c [Jae Pil Lee](#), ^b [Monu Joy](#), ^d [P. R. Annie Rilda](#), ^a [Rugma V. Randev](#), ^a [P. Nithyamol](#), ^a [Vijitha Vijayan](#), ^a [Sini T. Inasu](#), ^a [Githa Elizabeth Mathew](#), ^e [Krishnakumar K. Lohidakshan](#), ^f [Girish Kumar Krishnan](#)^g and [Hoon Kim](#)^{*b}

Author affiliations

* Corresponding authors

^a Division of Drug Design and Medicinal Chemistry Research Lab, Department of Pharmaceutical Chemistry, Ahalia School of Pharmacy, Palakkad-678557, Kerala, India

E-mail: bjovilaventgu@gmail.com

^b Department of Pharmacy and Research Institute of Life Pharmaceutical Sciences, Sunchon National University, Suncheon-57922, Republic of Korea

E-mail: hoon@sunchon.ac.kr

^c Department of Pharmaceutical Chemistry, Jouf University, Al Jouf-2014, Sakaka, Saudi Arabia

^d School of Pure & Applied Physics, M.G. University, Kottayam, Kerala, India

^e Department of Pharmacology, Grace College of Pharmacy, Palakkad, India

^f Department of Pharmaceutical Chemistry, Nirmala College of Health Science, Chalakudy-680311, India

^g Department of Pharmaceutical Chemistry, College of Pharmaceutical Sciences, Government Medical College Trivandrum, India

Abstract

A series of 13 phenyl substituted thiosemicarbazones (**SB1–SB13**) were synthesized and evaluated for their inhibitory potential towards human recombinant monoamine oxidase A and B (MAO-A and

Supplementary files

Supplementary information

PDF (669K)

Supplementary information

PDF (368K)

Supplementary information

PDF (780K)

Supplementary information

RTF (57K)

Crystal structure data

CIF (18K)

Publication details

The article was received on 14 Aug 2018, accepted on 23 Sep 2018 and first published on 25 Sep 2018



Journal

International Journal of Polymeric Materials and Polymeric Biomaterials >

Latest Articles

58 | 0

Views

CrossRef citations to date

0

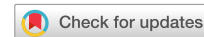
Altmetric

Articles

Development of biocompatible and biofilm-resistant silver-poly(methylmethacrylate) nanocomposites for stomatognathic rehabilitation

Sandhya Gopalakrishnan, Aby Mathew T., Miran Mozetič, Jayachandran V. P., Jiya Jose, Sabu Thomas & **Nandakumar Kalarikkal**  ...show less

Received 28 Sep 2018, Accepted 23 Nov 2018, Published online: 04 Jan 2019

 Download citation <https://doi.org/10.1080/00914037.2018.1552863>

Select Language | ▼

Translator disclaimer



Abstract

Recurrent prosthesis fracture and microbial contamination of the tissue bed or prosthetic materials remain the major clinical challenge for successful intraoral/faciomaxillary rehabilitation. Biocompatible and biofilm-resistant silver nanoparticle (AgNPs) based on poly(methyl methacrylate) was successfully developed by a compression-molding technique. The AgNP-loaded PMMA were characterized using TEM, SEM, FT-IR and XRD analysis. The nanocomposites were found to be biocompatible and biofilm-resistant against *Streptococcus mutans* and *Candida albicans*. Mechanical performance of the nanocomposite was statistically